NAVAL POSTGRADUATE SCHOOL
Monterey, California

THESIS

The Design of a FLIR Sensor
for the Korean Army RPV

by

Byung Gook Choi

September, 1991

Thesis Advisor: Donald L. Walters

Approved for public release; distribution is unlimited.

Unclassified

Security Classification of this page

REPORT DOCUMENTATION PAGE

1a Report Security Classification: Unclassified		1b Restrictive Markings	
2a Security Classification Authority		3 Distribution Availability of Report: Approved for public release; distribution is unlimited.	
2b Declassification/Downgrading Schedule			
4 Performing Organization Report Number(s)		5 Monitoring Organization Report Number(s)	
6a Name of Performing Organization: Naval Postgraduate School	6b Office Symbol (*If Applicable*): 3A	7a Name of Monitoring Organization: Naval Postgraduate School	
6c Address (*city, state, and ZIP code*): Monterey, CA 93943-5000		7b Address (*city, state, and ZIP code*): Monterey, CA 93943-5000	
8a Name of Funding/Sponsoring Organization	8b Office Symbol (*If Applicable*)	9 Procurement Instrument Identification Number	
8c Address (*city, state, and ZIP code*)		10 Source of Funding Numbers: Program Element Number / Project No / Task No / Work Unit Accession No	
11 Title (*Include Security Classification*): THE DESIGN OF A FLIR SENSOR FOR THE KOREAN ARMY RPV			
12 Personal Author(s): Byung Gook Choi			
13a Type of Report: Master's Thesis	13b Time Covered: From To	14 Date of Report (*year, month,day*): 1991, September	15 Page Count: 127
16 Supplementary Notation: The views expressed in this thesis are those of the author and do not reflect the official policy or position of the Department of Defense or the U.S. Government.			

17 Cosati Codes			18 Subject Terms (*continue on reverse if necessary and identify by block number*)
Field	Group	Subgroup	RPV, Thermal Imaging , FLIR, Design

19 Abstract (*continue on reverse if necessary and identify by block number*)

This thesis considers a forward looking infrared (FLIR) sensor system fot the Korean Army mounted in a remotely piloted vehicle such as the Pioneer RPV. Potential missions considered for this system included tactical reconnaissance, surveillance and intelligence gathering, target acquisition and location, artillery fire adjustment and damage assessment. The FLIR system provides high resolution thermal images in the 8-12 micrometers spectral range under day and night conditions, with a real time data link to the control center. Based on current technology a 55 element HgCdTe detector array cooled to 77 K was selected that provides a TV compatible video output. In the future, as improvements in quality occur with a corresponding reduction in cost, staring focal plane arrays such as PtSi or InSb should be considered.

20 Distribution/Availability of Abstract: (X) unclassified/unlimited ( ) same as report ( ) DTIC users	21 Abstract Security Classification: Unclassified	
22a Name of Responsible Individual: Donald L. Walters	22b Telephone (*Include Area code*): (408) 646-3207	22c Office Symbol: PH/We

DD FORM 1473, 84 MAR 83 APR edition may be used until exhausted security classification of this page

Approved for public release; distribution is unlimited.

The Design of a FLIR Sensor
for the Korean Army RPV

by

Byung Gook Choi
Captain, Republic of Korea Army
B.S., Korea Military Academy, 1985

Submitted in partial fulfillment
of the requirements for the degree of

MASTER OF SCIENCE IN SYSTEMS ENGINEERING
(ELECTRONIC WARFARE)

from the

NAVAL POSTGRADUATE SCHOOL
September 1991

Joseph Sternberg, Chairman, Electronic Warfare Academic Group

ABSTRACT

This thesis considers a forward looking infrared (FLIR) sensor system for the Korean Army mounted in a remotely piloted vehicle such as the Pioneer RPV. Potential missions considered for this system included tactical reconnaissance, surveillance and intelligence gathering, target acquisition and location, artillery fire adjustment and damage assessment. The FLIR system provides high resolution thermal images in the 8-12 μm spectral range under day and night conditions, with a real time data link to the control center. Based upon current technology a 55 element HgCdTe detector array cooled to 77K was selected that provides a TV compatible video output. In the future, as improvements in quality occur with a corresponding reduction in cost, staring focal plane arrays such as PtSi or InSb should be considered.

TABLE OF CONTENTS

I. INTRODUCTION 1

II. BACKGROUND 4

A. RPVS AND RPV PLATFORMS 4

B. SPECIFIC ENVIRONMENTAL CONDITIONS 14

C. THE KOREAN ENVIRONMENTAL CONDITIONS 14

D. ESTIMATED DESIGN FACTORS 17

III. INFRARED SENSOR CONSIDERATIONS 18

A. THE CHOICE OF IR SENSOR FOR RPV 18

B. PAYLOAD CONSIDERATIONS FOR RPV 18

1. Mission 18

2. EO Sensor Bandwidth and Resolution 20

3. Optical Considerations 22

IV. INITIAL DESIGN CONSIDERATIONS 28

V. SYSTEM REQUIREMENT ANALYSIS 30

A. PROBLEM DEFINITION 30

1. Mission and Functional requirements 30

2. Measure of Performance 30

B. SUMMARY OF REQUIREMENT 34

1. Optics 35

2. Optical Filters 35

3. Detector and Cooling Sytem 35

4. Preamplifier 35
5. Algorithm 36
6. Signal Processor 36
VI. SYSTEM DESIGN 37
A. OPTICAL DESIGN 37
1. Optical Configuration of FLIR 37
2. Optimum Configuration 38
3. IRdome and Stabilizing System 38
4. Optics 40
5. Scanning Mechanism 41
B. DETECTOR DESIGN 57
1. Selection of Detector Material 57
2. Detector Size and Array 61
3. Cooling System 63
C. ELECTRONICS 63
D. DISPLAY 64
E. SENSOR CONFIGURATION 64
VII. CONCLUSION / RECOMMENDATION 69
APPENDIX.A INFRARED (IR) FUNDAMENTALS 72
1. THE ELECTORMAGNETIC SPECTRUM 72
2. IR RADIATION 73
3. PLANCK'S LAW 74

4. PLOT OF SPECTRAL RADIANT EMITTANCE AS A FUNCTION OF WAVELENGTH 75
5. ATMOSPHERIC TRANSMISSION BASIC CONCEPTS OVERVIEW 76
6. ATMOSPHERIC TRANSMISSION 77
7. ATMOSPHERIC COMPUTER MODEL 78
8. EMISSIVITY 79
9. SPECTRAL DISTRIBUTION OF THERMAL AND SELECTIVE RADIATOR 80
10. SPECTRAL RADIANCE OF VARIOUS NATURAL SOURCES 81
APPENDIX.B BASIC IR OPTICS 82
1. BASIC OPTICAL TERMS 82
2. DETERMINING SENSOR FOV 83
3. LENS SYSTEM TYPES 84
4. PROBLEMS WITH OPTICS THAT AFFECT SENSOR PERFORMANCE 85
5. MEASURING LENS QUALITY MODULATION TRANSFER FUNCTION 86
6. LENS MATERIALS 87
7. IR FILTERS 88
APPENDIX.C IR DETECTORS / COOLERS 89

1. THERMAL DETECTORS 89
2. COMPARISON OF IR DETECTORS 90
3. CHARACTERIZING A DETECTOR 91
4. DETECTOR PERFORMANCE 92
5. DETECTOR RESPONSIVITY 93
6. DETECTOR DETECTIVITY 94
7. COMPARISON OF IR DETECTOR COOLERS 95
8. DETECTOR UNIFORMITY 96
APPENDIX.D ELECTRONIC 97
1. PREAMPS / POWER SUPPLIES 97
2. NOISE SOURCES 98
APPENDIX.E IR SENSOR SYSTEM AND PERFORMANCE 99
1. PASSIVE IR SENSOR99
2. PASSIVE IMAGING IR SENSOR 100
3. COMPARISON OF OTHER MEASURES FOR INFRARED SYSTEM 101
4. FUNDAMENTAL BLOCK DIAGRAM FOR A PASSIVE IR SENSOR 102
5. ANALYSIS OF IMAGING SYSTEM 103
6. PROBABILITY OF DETECTION 104
7. PROBABILITY OF DETECTING A REAL TARGET 105

8. PROBABILTY VS. RANGE 106
9. IR DETECTION PERFORMANCE 107
10. FALSE ALARM RATE 108
APPENDIX.F SENSOR GEOMETRY 109
1. DEFINITION OF TERMS 109
2. ANGULAR FIELDS AND TERMS 110
3. SENSOR FOOTPRINT 111
4. POINT SOURCE TARGET ANAYSIS 112
5. SENSOR FOV 113
REFERENCES 114
INITIAL DITRIBUTION LIST 117

LIST OF TABLES

TABLE 1.1 VARIOUS RPV STATISTICS 5-8

TABLE 2.1 GENERAL CHARACTERISTICS OF RPV 12

TABLE 3.1 COMPARISON OF 3 TO 5 AND 8 TO 14 μM WINDOW 27

TABLE 4.1 SENSOR PERFORMANCE GOAL 29

TABLE 5.1 SENSOR REQUIREMENTS 34

TABLE 6.1 CHARACTERISTICS OF A POLYGONAL MIRROR 46

TABLE 6.2 V/H RATIO AND OPTICAL PARAMETER 50-51

TABLE 6.3 RPV SPEED AND SENSOR FOOTPRINT 54-55

TABLE 6.4 CHARACTERISTICS OF THE DESIGN FOR
A FLIR SENSOR 67

TABLE 6.5 ESTIMATED SENSOR DIMENSION 68

LIST OF FIGURES

FIGURE 2.1 THE PIONEER REMOTELY PILOTED VEHICLE ... 11

FIGURE 2.2 THE PIONEER RPV FUSELAGE (SIDE VIEW) 11

FIGURE 2.3 THE PIONEER RPV FUSELAGE (BOTTOM VIEW) . 11

FIGURE 2.4 RPV FLIGHT SCENARIO 10

FIGURE 4.1 COMMON MODULE FLIR ZERO AZIMUTH SCAN . 23

FIGURE 4.2 NARCISSUS OF FLIR SCANNER 25

FIGURE 4.3 PUPIL DISTORTION DUE TO VIGNETTING 26

FIGURE 5.1 PROBABILITY OF DETECTING A REAL TARGET . 31

FIGURE 5.2 SENSOR FOOTPRINT 31

FIGURE 5.3 COMPARISON OF MTF FOR FLIR SENSOR 33

FIGURE 6.1 FLIR OPTICAL SCHEMATIC CONFIGURATION ... 37

FIGURE 6.2 IRDOME CONSTRUCTION 41

FIGURE 6.3 ASTRONOMICAL TELESCOPE FOR PARALLEL BEAM SCANNER 41

FIGURE 6.4 A PARALLEL AND CONVERGENT BEAM SCANNER 42

FIGURE 6.5 SCANNING AND STARING FORMAT OF FLIR IMAGE 43

FIGURE 6.6 PUSHBROOM SCANNING USING ROTATIONAL POLYGONAL MIRROR 45

FIGURE 6.7 DIMENSION OF A POLYGONAL MIRROR 46

FIGURE 6.8 MIRROR MOTION WITH ROTATION 46

FIGURE 6.9 GEOMETRY FOR THE DETERMINATION OF RESOLUTION CHANGE IN THE DIRECTION OF PERPENDICULAR TO THE RPV FLIGHT DIRECTION 53

FIGURE 6.10 GEOMETRY FOR THE DETERMINATION OF RESOLUTION CHANGE IN THE DIRECTION PARALLEL TO RPV FLIGHT DIRECTION 53

FIGURE 6.11 HgCdTe DETECTIVITY 58

FIGURE 6.12 $Hg_{1-x}Cd_xTe$ DETECTOR PERFORMANCE 60

FIGURE 6.13 IR DETECTOR CONFIGURATION 62

FIGURE 6.14 TENTATIVE FLIR SENSOR DESIGN 68

TABLE OF SYMBOLS AND ABBREVIATIONS

A	Gravitational Force
A/C	Aircraft
AF	Air Force
All Alt	All Altitude
APC	Armored Personnel Carrier
Ar	Army
Au	Aurum (Gold)
α	Instantaneous Field of View in Down Range
B	Electrical Bandwidth
BIT	Built In Test
BLIP	Background Limited Performance Detector
ß	Instantaneous Field of View in Azimuth
CCD	Charge-coupled Device
γ	Beam Deflection Angle by the Scan
D_o	Diameter of the Entrance Pupil
D	Diameter of the Lens
D^*	Detectivity
d	Lens Distance
D/A	Digital-Analog
δ	Beam Deviation at the Midpoint of the Scan
EO	Electro-Optical

F	Frame Time
f	Focal Length of Lens
f	Field of View change in Azimuth
F/#	Optical Focal Ratio (F number)
FLIR	Forward Looking Infra Red
FOV	Field of View
FPA	Focal Plane Array
FT	False Target Density
Δf	Electrical Bandwidth
GCS	Ground Control Station
Ge	Germanium
h	RPV Altitude
HgCdTe	Mercury Cadmium Telluride
θ	FOV
θ_f	Rotational Drum Facet Angle
θ_R	Angular Rotational Displacement
Id	Identification
IFOV	Instantaneous Field of View
InSb	Indium Antimone
Int	Intelligence
IR	Infrared
J	Radiant Intensity

J.T.	Joule-Thompson Refrigerator
κ	Dwell Time in the Detector
l	Number of Detector
L_{az}	Foot Print in Azimuth
L_{dr}	Foot Print in Down Range
LLLTV	Low Light Level Television
λ	Wavelength
M	Magnification of the Lens System
Min	Mini
MRTD	Minimum Resolvable Temperature Difference
MTF	Modulation Transfer Function
Mul	Multiple Purpose
N	Radiance
n	Number of Rotational Drum Facets
n	Refractive Index
n'	Number of Noise Pulse
NA	Numerical Aperture
NEP	Noise Equivalent Power
NET	Noise Equivalent Temperature
NETD	Noise Equivalent Temperature Difference
p	FOV change in Down Range
PC	Photoconductive

PCDM	Pulse Code Data Modulation
P_d	Probability of Detection
P_{rt}	Probability of Real Target Density
PtSi	Platinum Silicon
PV	Photovoltaic
R	Responsivity
R	Turn Radius of RPV
r_i	Radius of Rotational Mirror on the Inside
r_o	Radius of Rotational Mirror on the Outside
REC	Reconnaissance
RF	Radio Frequency
R_{max}	Maximum Range
R_o	Idealized Range
rpm	Revolution Per Minute
rps	Revolution Per Second
RPV	Remotely Piloted Vehicle
RRS	Remote Receiving Station
SAM	Surface to Air Missile
SAR	Synthetic Aperture Radar
Si	Silicon
SIGINT	Signal Intelligence
SNR	Signal to Noise Ratio

SR	Short Range
SUR	Surveillance
τ	Time Constant of Detector
τ_o	Transmittance of the Optics
τ_a	Transmittance of the Atmosphere
Tac	Tactical
TCU	Tracking Control Unit
TDI	Time Delay and Integration
US	United States
USN	United States Navy
USMC	United States Marine Corps
v	RPV speed
V_1	Dispersive Index of Lens 1
V_2	Dispersive Index of Lens 2
Ω	Search Field in Steradians
$\dot{\Omega}$	Search Rate
X	Scan Motion in azimuth
Y	Scan Motion in Down Range

ACKNOWLEDGMENT

It was a great experience to study electronic warfare at USNPS. I wish to express my cordial appreciation to the Korean Army for providing the valuable opportunity to study. I would like to personally thank Professor Donald L. Walters. Without his help, my effort would never have been successful. I am also very grateful Professor Milne, and Ron J. Pieper of the US Naval Postgraduate School who carefully read and correct this thesis. Their expertise and dedication were critical to the completion of this thesis.

A special thank you goes to my wife, Myung-Ja, Park, whose patience and understanding have been most supportive during my study at the Naval Postgraduate School, and to my little son, Sung-Jo, Choi, whose pure smiles and peaceful face have been another great contribution.

placed a new premium on sensors versatile enough to detect not only airborne targets but the entire broad spectrum of tactically interesting ground targets. FLIR sensors meet these goals [Ref.9 p:c-15].

The purpose of this thesis is to provide an overview of designing an IR system and to consider a tentative FLIR sensor for the Korean Army under the specific Korean environmental conditions.

In particular, this thesis will be focused on a FLIR sensor carried by a RPV for the Korean Army. The elements of an IR system involve radiating targets, an attenuating atmosphere, optics, detectors, and electronics. The system should detect the presence of the target, to track it as it moves, to relay targeting information, and to display the information for interpretation by a human observer. This system design process comprises the several steps necessary to translate the optimum system concept into physically realizable hardware. The first step is to determine the system requirements for the IR search system needed by the Korean Army. Next this thesis makes a tentative system design and a preliminary estimate of its performance. The design process will involve iterations through a preliminary design and back to systems analysis in order to estimate the overall performance. Finally a decision will be made on a final system design.

Chapter II contains background information related to the proper RPV for the Korean Army application and specific Korean environmental conditions, Chapter III covers the RPV infrared sensor and payload considerations, Chapter IV considers the initial system design, Chapter V depicts a system requirement analysis for the FLIR sensor, Chapter VI contains the FLIR optical design, scanning mechanism, detector configuration, and

electronics, and finally Chapter VII states the final conclusions and recommendations to the Korean Army.

II. BACKGROUND

A. RPVS AND RPV PLATFORMS

Israel's Bekaa Valley Operations are a classic example of the use of RPVs to gather signal intelligence (SIGINT). When Israel invaded Lebanon in 1982, the presence of Soviet built Syrian SAM 6 missiles could have caused heavy losses to Israel aircraft. Instead, Scout and Mastiff RPVs were sent ahead to act as decoys and identify missile radar locations and their frequencies. The proper employment of these RPVs provided front commanders timely information on the enemy missile activity. The RPVs became one of the major factors in destroying missile facilities, accelerating the tactical victory against Lebanon [Ref.1 p:17].

Another remarkable example was shown in " Desert Storm Operation" in the Gulf War by the Coalition troops against Iraqi-troops. Three kinds of RPVs were employed by the US Navy and US Marine Corps. The small Pioneer were used for naval gunfire aerial target observation and bomb damage assessment. The Pioneer produced by the AAI Corporation, were equipped with television cameras and forward looking infrared (FLIR) sensors for accurate surveillance and reconnaissance missions in hostile environments. An even smaller and less expensive second RPV system, also used in the Gulf War, was the Pointer, a battery - powered platform equipped with a very small charged coupled detector (CCD) camera for black and white electro - optic imagery. The Pointers built by Aero Vironment Incorporated, were operated by the US Marine Corps. In addition to the Pioneer and Pointer systems, very low-cost, close-range RPVs called Exdrone were used by the US Marine Corps. The Exdrone designed by the Applied Laboratory was a system to

disrupt enemy communications by loitering with an active barrage jamming up to three hours [Ref.1:pp.15 - 16]. RPVs have been used for a only few years, thus historical data is sparse. Table 1.1 shows various RPV statistics including the Pioneer, and Pointer.

TABLE 1.1 VARIOUS RPV CHARACTERISTICS

RPVs	Type of Mission	Wing Span(m)	Length (m)	Power (watt)	Max Pay-load(kg)
R-20	Sur & Tgt Id	3.72	7.71	1088	150
Mart	Rec & Sur	3.40	3.30	1625	30
CL - 289	Sur & Int	1.32	3.52	297	N/A
Pioneer	SR Sur & Int	5.15	4.26	1950	45
Impact	LE Mul RPV	8.00	6.20	3375	68
Mastiff	Rec & Sur	4.25	3.30	1650	37
Scout	Mul Tac Min	4.96	3.68	1650	38
Ranger	Rec & Sur	5.68	4.96	2850	50

Sur : surveillance, Tgt : target, Id : identification, Rec : reconnaissance, Int :intelligence, SR : short range, Mul : multiple, Tac : tactical, Min : mini

TABLE 1.1 (CONTINUED)

RPV	Ceiling & Endurance (m & h)	Max Speed (km/h)	Max Weight (kg)	Contractor (Company)	Service Armed Forces
R - 20	1000 & N/A	792	850	Aerospatiale	France Ar
Mart	1000 & 3.5	220	115	Alpilles SA	France Ar
CL-289	N/A & N/A	N/A	N/A	Canad Air	Germany Ar
Pioneer	4575 & 8	150	190	IAI(Malat)	USMC
Impact	5490 & 10	204	560	IAI(Malat)	USN & MC
Mastiff	4480 & N/A	98	138	IAI(Malat)	Israel Ar
Scout	4575 & N/A	102	159	IAI(Malat)	IsraelA,AF
Ranger	4575 & 5	220	220	Contraves	Swiss Ar

Ar : Army,

USMC : United States Marine Corps,

AF : Air Force

USN : United States Navy

TABLE 1.1 (CONTINUED)

RPVs	Type of Mission	Wing Span(m)	Length (m)	Max Power(watt)	Max Payload(kg)
Sparro Hawk	Sur & Mini	5.68	4.96	1875	N/A
Phoenix	TgtAcq & Sur	4.27	N/A	1875	N/A
Aura	Rec A/C	7.96	5.12	8625	181
Pointer	Man Portable	2.74	1.83	300	N/A
Skyhawk	Mul Mission	6.10	4.12	3450	79.5
Heron 26	Mul Role	6.00	3.63	1950	34
Scarab	Tac Rec	3.34	6.15	1186	113.5

Tgt Acq : target acquisition

A / C : Aircraft

All Alt : All Altitude

Mul : Multiple

TABLE 1.1 (CONTINUED)

RPV	Ceiling Endurance (m/h)	Max Speed (km)	Max Weight (kg)	Contractor	Service Armed Forces
Sparro Hawk	N/A & 1	300	59	Ael Ltd	French Army
Phoenix	N/A & 6	140	160	Gec Avionics	Brit AR
Aura	6100 & 12	309	725	Aero Met Inc	USAR,AF,NA
Pointer	150-300 & 1	55 - 74	3.4	Bell Helicopter Tetron	US NAVY
Sky Eye	5490 & 10	232	354	Development Science R4E	Royal Thai AF, Egypt
Heron-26	3510 & 5	139	225	Pacific Aero System	Italian Army
Scarab	13720 & N/A	853	1069	Teledyne Aeronatical	Egyptian AF

As shown in the RPV statistics, there are many RPVs available for military applications. Most of the RPVs are in active military service, but some of them are in development funded by each government. The Korean army is considering development of an all-weather close range surveillance and intelligence RPV. The Pioneer could satisfy the Korean Army need since it has proved its operability in Desert Storm Operation and several military services involving the US Marine Corps, US Navy, and Israel Army are using this type of RPV. In addition, this RPV is well suited for the close range surveillance capability , long endurance performance, and proper altitude needed by the Korean army.

In this survey, the Pioneer was used as a RPV model for adopting an FLIR sensor for the Korean army. The Pioneer is a close and short-range surveillance and intelligence gathering RPV. Pioneer incorporates considerable accumulated battlefield and technical experience of the Israel Aerial Industry (IAI) Scout and Mastiff RPV. It was ordered initially by the US Navy in Jan 1986 after a 1985 fly-off against the Pacific Aero System Heron 26. The Pioneer aircraft has a pod and twin tail boom configuration, with fixed tricycle landing gear and an arrest hook. A $0.1m^3$ bay in the center of the fuselage accomodates payloads with up to 500w of electrical power available for their operation. Catapult launch and net retrieval are standard for shipboard operation but the RPV can take-off and land conventionally on a suitable flat area, where the arrester hook engages a cable stretched between two energy absorbers. Rocket assisted zero-length launch is another option. Wings, booms and tail unit are detachable, to simplify dismantling and assembly in the field and facilitate prompt dispatch of several vehicles at one time.

Currently available sensors are gyro-stabilized high resolution TV camera, and a FLIR sensor for day and night or reduced visibility operations. The payload includes a radio relay communication package for VHF and UHF frequencies, and a radio frequency range extension pod. The air vehicle also includes an auto pilot, navigation, communication equipment and a two-way data link, allowing it to operate in either pre-programmed or manual control mode. Table 2.1 summaries specifications of Pioneer RPV [Ref.3 p:3-3].

The Pioneer system consists of several parts including a RPV, a ground control station (GCS) (see Fig.2.1, 2.2, 2.3), a tracking control unit (TCU), a portable control station (PCS), and a remote receiving station (RRS). TABLE 2.1 shows the general characteristics of the Pioneer RPV [Ref.3:pp.3-6]. The major RPV groups include an airframe system, propulsion system, electrical system, flight control system, mission payload, and communication system [Ref.3:pp 3-3 - 3-14].

Fig 2.4 shows a typical RPV flight scenario [Ref.28 p:28].

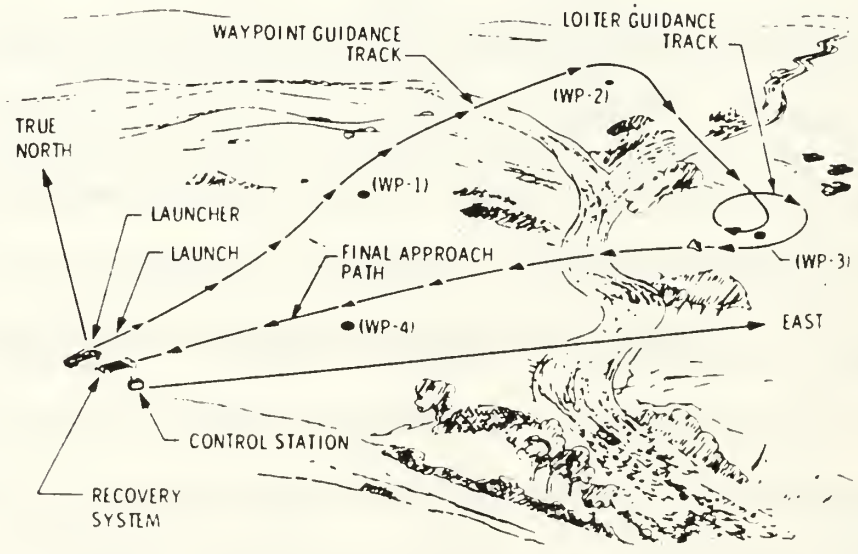

Fig 2.4 RPV Flight Scenario

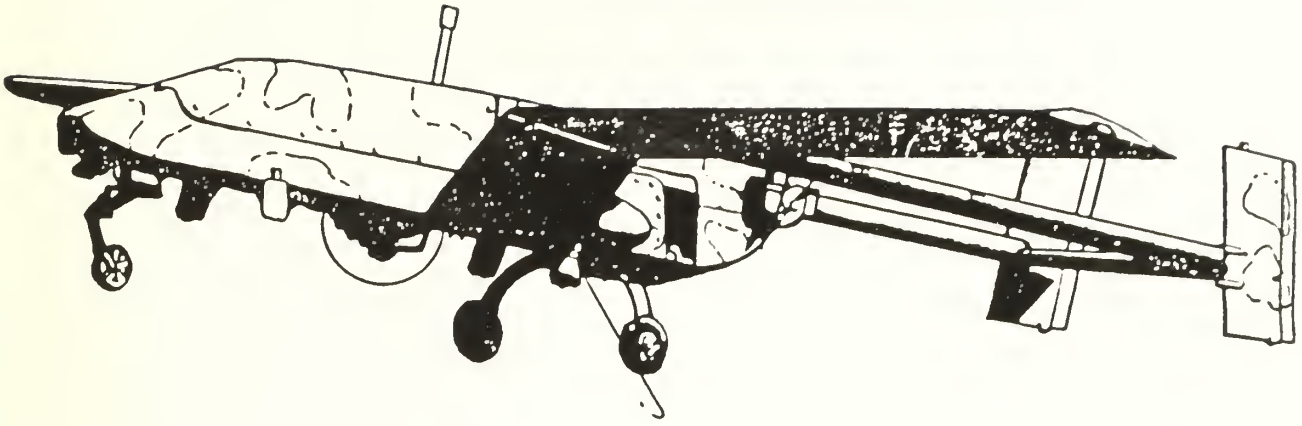

Fig 2.1 Remotely Piloted Vehicle

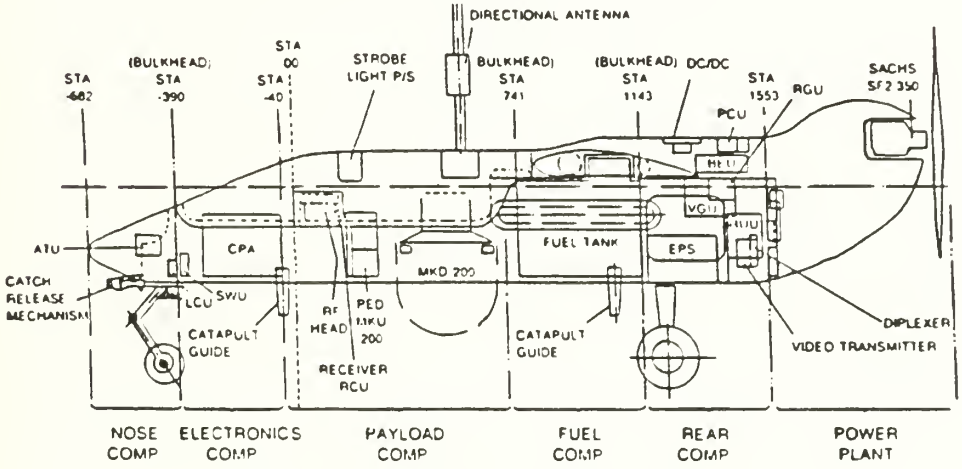

Fig 2.2 RPV Fuselage (Side View)

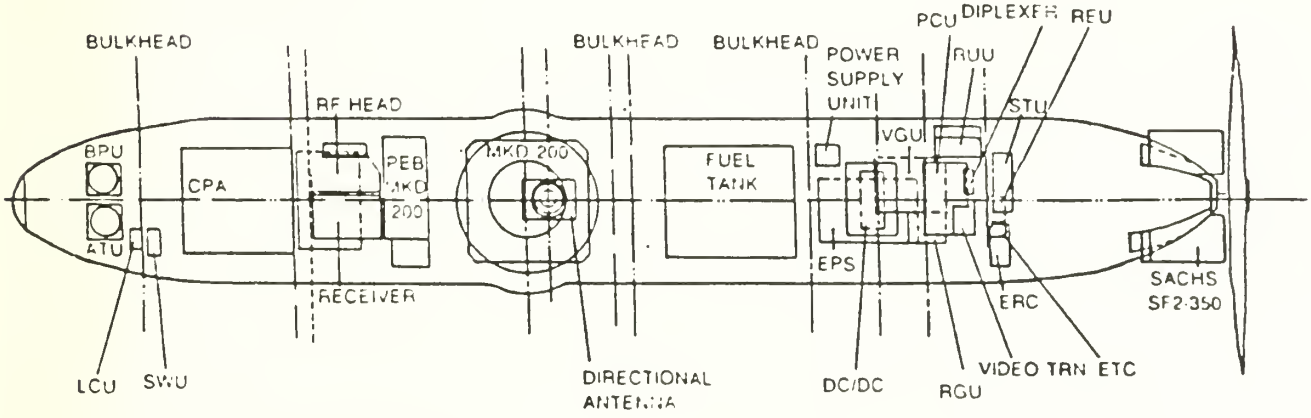

Fig 2.3 RPV Fuselage (Bottom View)

TABLE 2.1 GENERAL CHARACTERISTICS OF RPV

EXTERNAL DIMENSIONS:	
Wing Span	16.9 feet
Length, overall	14.0 feet
Height, overall	3.3 feet
WEIGHTS:	
RPV	267 pounds
Maximum payload	75 pounds
Full fuel tank	60 pounds
Maximum takeoff weight	429 pounds
PERFORMANCE:	
Dash speed	100 knots
Optimal cruise velocity	60 knots
Maximum dive velocity	106 knots
Stall speed	50 knots
Takeoff velocity	55 knots
Landing velocity	55-65 knots
Maximum altitude	15,000 feet
Maximum takeoff/landing altitude	3,500 feet
Flight endurance	5 hours minimum at 5,000 feet
Flight radius of action	109 nautical miles
Engine	26 horsepower
Fuel	RPV fuel (94-100 octane)
Oil type	2 cycle-BIA certified, type TCA
Fuel/Oil mixture ratio	50:1
LAUNCH AND RECOVERY:	
Rolling takeoff	210 meters
Pneumatic launch	21 meters
Rocket-assisted takeoff	0 dista
Arrested recovery	
Normal operations	130 meters
Special circumstances	70 meters
Rolling recovery	366 meters
ENVIRONMENTAL RESTRICTIONS:	
Temperature range	25°F to 125°F (-4°C to 51°C)
Rain	Up to 6mm/hr (less than ¼in.) over flight path distance of 40km
Icing conditions	Cannot operate
Wind	Up to 20km, with gusts up to 35km
Crosswind limitations on takeoff	16 knots steady, 24 knots gusting

There are several advantages and disadvantages of the Pioneer RPV system.

Pioneer RPV System Advantages include :

(1) A real-time datalink capability that provides for the acquisition, storage, interpretation, and discrimination of combat information using two means of data storage: digital cassette recorder, and video cassette recorder,

(2) A low probability of detection because the signature of the RPV (IR, radar, acoustic, visual..) is small,

(3) Rapid and accurate targeting for adjustment of supporting arms,

(4) A day (TV camera) and night (FLIR) system capability,

(5) A pre-programmed mode of operation that reduces radio frequency (RF) emissions,

(6) Reduced exposure of manned aircraft to lethal weapon systems such as missiles,

(7) No requirement to collocate ground control station and launch/recovery equipment.

Pioneer RPV Disadvantages :

(1) Environmental limitations such as icing and meteorological conditions, unit limitations,

(2) A line-of-sight transmission limitation between the tracking control unit and RPV, and also between RPV and remote receiving station,

(3) While more than one air vehicle may be airborne at any given time, the ground unit can process only one sensor package from a RPV at a time, and

(4) Transportation and handling requirements that include nonmil-spec equipment.

B. SPECIFIC ENVIRONMENTAL CONDITIONS

In the IR portion of the spectrum (see APDX A.1), water vapor and carbon dioxide absorption pose a far more serious problem than do scattering process. Fogs and clouds are strong scatterers (see APDX A.5) and are, in effect, opaque to IR radiation. IR system are not all-weather capable. On the other hand, transmission through the rain is surprisingly good and should not be overlooked in tradeoff studies of IR sensors. Other factors affecting the IR system include properties of terrestrial materials of the operation area and atmospheric turbulence. Terrestrial properties involve soil, rocks, road construction material, painted surfaces, marine background, snow, botanical material, and terrain emissivity and reflectivity. The terrestrial characteristics have effects on the reflectance, emissivity, index of refraction, at different wavelengths (see APDX A.8-10).

The effects of scattering by molecules, hazes, overcast, blowing dust, and fogs in the atmosphere are of major concerns in the visible portion of the spectrum, where they can be observed by the effect they have on visibility. But with the exception of scattering by fogs, they are of minor importance in the infrared. Infrared radiation penetrates the atmosphere better than visible light. Transmission of fogs in the infrared portion of spectrum is extremely poor for any reasonable path lengths due to the high scattering coefficient relativity. The deployment times of FLIR sensor should be evaluated by the military commander during the fog season.

C. THE KOREAN ENVIRONMENTAL CONDITION

Korea is one of the most mountainous regions in the world. Hills and scenic mountains extend down the length of the East Coast and cover approximately 70 percent

of the land. The solid granite and limestone base of the land is lifted and folded into some of the most magnificent mountains in the world. This is particularly true of the East Coast, where the mountains plunge precipitously into the sea. However the southern and western slopes descend gradually down to the coastal plains, which produce the bulk of Korea's rice crop and other agricultural products. In particular, the middle part of the Korean peninsula consists of two specific zones. Soft soils and road construction at elevation between 100 to 500 meters cover the broad open fields of the western area. On the other hand, rough and high mountainous range of the mid eastern area contain rocks and small water courses at elevations between 500 to 1500 meters. No marine topography exists except several small rivers in these operation areas.

Korea is within the temperature zone and has four distinct seasons. Spring begins in late March or early April as tree burst into leaf. Rainfall comes in the form of occasional drizzle from March to May. The spring mean temperature runs between 10 to 20°C. Summer in Korea is relatively hot and rainy, and the vegetation is very lush. In June the temperature rises up above 20°C, and then at the end of the month the monsoon rains usually begin. Rainfall is heavy in July. Autumn is rather short and lasts from the end of September into November. The air blows from the Asian continent bringing clear, dry weather, together with the golden and red leaves of autumn foliage. The temperature in this season varies between 0 to 10°C. Lastly, the winter weather is cold and dry from December to February, though spells of cold weather normally alternate with days and warm weather. In this season, snow falls and the temperature runs below zero and water freezes.

On the basis of the specific Korean terrestrial and atmospheric environmental

conditions mentioned above, IR system design is simplified. The absence of desert, tropical conditions reduces the environmental constraints. However, the environment must be considered to improve the effectiveness of the operation.

D. ESTIMATED DESIGN FACTORS

The suggested sensor system should include a passive IR sensor using the long wavelength IR (LWIR) atmospheric window (8μm to 12 μm). The system must attach to the Pioneer RPV platform as a short-range (within 10 km) surveillance IR sensor. The system should view a target at multiple, simultaneous, sensor wavelengths providing multiple discriminants and enhanced detection probability, and can have operational effectiveness in an ever-expanding countermeasure environment. All-weather operation and aimpoint selection must be possible, and the system must reject environmental clutter like clouds, fog, aerosols, and background, while maintains high target classification (see APDX B.5) ability. The total system must consider the following factors [Ref.6 p:1-11] :

(1) Range (distance),

(2) Resolution, rejecting of clutter, aiming accuracy or miss distance, countermeasures, rejection,

(3) Grazing angle (lookdown angle),

(4) Resolvable temperature difference(°K),

(5) Signal processing; algorithm and feature extraction, speed and complexity, countermeasures (robust), realtime processing (datalink),

(6) Physical size (weight, high, width),

(7) Cost-complexity-reliability, and

(8) Power requirement.

III.INFRARED SENSOR CONSIDERATIONS

A. THE INFRARED SENSOR CHOICE

The selection of a FLIR sensor is based upon the intended application or imagery. FLIR sensors have the following general criterion :

(1) Realtime imagery,

(2) Image mensuration and analysis is not required,

(3) Narrow FOV (40° x 30°) that provide details of small selected area (500m x 500m) is desired,

(4) Operator has full control over pointing of the sensor, and

(5) Sensor operation will not impose velocity/height restrictions on flight vehicles.

Existing and future infrared system should incorporate several capacities that would enhance the usefulness of the imagery. Two of these are : (1) determining thermal-dynamic temperature of features or objects in the imagery, (2) generation of temperature contour maps of a given objects by digital processing of the infrared imagery [Ref.13 pp:98-100].

B. PAYLOAD CONSIDERATIONS

1. Mission

Selecting payload components of a modern day RPV involves many factors. The limited air vehicle payload capacity constrains the real or near real time data acquisition capability. The RPV payload consists of a sensor, recorder/playback, and datalink components. The RPV must navigate and carry out complex missions autonomously. The autonomous nature of the RPV affects the sensor, recorder, and datalink systems greatly. The RPV must rely on accurate navigation, wide FOV, longer time

duration recording devices and higher power, steerable data link payloads. The autonomous or hands-off nature of the RPV also dictates a reconnaissance management system to coordinate the payload systems.

Present day mission categories have been set up to define range and expected target time or loiter time. Vehicles designed to meet those requirements also take on configurations according to four mission categories.

(1) A close range mission is 30 km maximum range with one to 8 hours loiter time. This vehicle flies the mission area and transmits data real time to the remote pilot location. The close range RPV is typically a small propeller driven vehicle with a small payload capacity (up to 50 Kg).

(2) A short range mission covers 150 km maximum with five to twelve hour loiter time. This vehicle enters a mission area and collects data upon command. The data is transmitted real time to the operator or remote location. The RPV remains in the mission area and is used as required. The longer loiter time dictates a small to medium size propeller driven vehicle. The payload capacity is greater than a close range operation (50-100 Kg).

(3) A medium range mission extends to 700 km no with loiter time. This vehicle navigates to distant targets, gathers intelligence and returns to a pre-arranged position, storing its data in a recorder-playback mode. The medium range RPV is a large airframe, jet engine driven, with a larger payload than the short range RPV (100 -150 Kg). The autonomous nature of this vehicle with no loiter time requires greater payload capacity to accommodate a large navigation, and system management package.

(4) A long endurance mission extends to greater than 300 km, which can reach extremely long range with its 36 hour loiter time. The endurance mission RPV remains in the target area and collects data over long periods of time. The sensors vary in spectrum and can be alerted to collect data as required by remote pilot or by sensors. This RPV is a much larger vehicle approaching manned aircraft size. The long range and high loiter time dictates a high altitude capability. The vehicle in this category is a long winged propeller driven large capacity airframe [Ref.13 pp:45-47].

Payload depends on RPV missions which will fly operation area with some mount of loiter time.

2. EO Sensor Bandwidth and Resolution

The need for real or near real time intelligence has changed the RPV payload configuration. The solution to time constrained intelligence gathering is the EO sensor. These sensors offer flexibility of format, real or near real time processing and display, electronic reliability, video display for interpretation, electronic recording, multiple target perspective data, and a vast reduction in the decision process time.

The detector dimensions determine the sensor's resolution and sensitivity. Scanned sensors usually contain one to twelve detectors arranged to collect ground information in a sequentially line scanned format. Pushbroom sensors rely on RPV motion to provide the sequential line direction while its clock rate determines the actual data rate. Scanning and pushbroom sensors collect target data in a line scanned below the vehicle. Synchronization must match the RPV forward velocity and the area scanned below the vehicle. Over-scanned or high pushbroom line rates images the same target detail repeatedly. This results

in a stretched out target on a video monitor. Underscanning or too slow a line rate results in compressed targets with gaps in the information. Area arrays do not require scanning or line rate detector operation. The area array images the target as a complete picture rather than a picture constructed line by line and is electronically scanned at the array.

Resolution of a system or the smallest target detail discernable is a result of the sensor lens focal length and detector size. The smallest single element of the detector determines the detector resolution. This element is called a pixel. The pixel can be looked upon as a single photo cell. Many pixels of differing density comprise a picture. The number of pixels covering the target controls target detail. According to empirical data, at least two pixels are required to detect a target which covers the target's minimum dimension. Target detail required for intelligence data is therefore dependent upon a large number of pixels covering all the target.

A large number of pixels requires a high bandwidth. Bandwidth is the result of the number of pixel lines, scan rate, and digital bits representing light magnitude for each pixel. Scanning and line scan sensors contain 4,000 to 10,000 pixels or more per line. Line rates vary from 100 to 2,000 lines per second. The systems usually have 8 bits per pixel. Multiplying pixel time rates times bits per pixels can result in 160 million bits per second. The digital rate for scanning systems are beyond the bandwidth of most airborne recorders. Increasing a recorder speed does improve its bandwidth to some degree but reduces its overall recording time. Typical digital airborne recorders will record at 240 Mega bits per second. Digital compression techniques using 3-8 bit PCDM (Pulse Code Data Modulation) will also reduce bandwidth prior to recording [Ref.13 pp:46-50].

3. Optical Considerations

a. Requirement for Scanning.

A conventional mechanically-scanning FLIR is considered by some to be an inelegant, inefficient, and unacceptably costly technique for thermal imaging. Raster, framing, detector cryogenic cooling, electronic signal processing, and moving optics are often-cited defects of conventional FLIR's which stimulate continuing interest in mechanically and electronically simpler device. Although many devices with more desirable features have been conceived, none has yet achieved the thermal sensitivity, the resolution, and the response time necessary to displace scanners. The problem is not that fundamental physical limitations exists. It is rather that the poor radiation contrast in the infrared make severe uniformity demands and necessitate that a linear energy conversion be followed by a background subtraction. Thus all non-scanning imagers which work well in the visible will not function in the infrared without compensating for non-uniformity with a complicated electronic or eletro-optical background subtraction scheme. This is why this author recommends the scanning design [Ref.25p:353]. The function of a FLIR scanner is to move the image formed by the optical system in the plane of the detector array in such a way that the detectors dissect the image sequentially and completely [Ref.25 p:283]. When designing the common module FLIR, the effect of the scanning mechanism must be taken into account. Fig 4.1 shows the common module FLIR IR image [Ref.16 p:303].

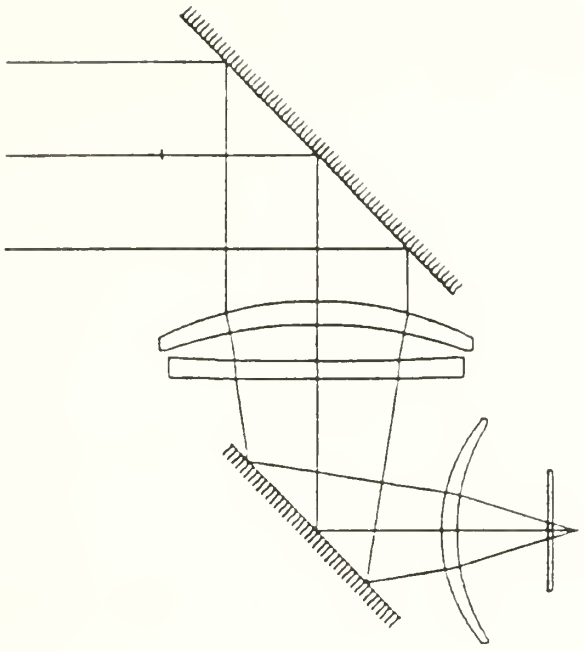

Fig 4.1(a) Common Module FLIR Zero Azimuth Scan

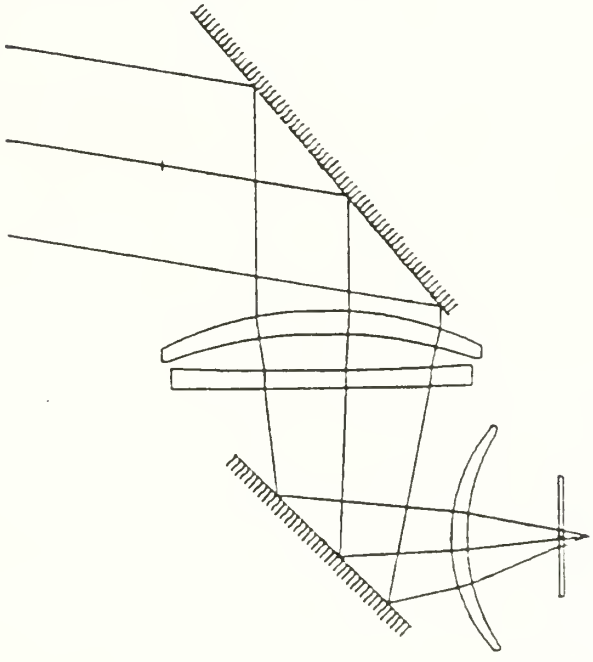

Fig 4.1(b) Common Module FLIR Full Azimuth Scan

Fig 4.1(a) shows the scanning mirror in the zero scan position (on axis). Fig 4.1(b) shows the scanning mirror tilted 5°, the edge of the scan. The FOV is then 10°off axis.

The off-axis aberrations are a function of azimuth scan position. In a common module FLIR, this effect is somewhat exacerbated by the non-coincidence of the entrance pupil and the scan mirror, which causes beam migration over the imager lenses [Ref.16.p:304].

b. Narcissus

The non-coincidence of the IR imager entrance pupil and the azimuth scan mirror tends to make the FLIR sensitive to Narcissus. Fig 4.2 shows two cases when Narcissus can occur. Fig 4.2(a) shows an afocal telescope attached to a FLIR scanner with the plano-side of the second lens facing the scanner. At the center of the scan, the detector retro-reflects onto itself and sees a warmer background, hence there will be a Narcissus spot in the center of the display. Fig 4.2(b) shows the same telescope but with a field lens at the afocal telescope focus. Retro-reflections from the field lens will be in focus at the detector, also causing a Narcissus spot. A second potential source of Narcissus includes on axis marginal ray of near zero heights at any surface.

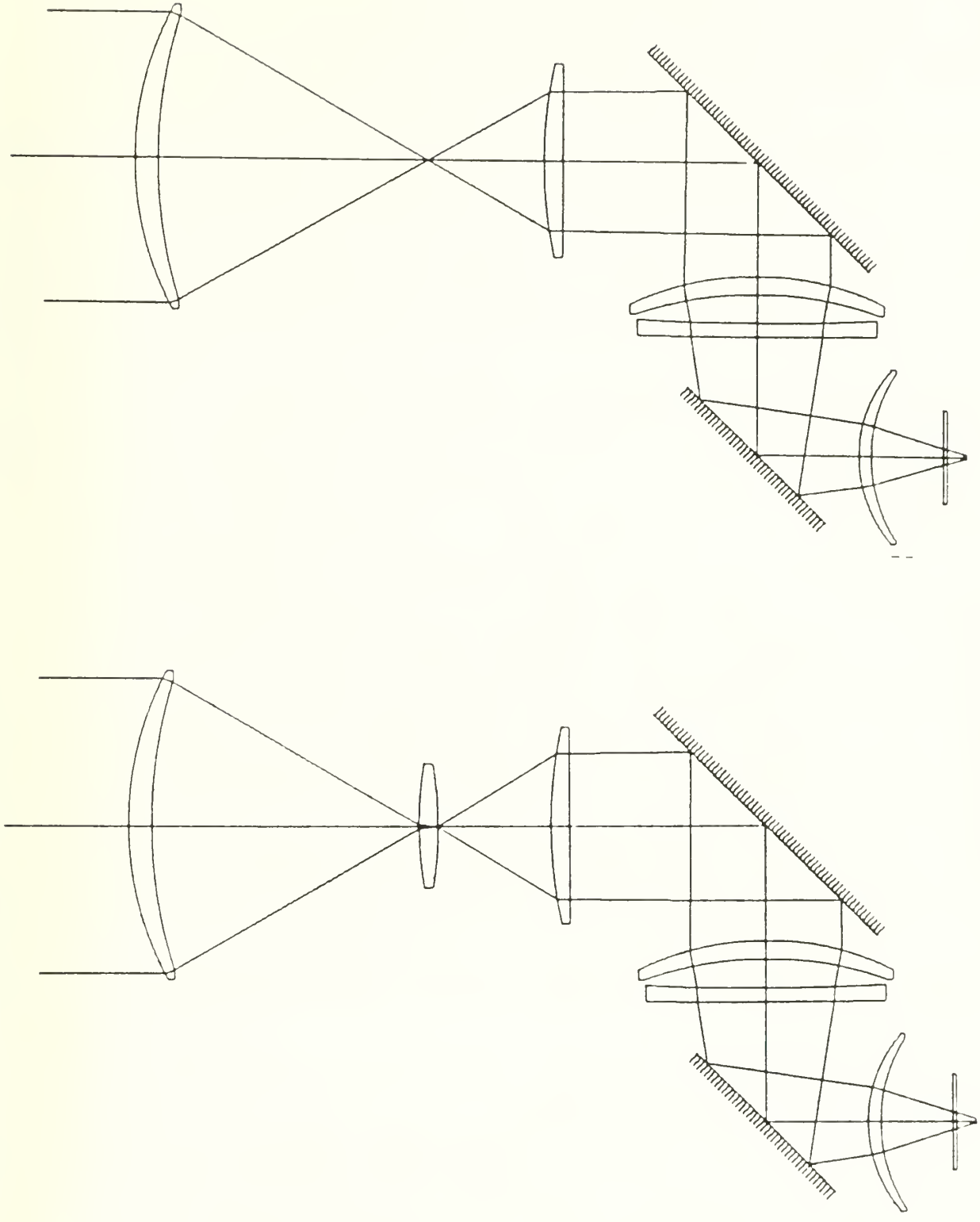

Fig 4.2 Narcissus of FLIR scanner

c. Vignetting Consideration

Since a FLIR operates on low contrast, typically in the one to two percent range, vignetting can be a significant problem. Vignetting which varies with field position may at worst be interpreted as a spurious signal, and at best will give a shading across the picture which can be very distracting. If the aperture stop is at the front surface, then control of vignetting is straightforward. However, if the aperture stop is at an internal surface, then knowledge of what happens during ray tracing is essential to prevent problems. The problem arises mainly as a result of pupil distortion. Fig 4.3 shows the problem [Ref.16 p:307].

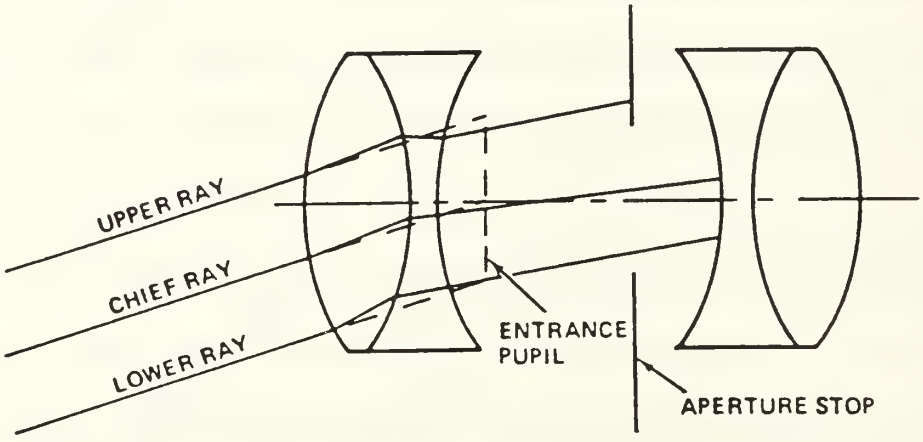

Fig 4.3 Pupil Distortion Due To Vignetting

Due to pupil distortion (see APDX B.4), the aperture stop constrains a ray traced from an off axis field point to the upper and lower parts of the entrance pupil diameter producing vignetting.

d. Atmosphere Windows

Both the 3-5μm and 8 to 14 μm windows must be considered to achieve the proper IR system, cost, size, and performance tradeoffs. TABLE 3.1 shows the comparison of these two windows.

TABLE 3.1 COMPARISON OF 3 TO 5 μM AND 8 to 14 μM WINDOW [Ref.19].

Parameter	3 to 5	8 to 12
Targets	Colored Body Targets	Natural Targets
	300°f - 100°f	-20°f - 120°
	More Signal in 3 to 5 Band	More Signal in 8 to 12 Band
Atmosphere	3-5 has poor penetration in Dust and Smoke	8-12 has better penetration in dust and smoke
	Good H_2O Penetration	H_2O severe attenuation
	3-5 has sun glint problem	No sun glint problem
Optics	3-5 smaller optics less expensive, less weight	8-12 requires larger optics, and more weight (coating)
	No scanners/staring arrays	Scanning optics
	Radome materials	Radome materials
Detectors	Lower Detectivity, lower cost	Highest Detectivity, highest cost
	Larger arrays 512 x 512, staring	Limited size arrays, scanning mode
	Cooled and uncooled	Cooled and uncooled

IV. INITIAL DESIGN CONSIDERATIONS

The Korean Army has a problem gathering military intelligence on the enemy activity in the night due to the lack of a night sensor. A detailed analysis of this problem suggests that a FLIR system could supplement the day and night ground surveillance using the Pioneer RPV over the enemy area. It would be most useful at night by detecting heating target such as tanks, hot trucks, and personnel targets. While the RPV cruises at a preplanned altitude, the FLIR sensor can provide realtime information to the military commanders. The FLIR system should be highly reliable, easily maintainable, and highly interchangeable. It also should require a minimum of special support equipment and no specially trained personnel for its operation. It should be possible to perform a single built-in-test (BIT) of the systems on the ground or in the air. All weather operation should be possible. Installation procedures should require an absolute minimum of structural change to the RPV in order to accommodate different sensor system. The signal processor and power supplies should be interchangeable with other payloads aboard the RPV without the need to relocate previously installed equipment. One of the major functions of the system is to detect the presence of the enemy activity in the operation areas. Consequently, it is essential that it have a wide search field and aimpoint capability.

The FLIR sensor uses parallel scanning with a linear array of detectors raster-scanned across the scene. The background limited performance (BLIP) detectors must operate at lower temperatures (70°K) to cover 8 to 14 μm window and have high detectivity for the FLIR application.

A stabilized gimbaled telescope platform can view any forward direction area with

a hemispherical irdome. The FLIR can sweep 360° in azimuth and from +5° to -90° in elevation. The FOV for the wide aperture is 34° x 40°, 3.4° x 4.8° for the narrow angle, 1.7° x 2.3° for beam expander having a 4:3 aspect ratio FOV and 30 frames per second, 60 fields per second scan format. The angular resolution requires a IFOV of 1 mrad x 1 mrad. A gimbaled telescope assembly can slew as fast as 250° per second. In the interest of long operation (max 8 hours) life, it was decided that the scan rate for the initial design should not exceed 100° per second. There is, of course, some dead time at the end of each scan line, while the scan motion reverses. It should detect and identify an armored fighting vehicle at a range 10 km. Table 5.1 shows the sensor performance goals [Ref.28 p:28].

TABLE 4.1 SENSOR PERFORMANCE GOALS

Performance	Detection Range	Recognition Range
High Performance	15 km	8 km
Austere	6 km	4 km
Designation Range	8 km	

FLIR sensor will have high performance for day and night and limited performance under adverse weather. It must transfer realtime image data from the RPV to the ground stations. Image data for the FLIR should be compressed using the 8 bit pulse code data modulation (PCDM) technique, encrypted and then channelled into the data link. At ground station, an expansion assembly simultaneously decodes, demultiplexes and expands the data without affecting the image resolution. The FLIR sensor should be mounted in a $0.1m^3$ bay in the center of fuselage of the Pioneer RPV.

V. SYSTEM REQUIREMENT ANALYSIS

A. PROBLEM DEFINITION

1. Mission and Functional Requirements

The Pioneer RPV equipped with a FLIR sensor will be launched by a pneumatic launcher from the ground for the purpose of detecting, recognizing, identifying, and locating ground targets at night. It will be used to conduct real time reconnaissance, close range surveillance, and intelligence collection. The RPV shall cruise over the operation area at a speed of over 30 m/sec, having a 8 hour maximum endurance at 1.5 km. It shall be capable of identifying an armored fighting vehicles (such as tanks, APC, trucks, etc,.) at a range of 10 km and of detecting such as vehicle at 15 km.

The RPV shall be capable of all-weather operation (during snow, fog, rain, clear) and day and night operation with a 0.95 probability of detection and 0.05 of false alarm against ground area such as forest, desert, grassland, rice flat including group troops, vehicles, tanks.

The RPV shall have a 360° sweep angle in azimuth, and +5° to -90° in elevation. The RPV shall utilize a FLIR sensor for target detection, tracks, aimpoint selection operated by remote control. The operation temperature lies between -50°C to 125°C.

2. Measure of Performance for FLIR Sensor

Probability of FLIR sensor detecting a real target P_{rt} [Ref.6 p:8-7] is

$$P_{rt} = \frac{RT\ P_d}{RT\ P_d + FT}\ [1 - e^{-(RT\ P_d + FT)\ A}]$$

where RT is real target density, FT is false target density, A is area searched by RPV, and

P_d is the probability of acquisition of the target. Fig 5.1 shows the probability of detecting a real target for the given data (see APDX E.9).

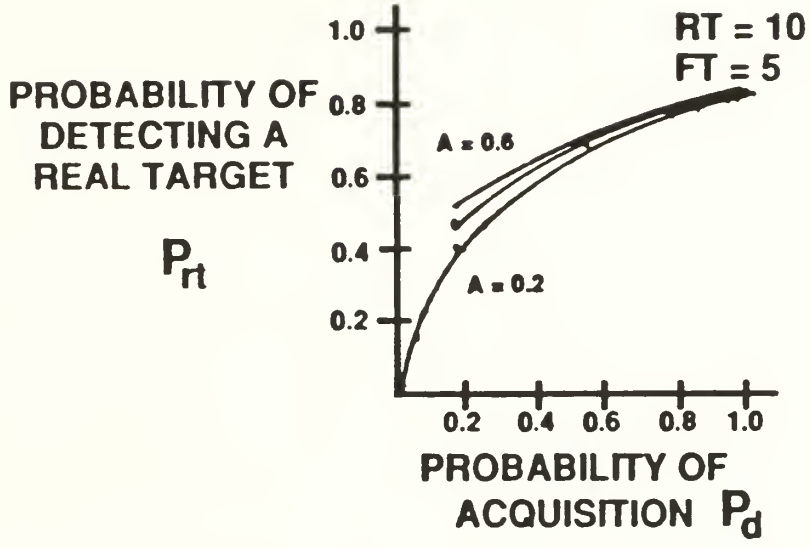

Fig 5.1 Probability Of Detecting A Real Target [Ref.6]

Sensor footprint and slant range (see APDX F.3) for detection are the key factors for measuring the performance for a FLIR sensor. Fig 5.2 shows the FLIR sensor foot print and slant range.

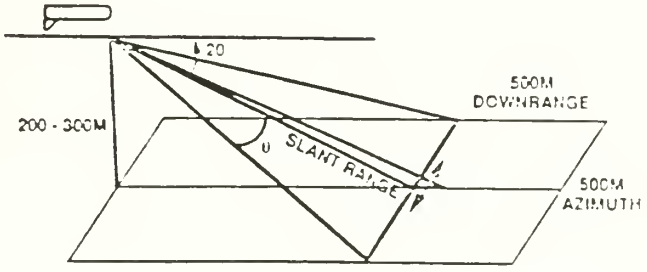

Fig 5.2 Sensor Footprint [Ref.6]

Slant range for sensor detection is a function of turn radius, the speed of the RPV, and gravitational force. Assume that the RPV is flying at a speed of 60 knots (30.86 m/sec), and

RPV has 2 G. The gravitational force A is $A = V^2/R$, therefore turn radius $R = V^2/A = 30.86^2/2(9.8) = 48$ m. Therefore a FLIR sensor needs a slant range greater than or equal to 48m, plus processing delay.

The sensor resolution shall be expressed in terms of FOV, IFOV, and aimpoint selection criterion (see APDX B.2). Assume 1 m target size with 20 pixels on the target at detection , then IFOV $= \tan^{-1}[\ 1/20(48)] \approx 0.0585°$ (1 mrad), and we need (1° x 17.45 mrad/deg)/(1 mard/pixel) ≈ 18 pixels across field of view for a sensor 1° FOV. Thus about 698 pixels per line are needed to achieve the 40° FOV in azimuth. The slant range depends of the speed of the RPV, and sensor resolution is a function of altitude and slant range of RPV.

Fig 5.3 shows a comparison of MTF for FLIR sensor [Ref.6 p:II-49b].

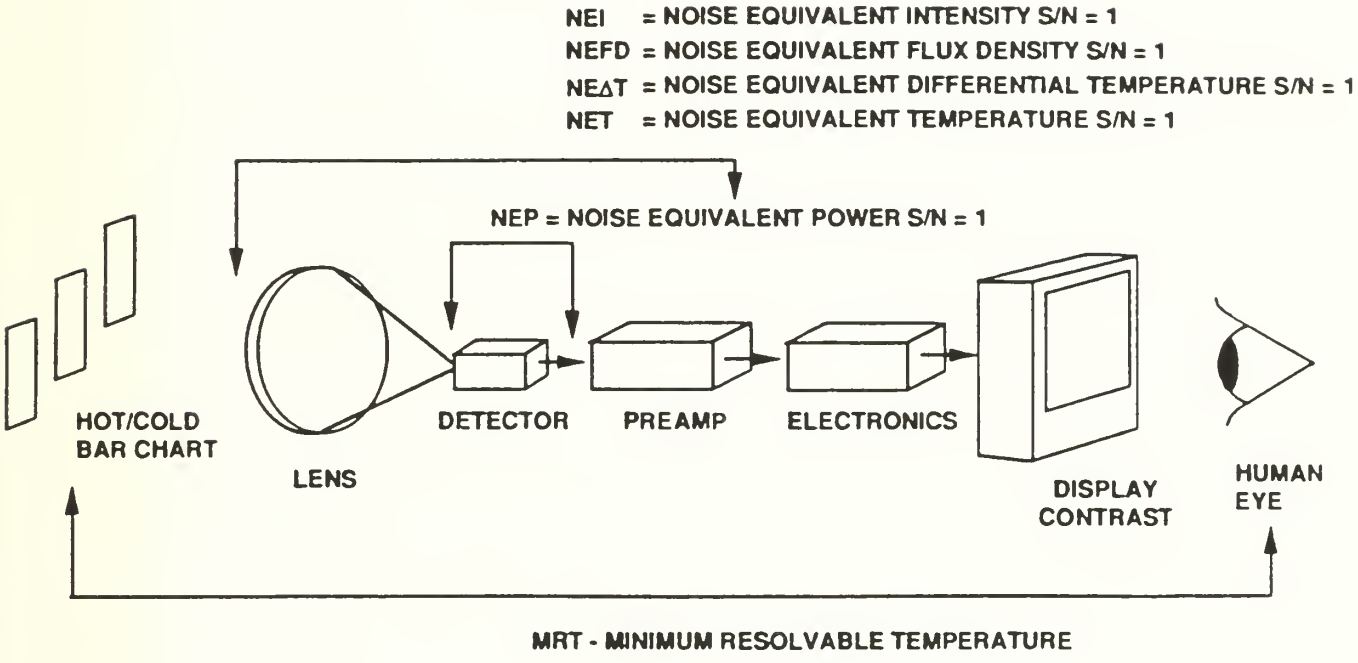

Fig 5.3 Comparison of MTF for FLIR Sensor [Fef.6]

B. SUMMARY OF REQUIREMENTS

We must design the FLIR sensor system on the basis of the requirements of the whole FLIR sensor and each components. Table 5.1 shows the FLIR sensor requirements.

TABLE 5.1 FLIR SENSOR REQUIREMENTS

Functions	Requirements
Operational/ Mission	A close range realtime surveillance Pioneer RPV airframe
Target Element	Tanks, self-propelled gunnery, SAM site, trucks cold targets, hot targets, troops, topography,
Target Complexes	Assembly area, rear area
Weather	all terrain, all weather rain, smoke, fog, dust, mountain, ocean, river -50° to 125°C,
FLIR sensor	P_d: 0.95 at minimum target range (15 km), mode : passive IR, functions : detect, track, aimpoint, locate, countermeasure resistance, weight : 45 kg, size : 45.72 cm (18") long x 30.48 cm (12") in diameter, power : 1950 watt, stabilization : telescope gimbal platform, FOV : 40° in azimuth x 30° in down range, aperture: 1.8 cm, maximum range : at least 15 km, frame / field rate : 30 / 60, sweep angle : -5° to 90 ° in elevation and 360° in azimuth, pixel resolution (IFOV) : 1mrad x 1mrad per pixel, slant range : 500 m at the altitude of 200 m, scanning mode : pushbroom (parallel scan using rotational polygonal exterior mirror), and scan lines per frame: 525.

1. Optics

aperture :
wavelength operation :
focal length :
distortions :
fields stop :
MTF :
antireflection coating :
number of elements :
optic materials :
reflective / refractive :
transmission :
cost :

2. Optical filters

passive band :
filter type :
transmission (inland / outband)
cost :

3. Detectors / cooling system

number of elements :
shape of detector :
detector material :
detectivity :
cooling / non cooling :
operating temperature :
bias voltage :

4. Preamplifier

dynamic range :
impedance matching :
number of channel :
electronic passband :
data compression :

5. Algorithm

IR hot spot size :
combo logic :
functions :

6. Signal Processor

input data rate :
output data rate :
I/O interface :
memory size :
thorough put :
functions :
lines of code :
testability modes :
cost :

VI. SYSTEM DESIGN

A. OPTICAL DESIGN

1. Optical Configuration of FLIR

The FLIR sensor module design process had several different categories. Each category was analyzed separately to determine the appropriate size of the individual components. These categories involve IR imaging optics with scanner, detector/detector array, appropriate electronics and output device (see APDX E.4). Only the optics and detector part were covered in this thesis. Fig 6.1 illustrates the basic optical configuration of the TV-compatible FLIR sensor [Ref.16 p:125].

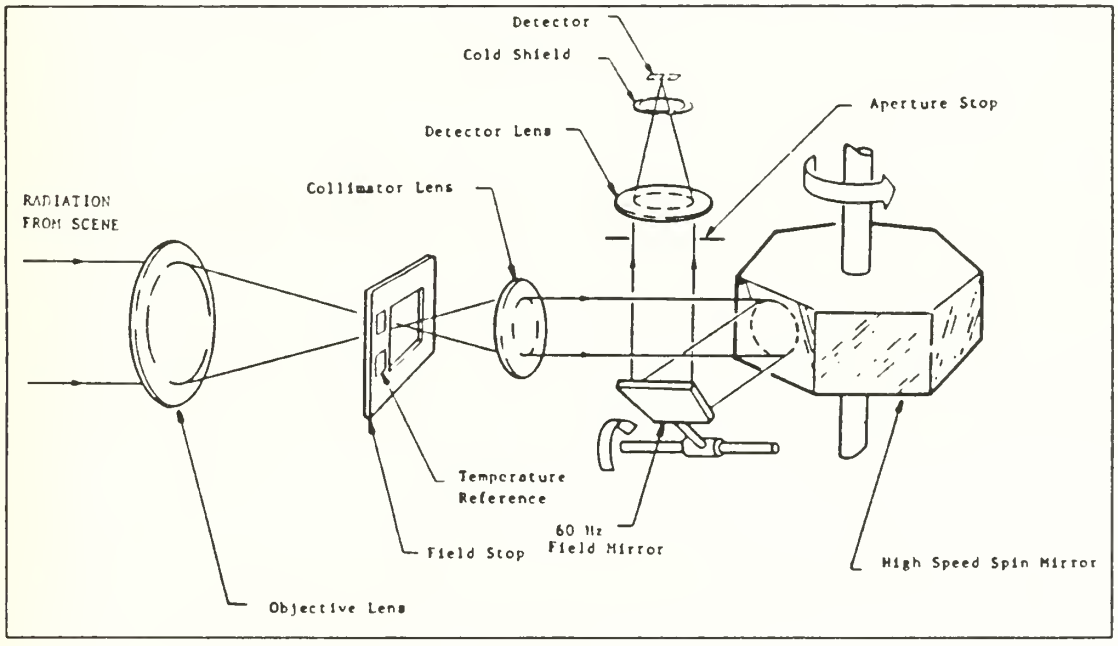

Fig 6.1 FLIR Optical Schematic Configuration [Ref.16 p:125]

2. Optimum configuration

The selection of the optimum optical system is most critical, especially in the infrared due to the limited number of available refractive materials, environmental sensivities, and other factors. The FLIR system will be basically refractive (see APDX B.3). The refractive system advantages include : (1) a full clear aperture with no central obstruction, (2) spherical surfaces. But this system has several disadvantages such as : (1) limited number of materials, (2) cost, (3) difficult materials to fabricate, (4) expensive coatings, (5) thermally sensitive, (6) difficult in testing [Ref.15 p: 55] .

Refractive system configurations in the infrared are often simpler than their visible counterpart due to the inherently higher refractive index of the materials and inherently low dispersion of many IR materials.

3. Irdome and Stabilizing Platform design

A hemisphere irdome will accommodate wide azimuthal scanning angles wider. Since it mounts on the end of a cylindrical package that has a diameter 30 cm, the diameter of the irdome is 30 cm and the radius of its outer surface is 15 cm. Because it is not mounted inside the RPV, the irdome must withstand the effects of aerodynamic forces, abrasion by dust, dirt rain and insects during takeoff and cruising and landing.

Of the possible optical materials (see APDX B.6), silicon is an excellent material for such an application when given an antireflection coating using aluminum-oxide because its transmission is excellent in the 8 to 14 μm window. The thickness of the irdome must be sufficient to withstand the anticipated aerodynamic forces. Stress analysis indicates that a silicon thickness of 0.25 cm is adequate for the maximum RPV cruise speed. The inner and

outer surface should, for optical sensor, be accurately concentric. Therefore the outer surface of the irdome has a radius of 15.24 cm and the inner surface a radius of 15 cm. Fig 6.2 shows the construction of an irdome for the FLIR sensor.

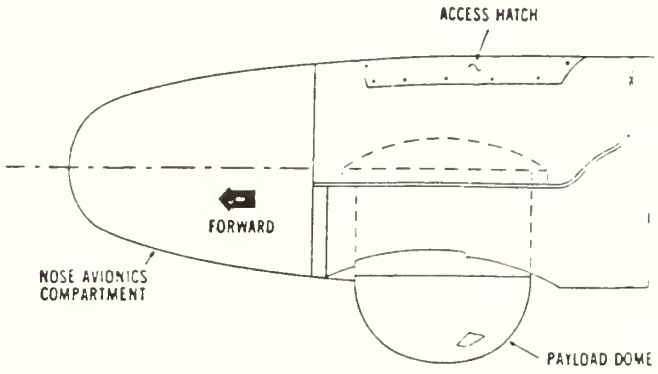

Fig 6.2 A Irdome Construction

High performance EO sensors are stabilized to minimize the effects of linear and angular perturbations. It is common to design the platform with dual mode servos, a rate system for target tracking and a position loop to maintain reference to the RPV when turning or holding constant standoff angle. The need to keep a crosshair or beam spot on a tank size at 14 km for 95% of the tracking period requires a stabilization accuracy of 50 micro-radians [Ref.28 p:35].

Gimbaling and mounting schemes for the FLIR sensor follow aircraft gimbal mounting designs.

An absorption filter using dyes and an interference filter using multiple index layers can remove unwanted wavelength (see APDX B.7).

4. Optics

Multielement reflective system provide imagery equal to the best obtainable with mirrors. The optical system consists of an afocal telescope system, a scanning drum mirror, and a detector lens. A wide field mechanical scanning system is of the simplest form if the detector is located at the gimbal center and if the irdome is concentric about this center. Because refractive optics have a simpler mounting, they were chosen for use in the search system. Since the front surface of the lens can be within 0.25 cm from the inner surface of the irdome, it is possible to design the lens so that the scanned principal point coincides with its front surface. The focal length of the lens would be 14.7 cm.

A magnifying telescope will increase the resolution of the system. Magnification decreases the FOV, increases the angular resolution, and keeps the ratio of detector substense to clear aperture diameter constant so that thermal sensitivity does not change. Fig 6.3 shows a telescope for parallel beam scanning. The objective of this telescope is achromatic to reduce chromatic aberration. The focal length of this objective is given by

$$f_{12} = \frac{f_1 f_2}{f_1 + f_2 - d},$$

where f_1 is the focal length of first lens and f_2 is the focal length of second lens. The combined focal length then is

$$f_{12} = \frac{f_1 f_2 (V_1 + V_2)}{f_1 V_2 + f_2 V_1},$$

here V_1 is the dispersive index of the first lens and V_2 is the dispersive index of the second lens or $V = (n-1)/\Delta n$.

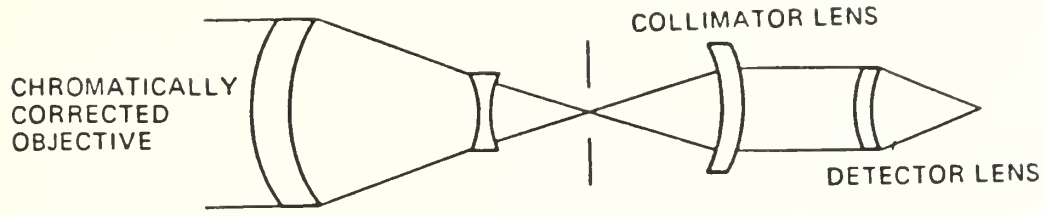

Fig 6.3 Parallel Beam Scanner Telescope For Chromatically Corrected Objective [Ref.25 P;252]

On the basis of the above mathematical relation, the first lens is made of germanium, V_1 = 1001.27 from 8 -14 μm, and second lens is zinc selenide, V_2 = 34.45 from TABLE 7.1 [Ref.25 pp:258-259]. If the focal length of both lenses is 14.7 cm, the distance between the lenses is also 14.7 cm.

Because each detector elements subtends an angle of 1 mrad, the F/# of the detector lens must be selected to achieve a blur circle no larger than this. From the blur-spot charts for diffracted-limited systems [Ref.12 p:9-25], an F/2 telescope lens has a total blur circle of 1.25 mrad, including 0.25 mrad of lateral chromatic aberration. A silicon lens could achieve this size blur circle if the surface of the lens were aspheric. Consequently, the detector lens was a F/2 silicon element with a focal length of 14.7 cm and a diameter of 7.4 cm.

5. Scanning Mechanism

The function of a scanner in a FLIR is to move the image formed by the optical system in the plane of the detector array. Fig 6.4 shows the basic two types of scanners : a parallel beam scanner consisting of an optical angle changing device such as moving mirror placed in front of final image forming lens, and a converging beam scanner

of a moving mirror between the final lens and image.

There are seven commonly-used optical scanning mechanism : the oscillating mirror, rotating polygonal mirror, the rotating refractive prism, the rotating wedge, the revolving lens, the rotating sensor, and the rotating V-mirror [Ref.25 pp: 283-284].

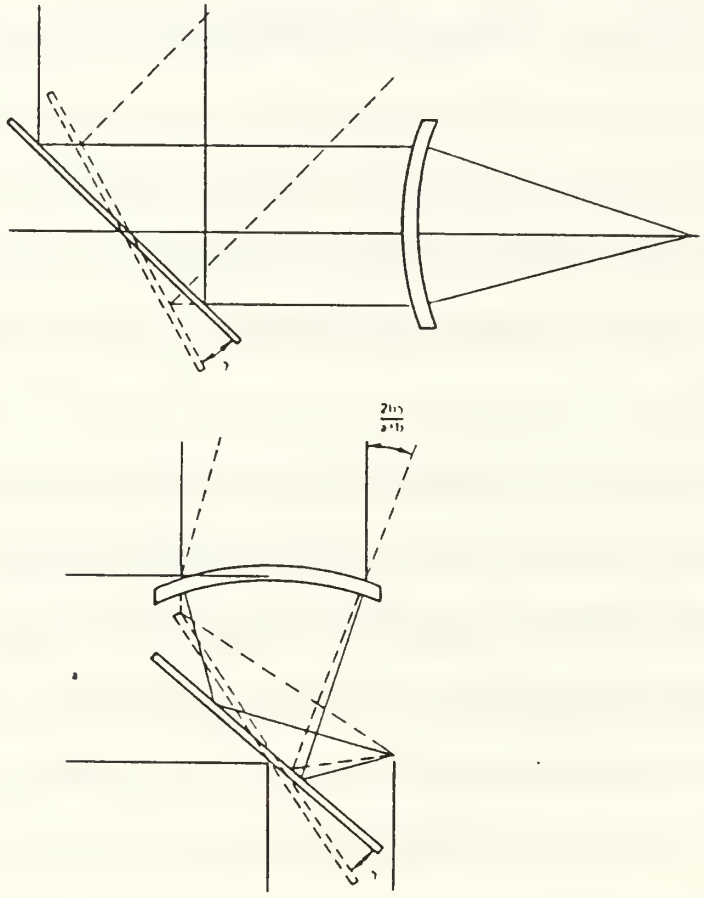

Fig 6.4 A parallel Beam and Convergent Beam Scanner [Ref.25 p:284]

Fig 6.5 shows three basic schemes for generating a FLIR image : serial scanning, parallel scanning or pushbroom, full format or staring arrays [Ref.15 p:53].

In the serial scanning case, a small detector array of perhaps 1-16 element scans across the FOV in order to construct the entire format. As shown, the array first sweeps across a narrow band at the top of the frame. Moving down to the second row, it sweeps across the

line. This process repeats for the full frame. The serial scan requires two motions, the scan motion in X (azimuth) and the increments from row to row in Y (down range). This scanning has the following properties : (1) poor sensitivity, (2) complex, high-speed, mechanical scan, (3) scan alignment problem, (4) a fast response detector problem (high bandwidth requires a fast response).

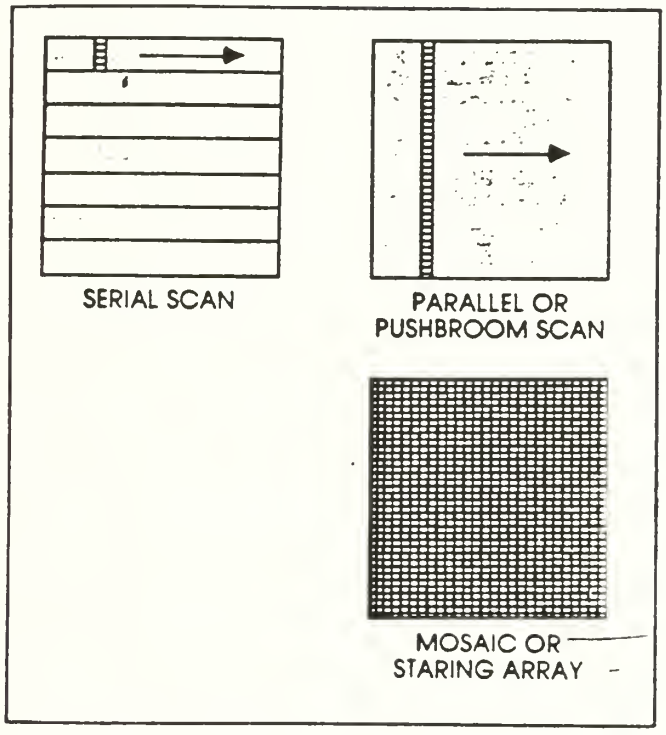

Fig 6.5 Scanning and Staring Format of FLIR image [Ref.15 p:53]

For parallel scanning, a one dimensional array scans across the object space in a "pushbroom" fashion. Although the detector is more complex and has an increased number of elements, the system requires only one scan motion simplifying the mechanical task. Several columns of detector elements arranged in a staggered form, help increase the resolution and SNR. This scanning method has the following advantages :

(1) Good sensitivity due to increased number of detector,

(2) Less complexity due to elimination of vertical scanning,

(3) Reduced alignment problem,

(4) Lower detector bandwidth, and

(5) Low speed scan.

Finally there are staring or mosaic detector arrays (see APDX.E.2). These detectors need substantially more elements, increasing production difficulties, but they do not require mechanical scanning. Comparing three scanning methods on the basis of sensitivity, mechanical complexity, detector bandwidth, simplicity, and cost, the "push broom technique is the best choice for the FLIR sensor system.

Fig 6.6 shows a push broom scanning system a using rotating polygon scan mirror, that was selected for this application [Ref.15 p:55].

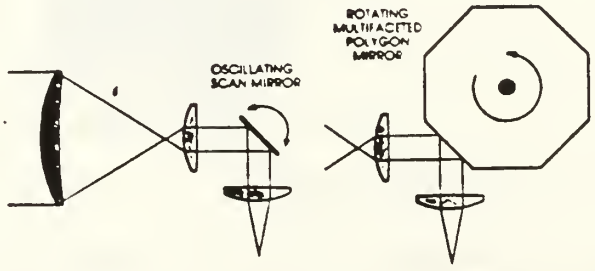

Fig 6.6 Pushbroom Or Linear Scanning Using Oscillating Scan Mirror [Ref.15 p:55]

Fig 6.6 illustrates the scan pattern for an RPV using a push broom. The Pioneer RPV cruising with speed v at an altitude h carries a scanner having a IFOV (resolution element) of angular size ß mrad. A rotating scanner moves the IFOV through an angle (α) at right angles to the RPV path (footprint). The RPV motion carries the scanner forward

so that successive scans cover different strips of the ground. The portion of ground swept during a single scan through angle α is called a "line". Underlap occurs when successive lines are not contiguous. This will occur if the vehicle speed is too high or if the rotating elements revolve too slowly. If successive lines scan over the same terrain the condition is called "overlap". Underlap is clearly undesirable, since information is missed between successive lines. Contiguous scanning is desirable because no ground remains unscanned. Overlap should be avoided to reduce the bandwidth and cost. Consider an exterior polygonal drum scanning mechanism. Fig 6.7 shows the dimensions of a polygonal mirror which has 6-facets [Ref.25 p:303].

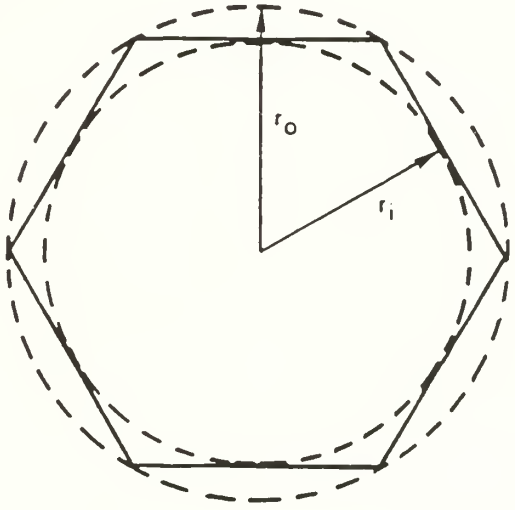

Fig 6.7 Dimension Of A Polygonal Mirror

The facet angle θ_f measured from the drum axis for n facets is $\theta_f = 2\pi/n$. If the facet is l, $l = 2\, r_o \sin(\theta_f/2)$, and the ratio of inner and outer radius of mirror is $r_o/r_i = [\cos(\theta_f/2)]^{-1}$. The ratio of the facet length to the outer radius and the outer radius are tabulated in TABLE 6.1 [Ref.25 p:305].

TABLE 6.1 CHARACTERISTICS OF A POLYGONAL MIRROR

Number of Facets	Facet Angle (°)	$1/r_o$	r_o/r_i
3	120	1.732	2.000
4	90	1.414	1.414
5	72	1.176	1.236
6	60	1.000	1.155
7	51.43	0.868	1.110
8	45	0.765	1.082
9	40	0.684	1.064
10	36	0.618	1.051

Now consider Fig 6.8 [Ref.25 p:305], which shows two drum angular positions with an angular rotational displacement θ_R.

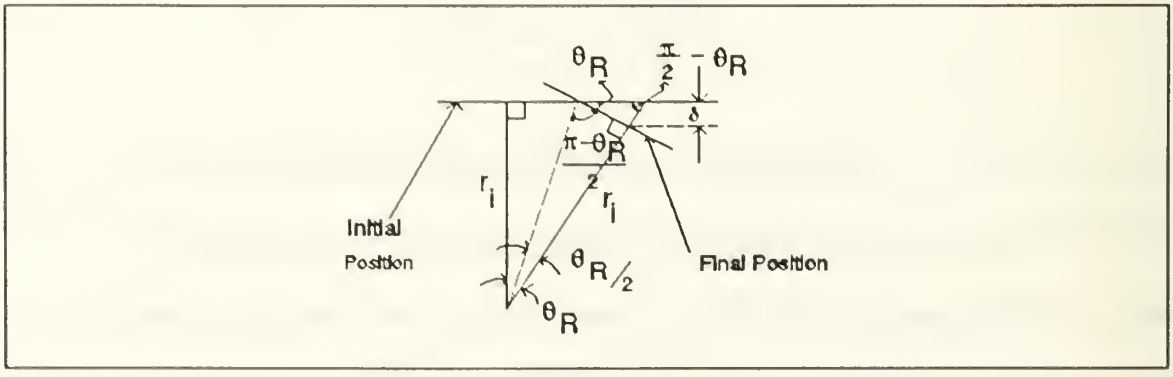

Fig 6.8 Mirror Motion With Rotation

The geometry demonstrates that the final displacement δ of the center of the facet in the direction normal to the initial undisplaced mirror surface is given by $\delta = r_i(1- \cos\theta_R) = r_o (1 - \sin(\theta_f/2) \tan(\theta_f/4)(1-\cos\theta_R)$.

Levi [Ref.26] has shown that the minimum outer surface radius r_o necessary to keep the beam unvignetted during the scan of a parallel beam is given by

$$r_o = \frac{D}{2\cos(\frac{d}{2})\sin(\frac{\theta_f-\gamma}{2})},$$

where D is the exit pupil diameter, δ is the beam deviation at the midpoint of the scan, 2γ is the beam deflection angle produced by the scan, and θ_f is the facet angle $2\pi/n$.

For the six facets, θ_f is 60°. Assume the scan beam deflection is 0, and δ is 90°. Then the polygonal mirror radius is

$$R = \frac{D}{\sqrt{2}\sin(\frac{60-\gamma}{2})} = \frac{D}{\sqrt{2}\sin 30}.$$

As shown above, the polygonal mirror radius is a function of the beam exit pupil diameter and the beam deflection angle.

The numerical aperture (NA) of the detector lens in an IR optical system is NA = 1 /(2 f/#) [Ref.5 p:179]. For a D of 7.4 cm the detector diameter which has a f/# of 2, NA is 1/4 D. The exit pupil diameter is 1.8 cm. The drum mirror radius becomes r_o = D /(1.414 sin 30) = 2.6 cm.

For 6 mirror facets using TABLE 7.1, the ratio of l/r_o is 1, and the length of a facet $l = r_o$ becomes 2.6 cm, and r_i is 2.3 cm.

A prism mirror with n facets rotates at a rate of r (rpm) about an axis that is parallel to the flight of the RPV. A single element detector scans n lines per revolution. Each face of the prism is inclined 45° to the axis of rotation. Normally, the detector acts as the field stop of the optical system, determining the angular dimensions of the IFOV. If the detector, instead of being a single element, consists of l identical elements arranged in a closely-spaced array, then n x l lines will be scanned per revolution. A significant detector characteristic is the time constant τ. The scanner must dwell on each resolution element for a time not less than $\kappa \times \tau$, where κ is a positive dimensionless number, representing the dwell time in terms of the detector time constant. Such a scanner must meet two conditions. The scanner must dwell on each resolution element for a time not less than $\kappa\tau$. The number of resolution elements scanned per second is $2\pi r/ß$, so the dwell time is $ß/2\pi r$. Hence, $(ß/2\pi r \geq 2)$. The scanner must operate at a rate so that under-lap does not occur (over-lap is permissible). In the RPV cruise direction, the swath (azimuth x down range) scanned by each face of prism is ßhl. The width of the strips scanned each second is ßhlnr. If no underlap occurs, $ßhlnr \geq v$ must be greater than or equal to the RPV speed. Combining the dwell time and underlap constraints gives $r < ß/2\pi\kappa r$, and $r \geq v/hlnß$ when all quantities are positive.

The range r has an upper limit set basically by the detector time constant and a lower limit set by the zero underlap requirement (by v/h). A third constraint upon r is also important, the maximum rotation rate permitted by mechanical considerations such as the strength of materials, vibrations, and allowable distortions. Eliminating r from the above inequalities, a constraint upon ß is

$$\beta = \sqrt{\frac{2\pi k}{nl}\ \frac{v}{h}\ \tau}.$$

Unlike r, ß is only constrained by a lower limit imposed by the joint action of v/h and τ. Under the limiting condition of contiguous lines, r and ß are

$$r = \sqrt{\frac{1}{2\pi knl}\ \frac{v}{h}\ \frac{1}{\tau}},$$

$$\beta = \sqrt{\frac{2\pi k}{nl}\ \frac{v}{h}\ \tau}.$$

The velocity v and height h are usually set by considerations relative to RPV operation. The properties of the detector material determine τ. They are not easily changed. K is normally not less than 2. The value selected for n determines α, the focal length width of the scan, since $\alpha = 360°/n$. Note that n=1, 2, 3 than α = 360, 180, 120..., degrees. Reconnaissance of a large area should avoid flying over the same ground twice. Therefore, α should be as large as possible e.g., n=2, so α=180°. Since maximum detail is desirable, ß should be as small as possible. Also, for mechanical reasons it is desirable to minimize r. In order to minimize both ß and r the designer has at his complete disposal only the factor l.

The following parameters represent a low-altitude, slow-speed FLIR system: k=2, n=6, v=30.86(m/sec), h=200, $\tau = 10^{-5}$sec. The revolution per second (rps) is

$$r = \sqrt{\frac{1}{2\pi knl}\ \frac{v}{n}\ \frac{1}{\tau}} = \sqrt{\frac{1}{2x3.14x2x6}\ \frac{30.86}{200}\ \frac{1}{10^{-5}}}\ \sqrt{\frac{1}{l}} = \frac{14.31}{\sqrt{l}}\ rps,$$

and ß is

$$\beta = \sqrt{\frac{2\pi k}{nl}\frac{v}{h}\tau} = \sqrt{\frac{2\times 3.14\times 2\times 30.86\times 10^{-5}}{2\times 200}}\ \frac{1}{\sqrt{l}} = 3.113\times\frac{1}{\sqrt{l}}\ (mrad),$$

where l is the number of detector arrays. For one detector, the simplest configuration to implement is r = 858.6 rpm, and ß = 3.113 mrads. Table 6.2 shows the various statistics of rpm and IFOV per square root l for n=6, k=2, and $\tau = 10^{-5}$.

TABLE 6.2 V/H RATIO AND OPTICAL PARAMETERS

RPV speed v(m/sec)	RPV altitude (m)	RPM (r/√l)	IFOV (mrad/√l)
30.8	200	858	3.113
50	200	1092	2.287
100	200	1545	3.2352
30.8	300	700	1.466
50	300	772	1.617
100	300	1261	2.641

(TABLE 6.2 CONTINUED)

RPV speed(m/sec)	RPV altitude(m)	RPM (r/√l)	IFOV(mrad/√l)
30.8	300	606	1.2691
50	400	772	1.6173
100	400	1092	2.2876
30.8	500	542	1.1350
50	500	691	1.4452
100	500	977	2.046
30.8	600	495	1.036
50	600	630	1.319
100	600	892	1.865
30.8	700	458	0.9587
50	700	584	1.220
100	700	826	1.729
30.8	800	428	0.8976
50	800	546	1.14

As shown in TABLE 6.2, the drum mirror RPM and the IFOV of the scanning mechanism strongly depend on the ratio of RPV speed and altitude, and the number of detector arrays. But from the above equation, the number of detector l need for 1 mrad is

$$l = 2\pi kv/nh\beta^2 \times \tau = (2x3.14x2x10^{-5}x30.86)/(6x200x1x10^{-6}) = 3.24 \fallingdotseq 4.$$

In this case, rpm are 429, and the IFOV becomes 1.5 mrad. Ten detectors will give a 1 mrad IFOV for an RPV speed of 30.8 m/sec at 200 altitude. In this case, the mirror rotates at the rate of 271 RPM. The number of detector arrays depends on the RPV speed and altitude, and the number of scanning mirror facets, and the IFOV per each element.

The Rayleigh criterion states that for a circular aperture of diameter D, the best resolution obtainable at a wavelength λ is given by $\beta = 1.22\ \lambda/D$. At a wavelength of 10μm, a desired β of 1 mrad requires a 1.2 cm diameter circular aperture.
However, Rayleigh criterion is an idealized limit assuming a perfect optical system. In practice, such performance can't be realized, and a larger aperture is needed.

There are two features of the operation of the scanner described above which must be considered to display the information. First, although the angular resolution is constant, the linear resolution on the ground is not. Secondly, for a linear detector array, the projection of the IFOV of the array on the ground (target) rotates as the scan angle increases. In Fig 6.9, assume a flat earth approximation. The angle away from vertical is θ, the range from the scanner to the earth at any instant is R, and p is the length of the IFOV in the direction of RPV. It can be seen from the figure that $p = \beta r$, and $R = h \sec\theta$ so that $p = \beta h \sec\theta$. To obtain an expression for the change in azimuth and down range of IFOV as a function of θ, see Fig 6.9 [Ref.27].

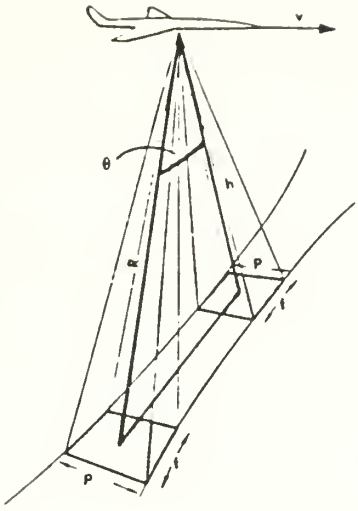

Fig 6.9 Geometry For The Determination Of Resolution Change In The Direction of Perpendicular To The RPV Flight Direction [Ref.16 p:250]

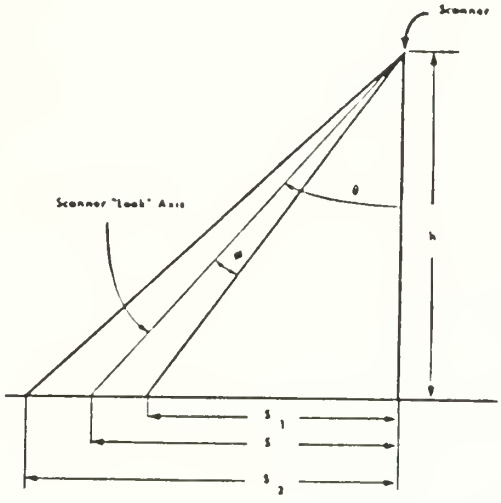

Fig 6.10 Geometry For The Determination Of Resolution Change In The Direction Parallel To The RPV Flight Direction [Ref.16 p:250]

Finally, $f \approx h\beta(1 + \tan^2\theta) = h\beta \sec^2\theta)$. We therefore have the result that the FOV changes as $\beta h \sec\theta$ in one direction and $\beta h \sec^2\theta$ in the other direction. TABLE 6.3 summarizes the various statistics for the changes of FOV and the sensor footprints for $\theta = 40°$, $\beta = 1$ mrad.

TABLE 6.3 RPV SPEED AND SENSOR FOOTPRINT

RPV Speed (m/s)	f (m)	p (m)	L_{az} (m)	L_{dr} (m)
100	0.17	0.13	73	54
200	0.34	0.15	146	107
300	0.51	0.39	218	161
400	0.68	0.52	291	214
500	0.85	0.65	364	268
600	1.02	0.78	437	321

TABLE 6.3 (CONTINUED)

PRV Speed (m/sec)	f(m)	p(m)	L_{az}(m)	L_{dr}(m)
700	1.19	0.91	510	375
800	1.36	1.04	582	429
900	1.53	1.17	635	482
1000	1.7	1.3	730	536
1500	2.55	1.95	1092	804
2000	3.4	2.6	1456	1071

As shown in the above relation, the sensor footprint is proportional to the RPV altitude and the FOV of the FLIR sensor.

Consider a close support mission at an altitude of 200 m and a velocity of 30.86(m/sec). This requires a FLIR sensor with a V/H capability of 0.154 radian/second for the FLIR FOV of 40° in azimuth (across) and 30° in down range (along the track), and the IFOV is 1 mrad. The number of resolution elements (across track)(see APDX.F.1-2) is

$$\frac{FOV}{\beta} = \frac{40(degree)}{1mrad} \times \frac{17.45mrad}{degree} = 698\ resolution\ elements\ ,$$

and resolution elements per second is

$$\frac{V/H}{\beta} = \frac{0.154\,(rad/second)}{1 \times 10^{-3} rad} = 154\ elements/second.$$

Therefore, the total resolution elements per second is

total resolution elements = (across-track elements) (along-track elements)/second = 107492.

B. DETECTOR DESIGN

1. Selection of Detector Material

Preliminary studies clearly indicated the advisability of using the 8-12 μm window and a detector cooled to 77°K. A possible choice for a detector is photovoltaic (PV) or photoconductive (PC) mercury cadmium telluride. APDX C.2 [Ref.12 p:11-86] shows a detailed comparison of different IR detectors produced by US manufacturers. IR detector materials separate into five basic groups : HgCdTe, Ge, Si, InSb, and PtSi. Comparing these on the basis of wavelength, and detectivity, PC HgCdTe, PC Ge:Au (p-type), and Ge are the best detector materials in the 8 -12 μm spectral range . Germanium has the highest detectivity of 5 x 10^{12} (cm $Hz^{1/2}$/w), but it must be cooled to below 77°K . The second good choice is PC HgCdTe that has the detectivity of 3 x 10^{11}(cm $Hz^{1/2}$/w). The responsivity of HgCdTe is 2 - 5000 times higher than it is for the other two. Upon comparison, HgCdTe is the best detector material for the FLIR sensor.

a. HgCdTe Characteristics

HgCdTe is a pseudo binary semiconductor whose bandgap varies with the Mercury-Cadmium ratio. Photoconductors can be made from the material with long wavelength sensitivity limit from about 1 to 30 μm. The ability to design a cutoff wavelength is of particular importance in applications requires minimum cooling. Choosing the largest bandgap consistent with the required operating wavelength generally assures optimum performance at the maximum operating temperature. A large proportion of the work on HgCdTe has been performed on material and devices sensitive in the 8 - 12 μm region of spectrum. Objects at room temperature emit thermal radiation band, within this

atmospheric transmission window. These detectors are useful for imaging or detecting any object near room temperature. Fig 6.11 shows a typical plot of detectivity as a function of frequency for a good HgCdTe photon conductor, sensitive in the 8-12 μm region [Ref.17 p:602].

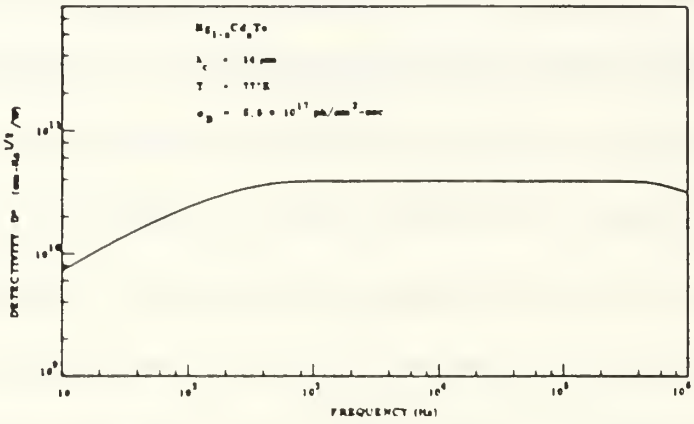

Fig 6.11 HgCdTe Detectivity As A Function Of Frequency [Ref.17 p:602]

The absorption coefficient of HgCdTe is also much greater than the impurity absorption coefficient of Ge:Te. This permits the construction of thinner detectors with larger quantum efficiency with normal incident backgrounds, at operating temperatures in the vicinity of 77°K. Photoconductors made from HgCdTe have two mobilities. The mobility ratio is such that the maximum photoconductive gain is about 500. The device has low impedance, about 50Ω for a typical detector, and will operate effectively into an amplifier with an input impedance exceeding a few hundreds ohms. Amplifiers with bipolar input stages and an equivalent input noise voltage of about 10^{-9}v/√Hz are commonly used [Rep.16 p:602].

In an ideal operating environment, in which there are no extraneous noise sources, a high D^* is desirable. An RPV, on the other hand, is a hostile environment for sensitive,

low-noise equipment. In such a noisy environment these are advantages to choosing the detectors with the highest signal level (responsivity) because its use will make it easier to achieve a detector-noise limited system. The severity of the noise pick up can be determined only after installing the equipment in its final operating environment. On the basis of these facts, since it represents conservative design and it is used in most of IR thermal imaging system, HgCdTe was selected as the detector for the FLIR sensor. But a HgCdTe detector has different characteristics depending on the HgCd ratio. Fig 6.12 [Ref.12 p:11-86] shows $Hg_{1-x}Cd_xTe$ detector performance data at 77°K. Fig 6.12 (a) shows the spectral responsivity of the detector responsivity for different x values. Curve A has clearly best responsivity in the spectral of 8-12 μm. This evaluation recommends $Hg_{0.79}Cd_{0.21}Te$ detector for the FLIR sensor detector.

$Hg_{1-x}Cd_xTe$

T_d = 77 K

A_d = 4 x 10^{-6} to 4 x 10^{-2} cm^2

R_d = 20 to 600 ohms

τ = 100 to 800 nsec

FOV = 10^0 to 130^0

Background temperature = 300 K

$\mathcal{R}_\lambda$ = 10^4 V W^{-1}

$\mathcal{R}_{\lambda_p}/\mathcal{R}_{bb} \approx 2$

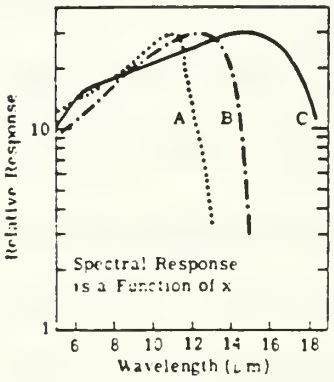

(*b*) Spectral response of detector responsivity. Curve A:x = 0.21; Curve B:x = 0.20; Curve C:x = 0.17.

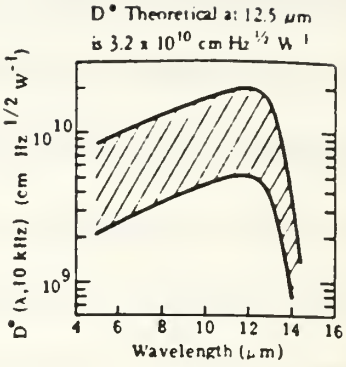

(*a*) Spectral response of detector D* (λ, 10 kHz).

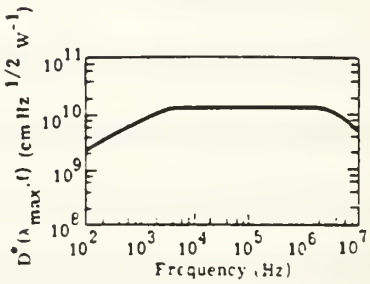

(*c*) Frequency response of detector D* (λ_p, *f*).

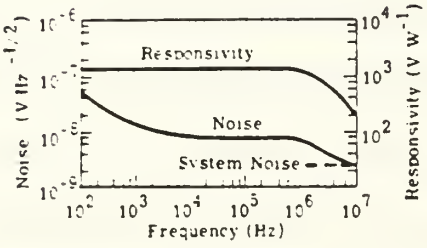

(*d*) Frequency response of detector noise.

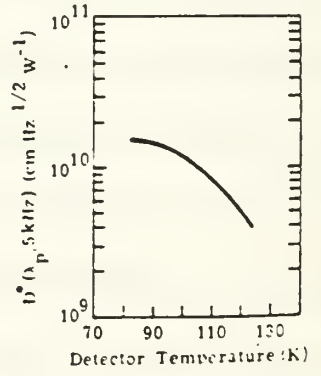

(*e*) Temperature of detector D* (λ_p, 5 kHz).

Note

Spectral response is determined by the alloy composition.

Fig 6.12 $Hg_{1-x}Cd_xTe$ Detector Performance At 77°K [Ref.12 p:11-86].

2. IR detector size and array

For any optical system associated with a detector, the limiting detector size is given by $S_d \geq (D\theta/n)$, where S_d is the diameter (or linear dimension) of the detector, D is the corresponding diameter or linear dimension of the entrance pupil of the optical system, θ is the half-angle of FOV or angular half field, and n is the refractive index of the medium containing the detector. From section A.4, the telescope object lens has a diameter of 7.4 cm, and silicon has the refractive index of 3.41 at room temperature. From the optical design, the entrance pupil of the telescope is 1.85cm.

The diameter of the IR detector for a 40° FOV in azimuth is 0.19 cm.

From the data sheet for $Hg_{0.79}Cd_{0.21}Te$ (see Fig 6.12) a cooled filter and a F/2 background shield should give a detectivity of 5 X 10^{10} cm$(Hz)^{1/2}w^{-1}$ in the 8 -12 μm region. Since the detector elements subtend an angle of 1 mrad x 1 mrad (0.0573°) when used with a detector lens of 14.7 cm focal length, each element is 147 nm on a size. Fig 6.12 also shows that elements of this size are well within current manufacturing capability (A_d = 4 x 10^{-6} to 4 x 10^{-2} cm^2) [Ref.12 p:11-86].

The FOV (see APDX F.3) is $\theta = 2 \tan^{-1}(d/2f)$ where f is the focal length of the detector lens, and d is the vertical size of the detector arrays. The FLIR sensor requires a FOV of 30° in down range and 40° in azimuth. Therefore, $d = 2f \tan(\theta/2) = 0.8$ cm. The detector size computed satisfies this criterion. Each detector element has a size of 0.015cm from the previous requirement. About 55 detectors are needed to achieve a 40° FOV in azimuth. In this case, the IFOV will be 1 mrad.

The detector array should have 55 elements, which gives a pixel size of (147 x 147)

μm^2. A photoconductive MCT (Hg Cd Te) detector in a 55 element staggered linear array configuration will achieve this (see Fig 6.13). The configuration provides a 10% overlap between scan lines in order to minimize signals from point objects while maintaining high resolution.

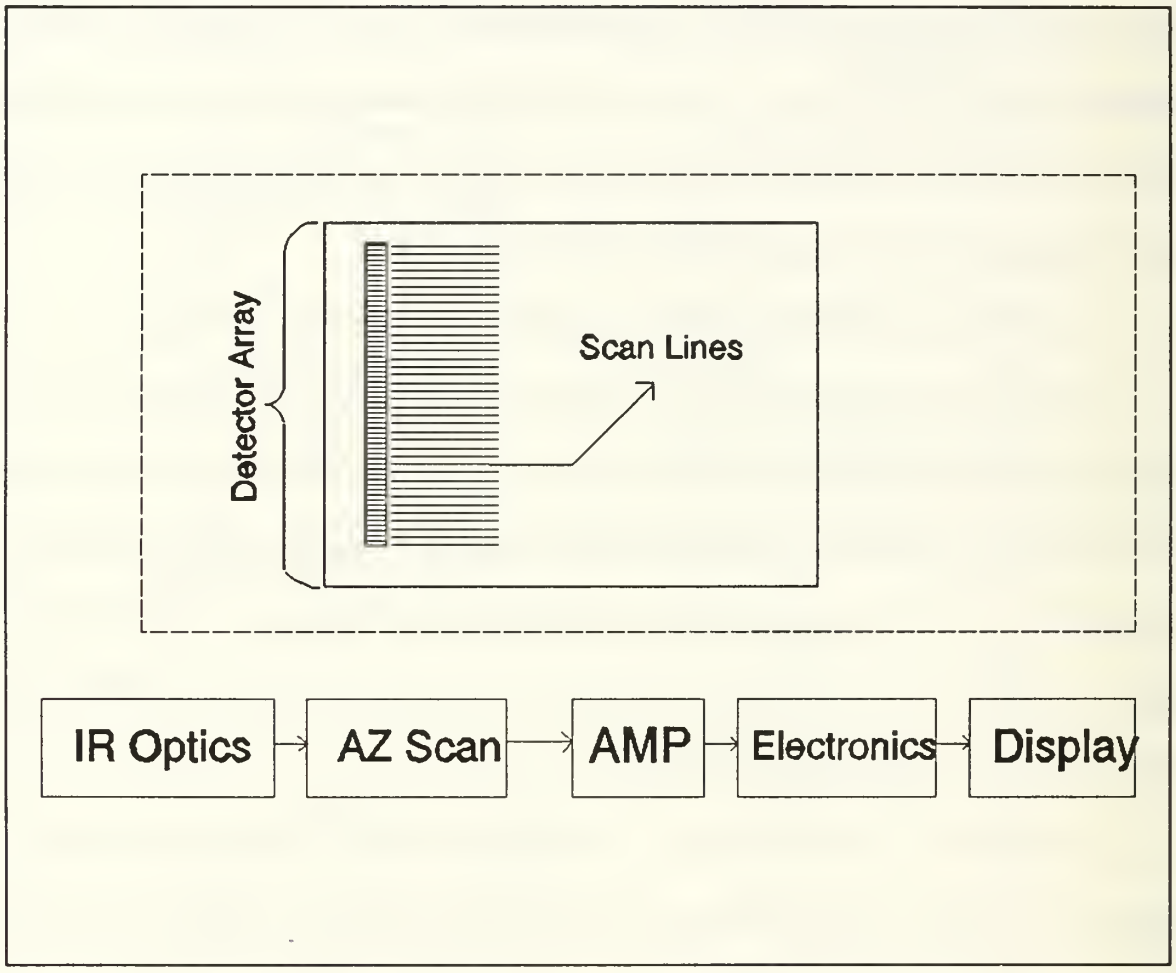

Fig 6.13 IR Detector Configuration

3. Cooling system

Currently thermal imaging devices use three cooling methods (see APDX C.7). Closed cycle mechanical cooler are used in applications that can tolerate the weight and power associated with this mode. Handheld systems use thermoelectric (TE) cooler because there are no moving parts. This method lends itself to the lowest weight, cost, and size option, but it is limited to temperatures around 200°K. The Joule-Thomson (J.T.) cooler achieves cryogenic temperatures from 20° to 77°. This method offers the lowest weight and quietest method for cooling to around 77°, but has severe logistic problems from the high compressed and pure gas supply [Ref.17 p:736]. In addition, the Hoffler thermo-acoustic refrigerator developed by NPS provides a high performance cooling capability for future consideration [Ref.8].

Comparing these cooling systems on the basis of temperature, cost, efficiency, and ease of servicing, the J.T. cooler is the best choice for a FLIR sensor. The externally supplied gas enters the sensor unit through a pipe in the platform. A separate gas supply unit incorporating a compressor using ambient air and a suitably chosen combination of filters for contaminant removal provides the compressed air . This unit cooldown time runs from several seconds to minutes.

C. ELECTRONICS

The first stage of analogue signal processing in a set of well shielded, low-noise individual preamplifiers for each detector element. With no noise amplifier, the sensor performance is detector noise limited. A further stage contains individually adjusted amplifiers, which corrects detector responsivity variations between elements. The system

should use an automatic gain control stage operating uniformly on all channels.

Fast multiplexing and A/D conversion circuits, should avoid information loss introduced by sampling effects. The scan converter uses a random access memory architecture to achieve fast image conversion. APDX D.1 covers the dynamic range as a function of preamp voltage and power supplies.

The video generator takes the D/A converted data from the scan converter, adjusts to the corrected voltage level and adds synchronization pulses to provide video output in accordance with the standard TV format.

APDX D.2 addresses different noise mechanisms.

D. DISPLAY

A standard TV-monitor displays the image, which is mounted on an operator display board. In flight, operator controls are minimal. The operator only needs to observe the displayed image, detect the target and initiate automatic tracking.

E. SENSOR CONFIGURATION

Fig 6.14 shows a tentative sensor design. It consists of the irdome, lens, detector, scanning mechanism (drive motor), gimbal structure and associated drive circuitry, a 55-channel preamplifier, and a flexible line to deliver the coolant to the detector. The estimated sensor package weight is about 11 kg.

The idealized sensor range [Ref.5 p:425] is

$$R_{max} = [\frac{\pi}{2} D_o NA D^* J \tau_a \tau_o]^{1/2} [\frac{\theta l}{\Omega}]^{1/4}$$

where D_o is diameter of the entrance pupil,

NA is the numerical aperture,

D^* is the detectivity of detector material,

τ_a is the transmittance of the atmosphere,

τ_o is the transmittance of the optics,

l is the number of independent detector element,

θ is the IFOV that is $\tau_d \omega / c$,

Ω is the search field in steradians,

F is the frame time,

$\dot{\Omega}$ is the search rate, and

Δf is the electrical band width.

The transmittance of the optics τ_o depends on the transmittance of the irdome and lenses. From the section III, the irdome and lens will result in a transmittance of 0.9 per element in the 8 to 12 μm spectral bandwidth. Thus the value of τ_o is 0.81. The optimum RPV altitude is about 200m. From the APDX A.6, the transmittance of the atmosphere τ_a is less than 0.7.

The effective FOV is to be 40 by 30 deg, with a frame time 1/30 sec. The search rate (to account for the scan dead time) is

$$\dot{\Omega} = \frac{\Omega}{F} = 10.9 sr \ sec^{-1}.$$

The detector dwell time [Ref.5 p:424] and the optimum 3 dB bandwidth[Ref.5 p:408] are

$$B = \frac{1}{2\tau_d} = \frac{1}{2 \times 5.016 \times 10^{-6}} = 100\ kHz.$$

Assume that the 3 dB bandwidth is equal to the noise equivalent bandwidth, the value of Δf is 100 kHz.

After determining the transfer function of the system electronics, we can compute the value of the pulse visibility factor υ. The data shows that the value lies between 0.25 to 0.75. Assume as a starting point that the value of υ is 0.5.

Assume that the exhaust port of the Pioneer RPV engine is a grey body with an emissivity of 0.9 and the exhaust gas temperature can range 350 to 400° C for normal cruise speed flight. The radiance is

$$N = \frac{\epsilon \sigma T^4}{\pi} = (0.9/3.14)(5.67 \times 10^{-12})(350+273)^4 = 0.24482\ W\ cm^{-2}\ sr^{-1}$$

The radiant intensity of the RPV engine is

$$J = NA = (0.24482)(314) = 77 W\ sr^{-1}.$$

About 4 percent of the radiant flux lies in the 8 to 12 μm region ; thus the effective intensity of the RPV engine is 3 W sr^{-1}. Therefore the idealized range is

$$R_o = [\frac{\pi}{2} x 7.366 x 1.8415 x 3 x 10^{11} x 3.0748 x 0.7 x 0.81]^{1/2} [\frac{0.5 x 55}{10.962}]^{1/4} = 42 km$$

For a false-alarm time of 1000 sec, the number of noise pulses[Ref.5 p:426] is

$$n' = \tau_{fa} \Delta f = 1000 \times 99681 \approx 10^8.$$

For a 0.95 probability of detection, the ratio of the actual to the idealized range is 0.35 ; therefore $R_{0.95} = 0.35\ R_o = (0.35)(42) = 14.7$ km

TABLE 6.4 shows the characteristics of the design for a FLIR sensor .

TABLE 6.4 CHARACTERISTICS OF THE DESIGN FOR A FLIR SENSOR

Quantity	Symbol	Value	Unit
Diameter of entrance aperture	D_o	7.366	cm
Numerical Aperture	NA	1.845	cm
Detectivity	D^*	3×10^{11}	$cmHz^{1/2}w^{-1}$
Transmittance of the optics	τ_o	0.81	-
Pulse visibility factor	υ	0.5	-
IFOV per element	ω	1×10^{-6}	sr
Search field(effective)	Ω	0.45	sr
Frame time	F	1/30	sec
Search rate	Ω	10.962	$sr\ sec^{-1}$
Electrical bandwidth	Δf	99.681	kHz
Spectral bandwidth	-	8 - 12	μm

TABLE 6.5 shows the estimated weight, volume, and power consumption of the FLIR sensor package.

TABLE 6.5 Estimated Sensor Dimension

Unit	Weight(kg)	Volume(m^3)	Power(watt)
Sensor	11	0.0261	153
Signal, Servo, Power supply	16	0.0697	223
Tie-in	3	0.0174	42
Joule-Tompson Cooler	15	0.0261	1532
Total	45	0.1393	1950

Fig 6.14 shows a tentative dsensor design.

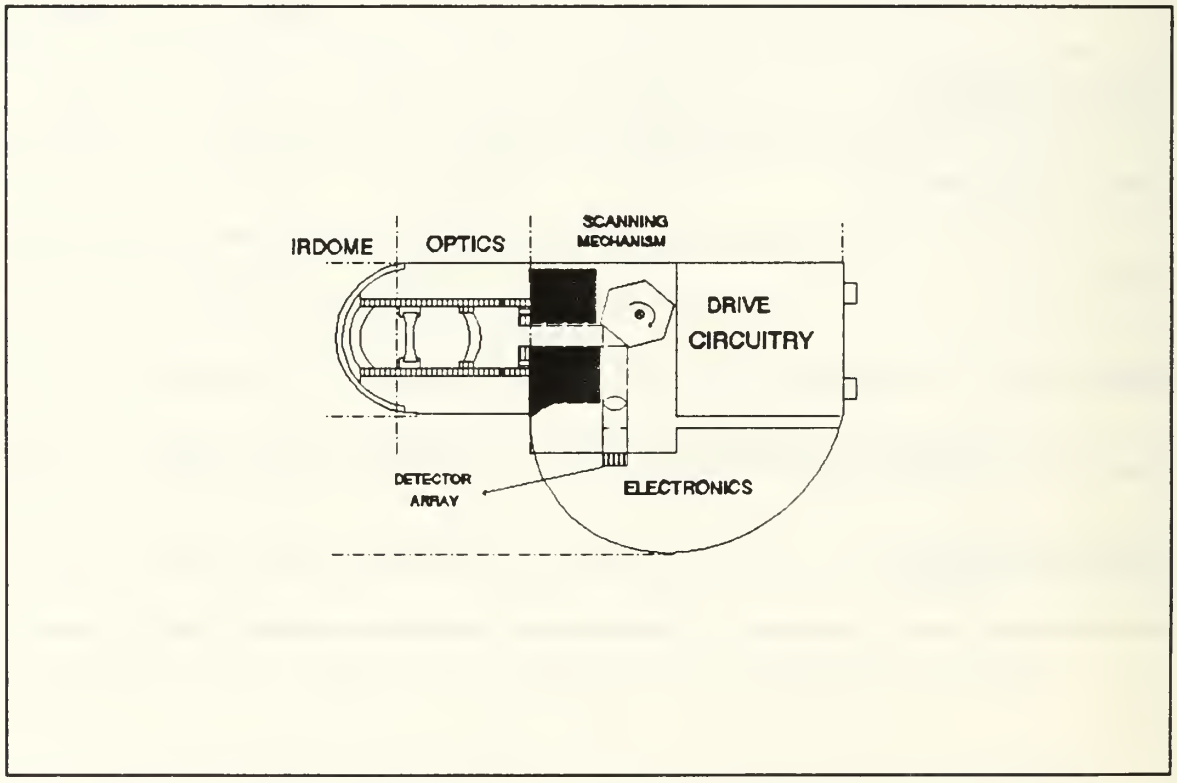

Fig 6.14 Tentative Sensor Design

VII. Conclusions and Recommendations to the Korean Army

This thesis introduced the concepts and design considerations of a FLIR sensor design for a RPV which could be used by the Korean Army. We adopted the Pioneer RPV as a close-range tactical unmanned vehicle model. The Pioneer RPV can provide military commanders unprecedent ability to see behind enemy lines in a timely manner by using various EW payloads involving FLIR, LLLTV, and SAR. The Pioneer RPV has proved its operability and effectiveness in the "Desert Storm Operation" during Gulf War by the US Navy and US Marine Corps. In particular, the employment of a television camera and FLIR sensor played a critical role for accurate surveillance and reconnaissance mission in hostile environments. The Pioneer RPV has a wing span of 5.15 m and length of 4.26 m with a maximum power of 1950 watt and maximum payload of 45 kg. It can fly manually or pre-programmed for up to eight hours at a maximum speed of 58 m/sec and a maximum altitude of 4 km. Its maximum range is 30 km and it can transmit jam resistant data up to 185 km. The FLIR sensor is a key payload which can provide day and night thermal imaging to the Korean Army. The FLIR sensor provides a real map-like image with a FOV of 40 degree by 30 degree. It consists of optics, scanning mechanism, electronics and display. A hemisphere irdome which has a diameter of 30 cm, protect the FLIR sensor from aerodynamic forces, abrasion of dust, dirt and insects during takeoff and cruising. The irdome is made of silicon and uses an aluminum oxide antireflection coating.

The optics are refractive, consisting of telescope lenses and a detector lens. The telescope lens comprised two different lens materials. The first lens is made of germanium with refractive index of 3.41. The second lens is made of zinc selenide. The telescope lens

is a F/2 design with a focal length of 14.7 cm, and a total blur circle of 1.25 mrad. The detector lens is made of silicon with a exit pupil of 1.8 cm.

The parallel linear beam scanner uses a six-facet polygonal rotational external mirror to move the object image over the detector array. The rotational mirror is made of aluminum and has a outer drum radius of 2.6 cm and a inner of 2.251 cm from the center of a drum mirror.

The sensor footprint is proportional to the RPV altitude and the FOV of FLIR sensor.

The number of resolution elements depends on the FOV and IFOV of the FLIR sensor. The total resolution element per second is proportional to across-track elements and along-track elements. We calculate the total resolution elements per second of 107492 to achieve the FOV of 40° by 30° at altitude of 200 m at a velocity of 30.86 m/sec.

A Joule-Thompson cooled photoconductive $Hg_{0.79}Cd_{0.21}Te$ detector was selected as the detector for the FLIR sensor. HgCdTe has the detectivity of $3 \times 10^{11}(Hz^{1/2}/w)$ using 8 - 12 μm spectral window and cooled to 77°K, and higher responsivity than the other materials.

The detector array will be configured with 55 x 1, and pixel size of 147 x 147(μm^2). The configuration will provide a certain overlap between scan lines in order to minimize signal from point objects while maintaining high resolution.

The FLIR has a FOV of 40° by 30° and an IFOV of 1 mrad per each detector with thermal resolution of 0.2°C to 0.4° C at the design frequency and 525 lines TV-compatible video signal.

Recognition range capability of the FLIR sensor is a function of target size, clarity of the atmosphere, temperature differential of the target relative background and size and resolution of the optics. The maximum estimated range is 14.7 km for a probability of 0.95 and a false alarm rate of 0.05.

Total estimated sensor and optical package is about 45 kg, and total power of 1950 watts, and total volume of 0.14 m^3.

This thesis investigated a close-range mission, parallel scanned FLIR RPV sensor. The performance of this FLIR sensor, selection of detector arrays between scanning and staring mode, multiplexing the output data, TV compatible output video format, and transmitting output data to the ground station (data link) in real time should be considered further. Cooled arrays using HgCdTe large focal plane arrays and superconductors can be used in the present applications. Future designs can consider active and passive IR sensor combinations.

APPENDIX.A IR FUNDAMENTALS

1. THE ELECTROMAGNETIC SPECTRUM [Ref.6]

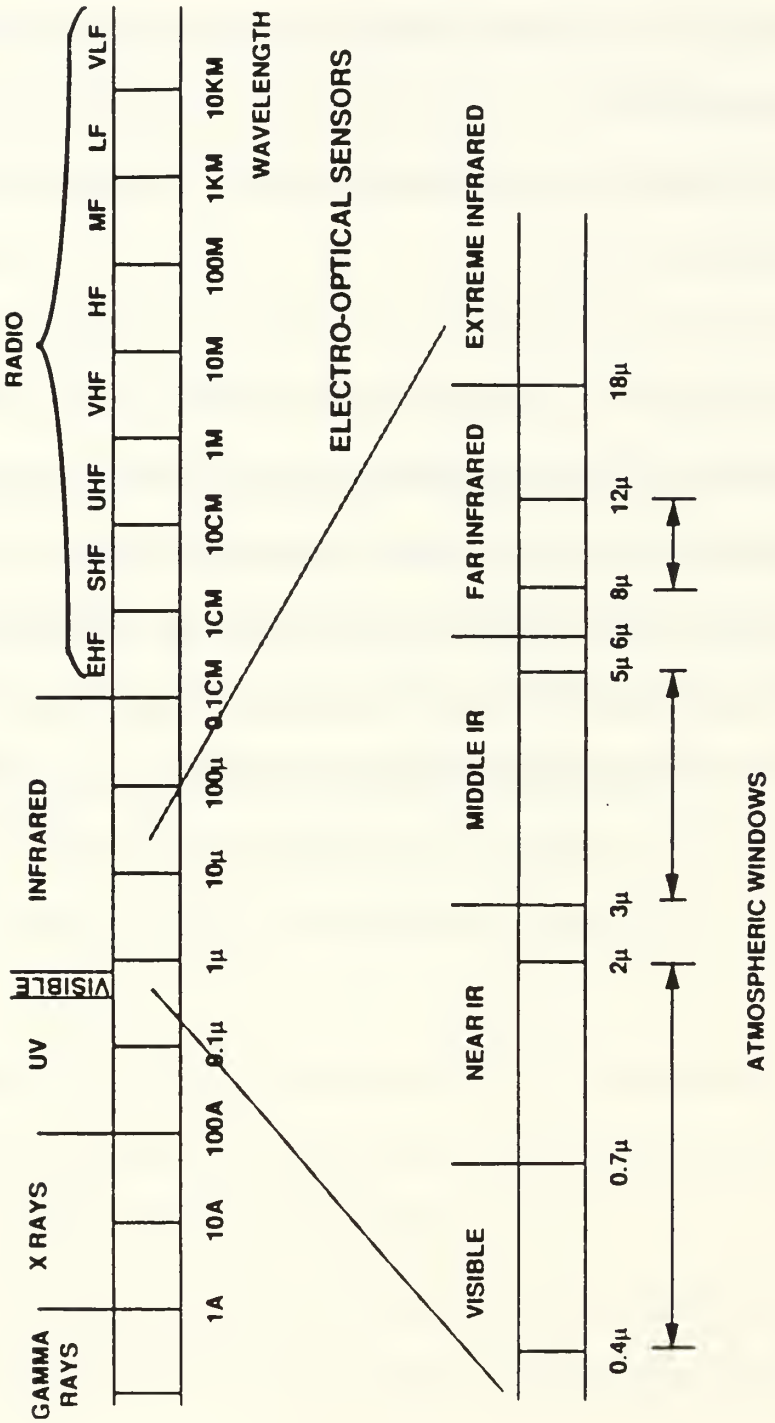

- EVERY OBJECT IN NATURE IS A SOURCE OF RADIATION
- RADIATION IS GENERATED BY VIBRATION AND ROTATION OF ATOMS AND MOLECULES WITHIN AN OBJECT
- AS THE TEMPERATURE OF AN OBJECT INCREASES, THE TOTAL RADIATED ENERGY OF THE OBJECT WILL INCREASE WITH A CORRESPONDING SHIFT IN THE PEAK OF THE RADIATION WAVELENGTH TOWARD A SHORTER WAVELENGTH
- IR ENERGY EMITTED BY AN OBJECT IS PROPORTIONAL TO THE FOURTH POWER OF ITS ABSOLUTE TEMPERATURE (BLACK BODY)

$$W_s = \sigma_s T^4$$

σ_S = STEFAN-BOLTZMAN CONSTANT (5.6697×10^{-12} WATTS $\cdot CM^{-2} \cdot °K^{-4}$)
T = °K
W_S = WATTS $\cdot CM^{-2}$

- STEFAN-BOLTZMAN LAW GIVES THE TOTAL RADIANT POWER OF A BLACK BODY AS A FUNCTION OF TEMPERATURE, BUT DOES NOT DESCRIBE THE WAVELENGTH DEPENDENCE

- PLANCK'S LAW DESCRIBES THE SPECTRAL DISTRIBUTION OF THE RADIATION FROM A BLACKBODY AS

$$W_\lambda = \frac{2\pi hc^2}{\lambda^5} \frac{1}{e^{ch/\lambda kT} - 1}$$

WHERE

W_λ	=	SPECTRAL RADIANT EMITTANCE $Wcm^{-2}\mu^{-1}$
λ	=	WAVELENGTH, (MICRON)
h	=	PLANCK'S CONTANT = 6.6256×10^{-34} $Wsec^2$
T	=	ABSOLUTE TEMPERATURE, °K
c	=	VELOCITY OF LIGHT = $2.99 \times 10^{10} cmsec^{-1}$
k	=	BOLTZMANN'S CONSTANT = $1.380 \times 10^{-23} Wsec°K^{-1}$

4. PLOT OF SPECTRAL RADIANT EMITTANCE AS A FUNCTION OF WAVELENGTH [Ref.5]

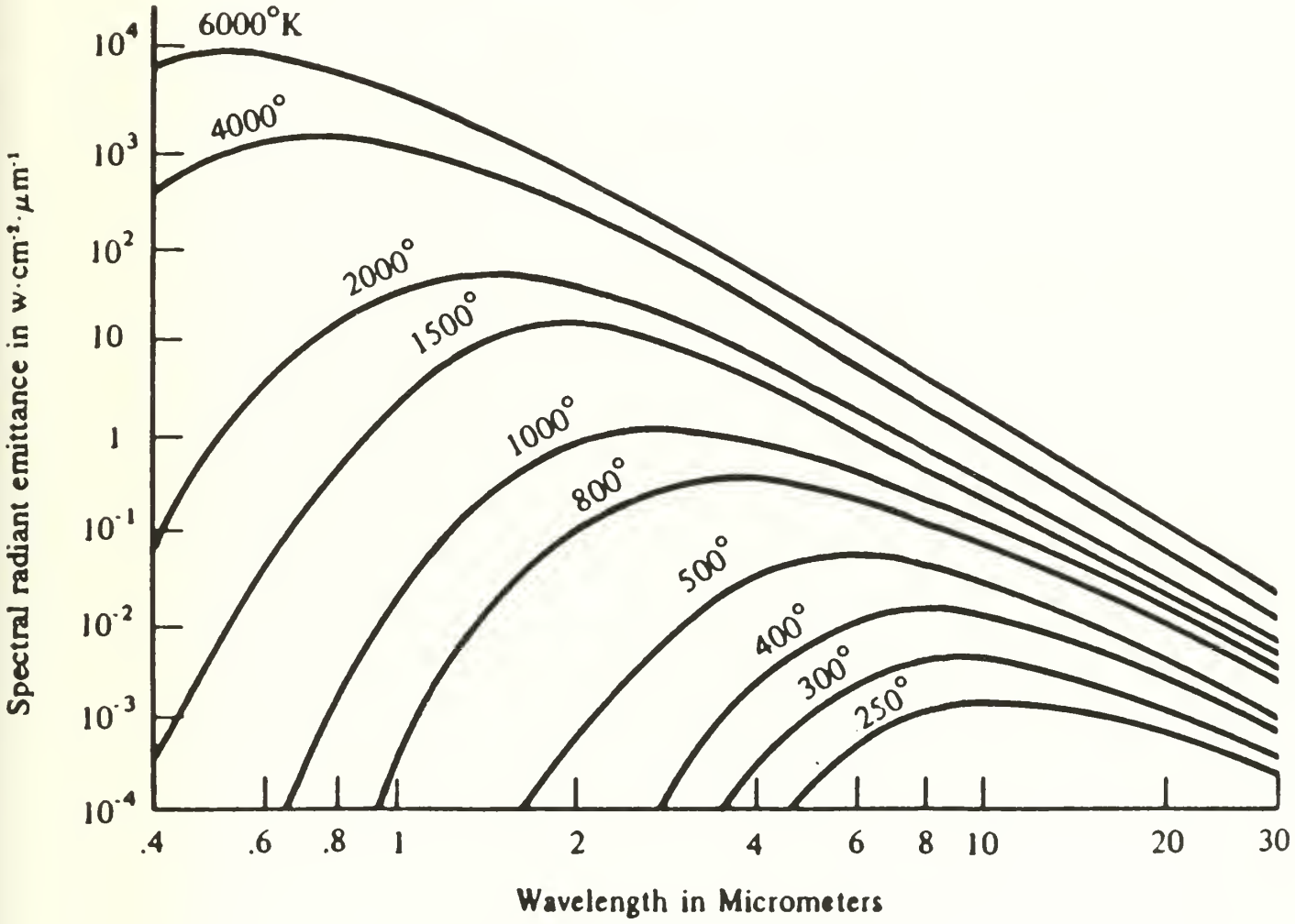

5. ATMOSPHERIC TRANSMISSION BASIC CONCEPTS OVERVIEW

DEFINITION: THE GENERAL PROCESS BY WHICH RADIANT FLUX IS ATTENUATED IN PASSING THROUGH THE ATMOSPHERE IS CALLED EXTINCTION

BASIC DESIGN RELATIONSHIPS:

$\tau = e^{-\sigma x}$, x = RANGE OR DISTANCE, τ = TRANSMITTANCE

$\sigma = a + \alpha$, σ = EXTINCTION COEFFICIENT

a = ABSORPTION COEFFICIENT, MORE IMPORTANT IN INFRARED REGION

α = SCATTERING COEFFICIENT, DERIVES FROM SCATTERING BY

- GAS
- MOLECULES
- HAZE
- FOG OR
- CLOUD
  SMOKE
  DUST

BOTH a AND α DEPEND ON WAVELENGTH, λ, AND VARY WITH WEATHER AND ALTITUDE

6. ATMOSPHERIC TRANSMISSION [Ref.5]

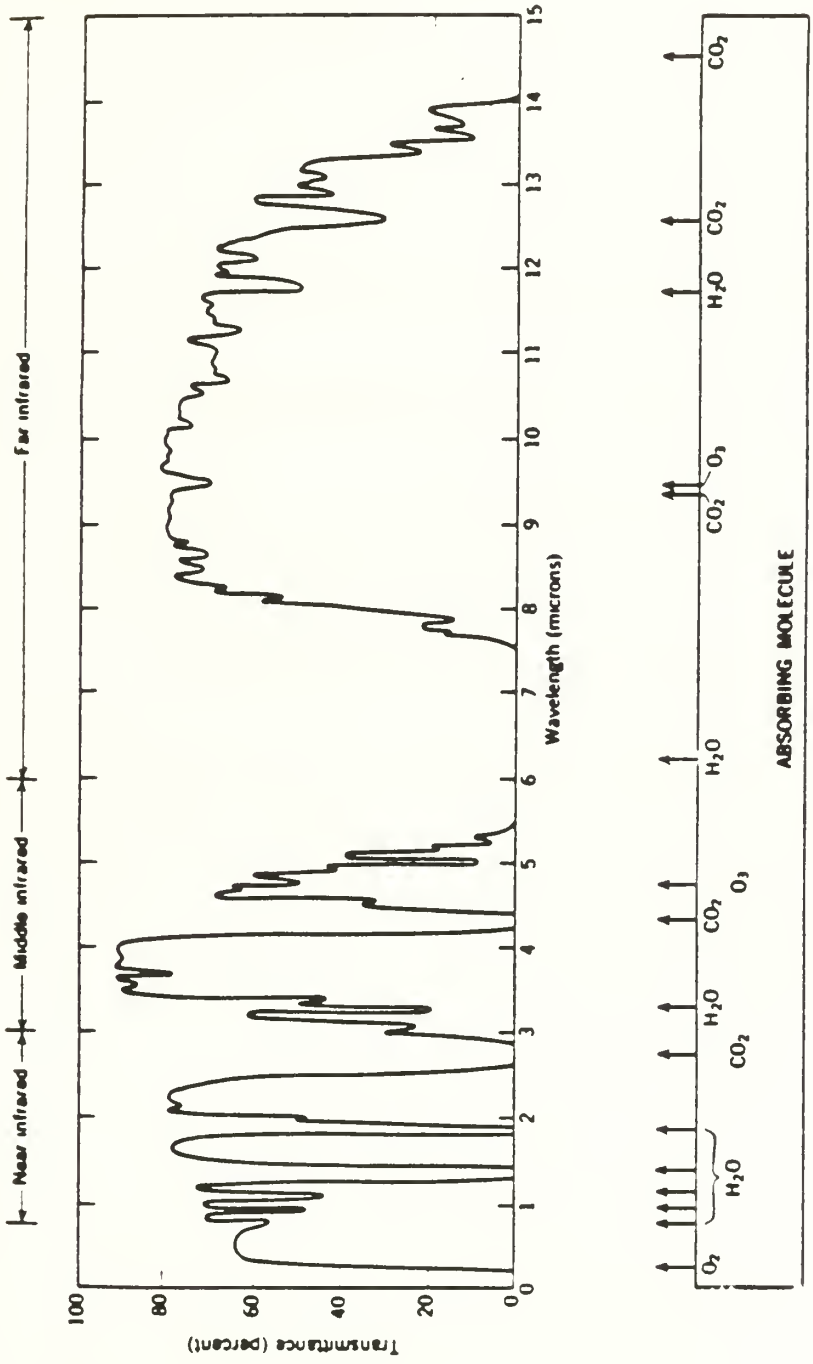

- **LOWTRAN VI (USAF)**
  - **33 LAYER MODEL OF ATMOSPHERE**
  - **.25 TO 28.5 MICRONS**

    MODERATE SPECTRAL RESOLUTION
  - **2 SEASONAL (WINTER, SUMMER)**

    3 CLIMATE (TROPICAL, MIDLATITUDE, SUB ARCTIC)

    6 VISIBILITY (RURAL, URBAN, CLEAR, HAZE, FOG [2])

8. EMISSIVITY [Ref.5]

EMISSIVITY (e) IS GIVEN BY THE RATIO OF THE RADIANT EMITTANCE OF THE SOURCE TO THE RADIANT EMITTANCE OF A BLACK BODY AT THE SAME TEMPERATURE

EMISSIVITY IS A NUMERIC VALUE BETWEEN 0 AND 1

BLACK BODY $e = 1$
GRAY BODY $0 \leq e \leq 1$

COLORED OR SELECTIVE BODY $e(\lambda)$ **VARIES WITH WAVELENGTH**

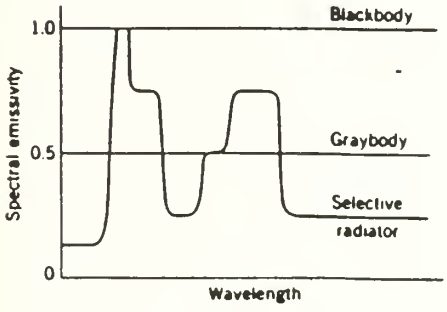

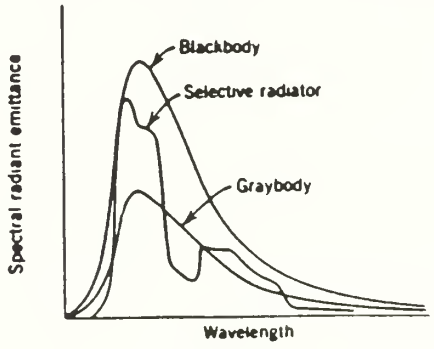

9. SPECTRAL DISTRIBUTION OF THERMAL AND SELECTIVE RADIATOR [Ref.5]

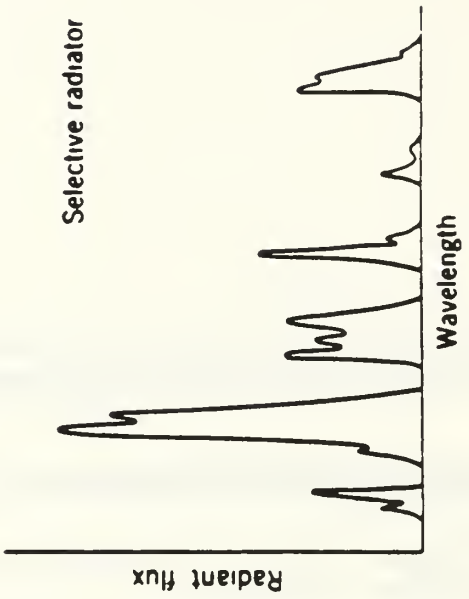

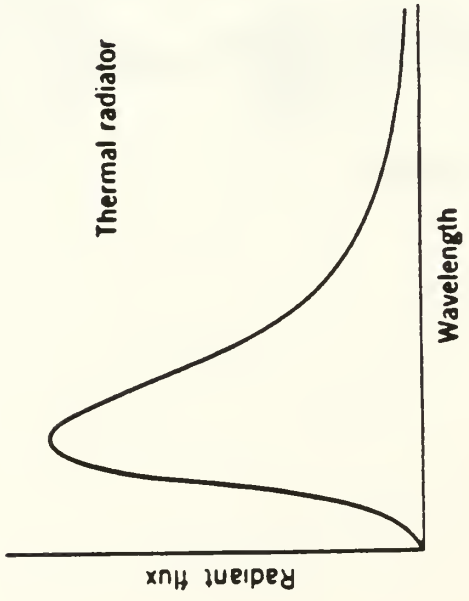

10. SPECTRAL RADIANCE OF VARIOUS NATURAL SOURCES [Ref.6]

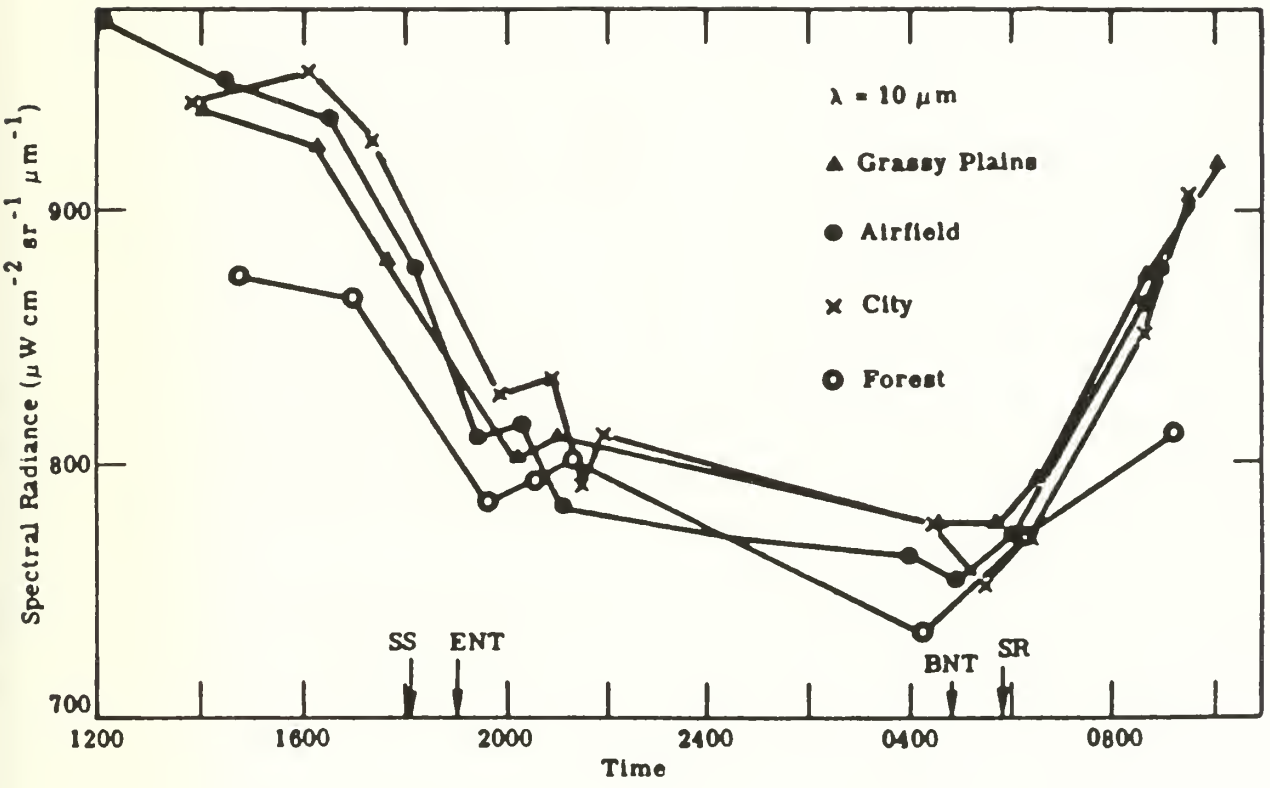

APPENDIX.B BASIC IR OPTICS

1. BASIC OPTICAL TERMS

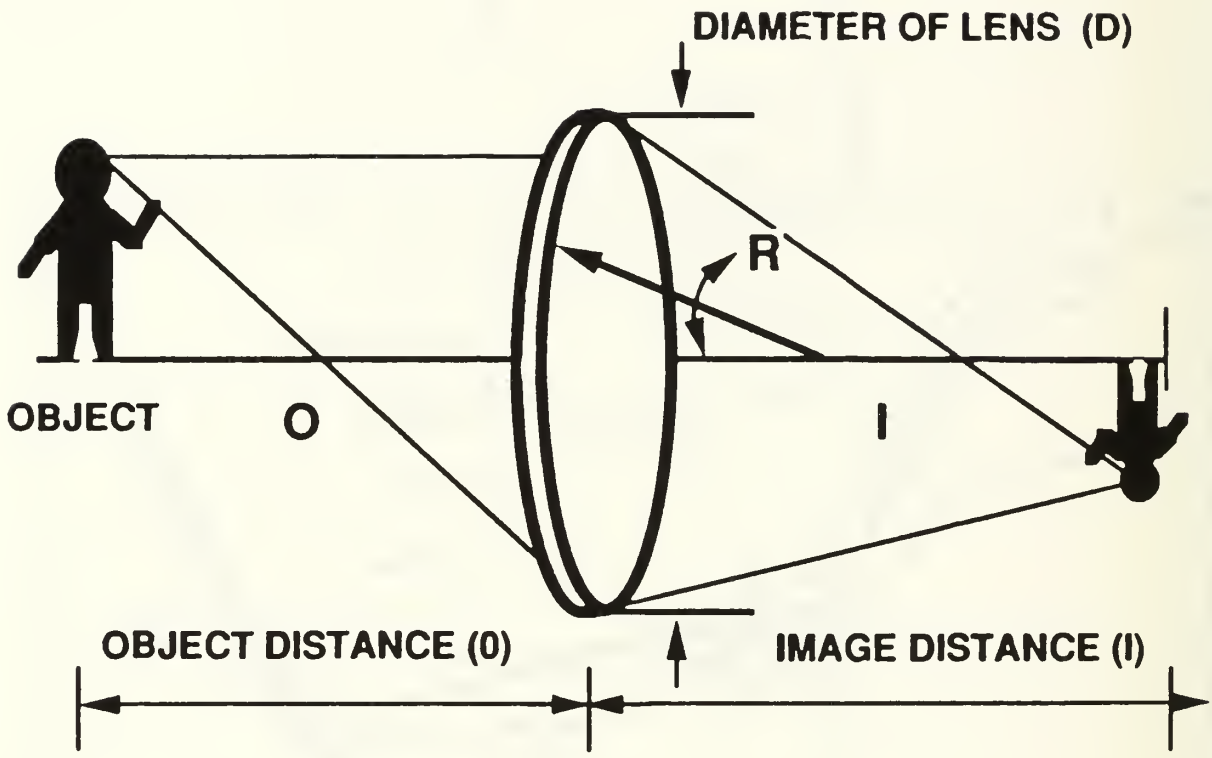

$$\frac{1}{f} = \frac{1}{0} + \frac{1}{I}$$

f = FOCAL LENGTH

$$\text{F NUMBER} = \frac{\text{FOCAL LENGTH}}{\text{DIAMETER}}$$

N (λ) = INDEX OF REFRACTION

$$\frac{1}{f} = (N(\lambda) - 1)\left(\frac{1}{R_1} - \frac{1}{R_2}\right)$$

D = DIAMETER LENS

(PRACTICAL LIMIT 0.5)

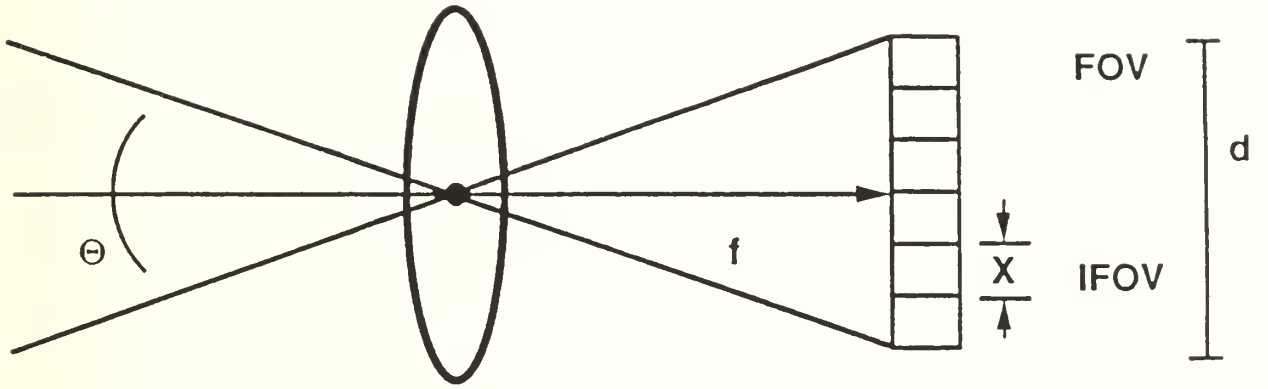

SENSOR FIELD OF VIEW (FOV)

$$\Theta = 2 \cdot TAN^{-1} \left[\frac{d/2}{f} \right]$$

INSTANTANEOUS FIELD OF VIEW (IFOV)

$$TAN\Theta \simeq \Theta = \frac{X}{f} \quad \text{PIXEL (IFOV)}$$

REFRACTIVE (TRANSMISSION)

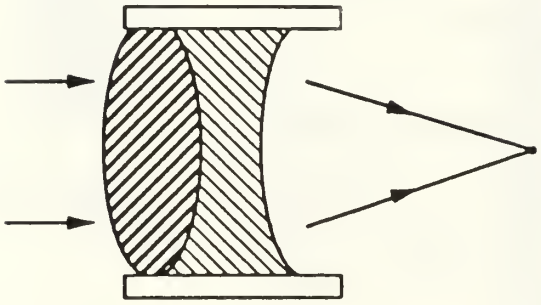

ADVANTAGES

- HIGH RESOLUTION (FLIR)
- LARGER FOV

DISADVANTAGES

- LOWER TRANSMISSION (HIGH N)
- HEAVY
- SOME LENSES ARE SALT BASED

CATADIOPTRIC (REFLECTIVE)

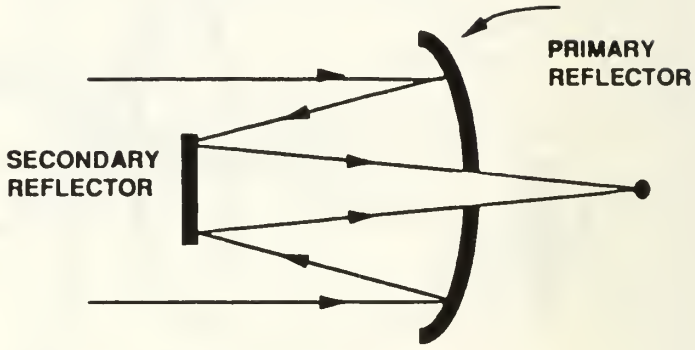

ADVANTAGES

- SMALL PACKAGE
- LIGHTWEIGHT
- EXCELLENT FOR SMALL FOVs
- HIGH TRANSMISSION

DISADVANTAGES

- SMALLER FOVs
- DEAD CENTER AREA

4. PROBLEM WITH OPTICS THAT AFFECT SENSOR PERFORMANCE [Ref.6]

• CHROMATIC ABERRATIONS

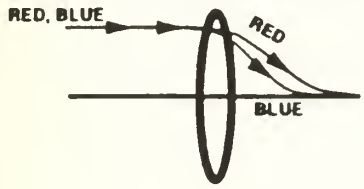

• BLUR SIZE/DEPTHS OF FOCUS

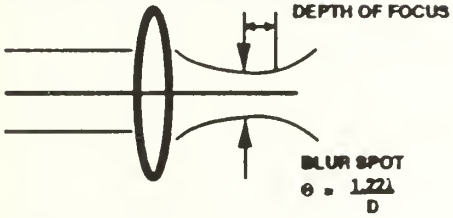

• FIELD CURVATURE

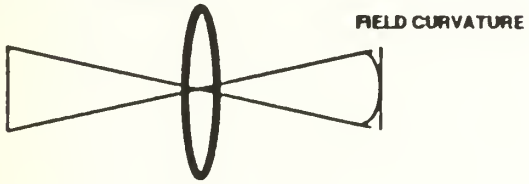

• DISTORTION

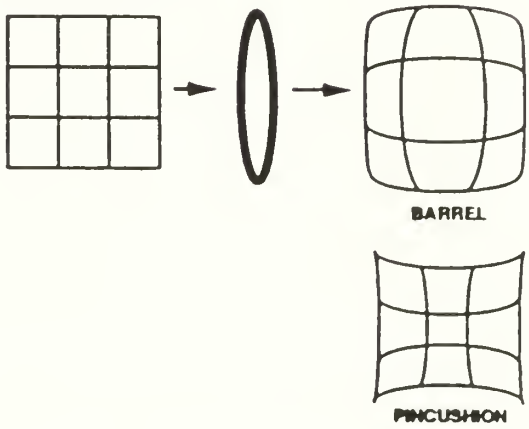

• INDEX OF REFRACTION (N)

HIGH N — HIGH REFLECTIVITY
LOW TRANSMISSION

$$\text{REFLECTIVITY} = \frac{(N-1)^2}{(N+1)^2}$$

N = 4.0 R = 36% PER SURFACE

5. MEASURING LENS QUALITY MTF [Ref.6]

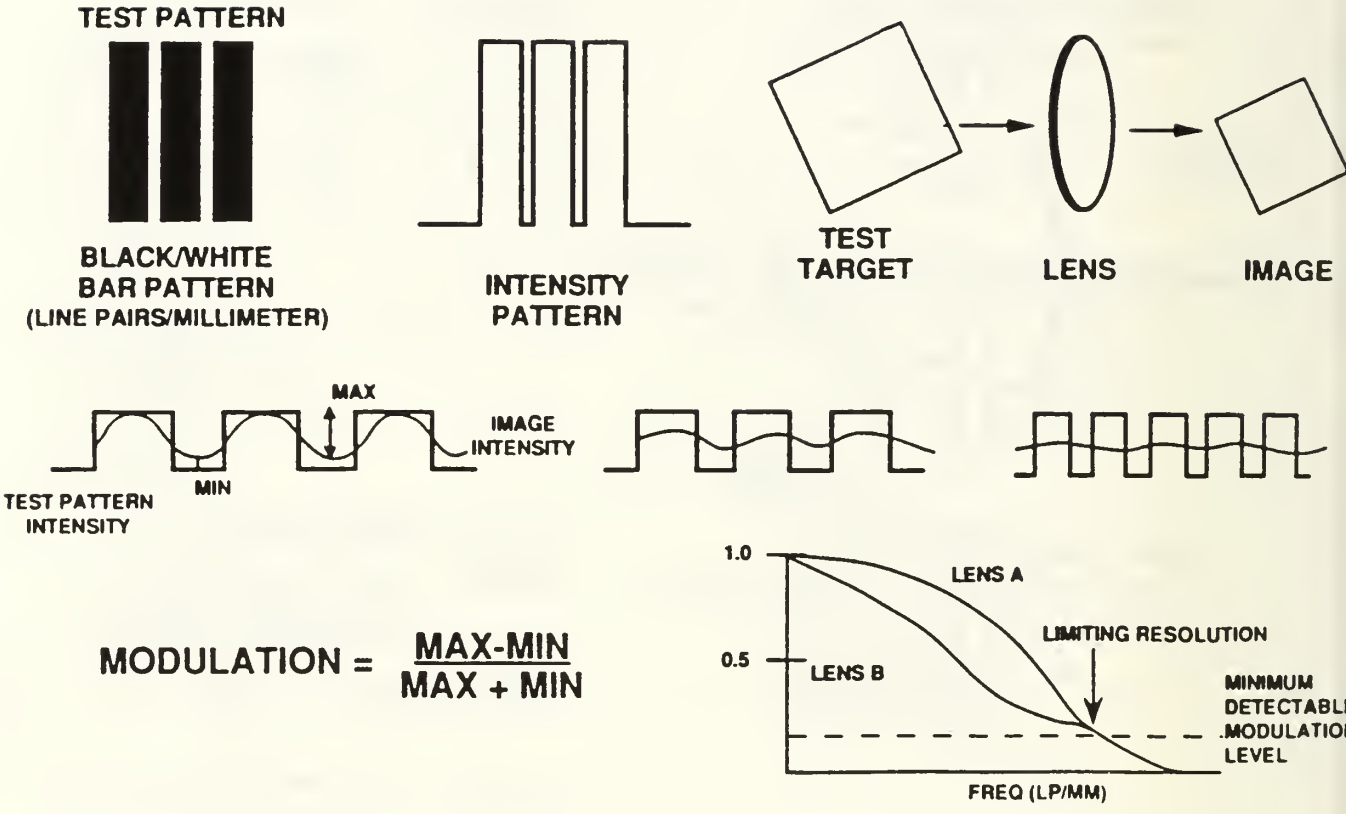

6. OPTICAL MATERIALS [Ref.5]

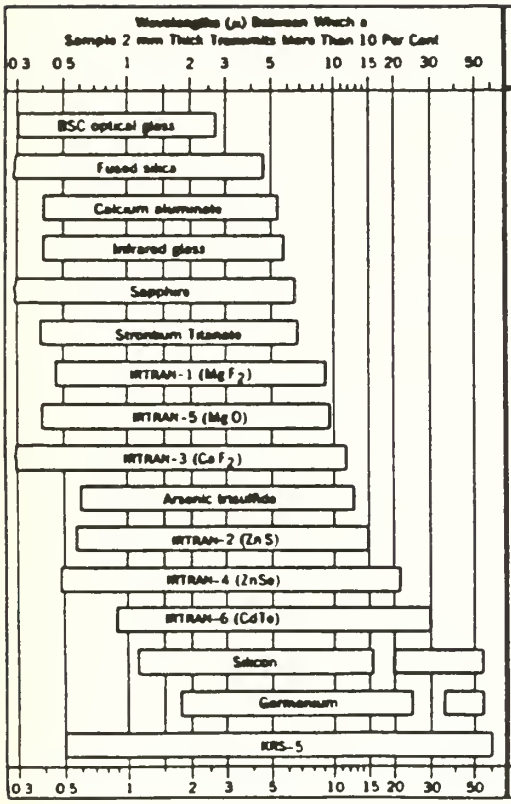

Maximum Window Diameter (in.)	Density (g cm^{-3})	Index of Refraction (Midpoint of Useful Range)	Coefficient of Linear Expansion ($°C^{-1} \times 10^{-6}$)	Thermal-Stress Figure of Merit ($\times 10^{-4}$)
~30	2.52	1.48	9.9	0.2
18	2.20	1.43	0.5	5.3
5	3.07	1.63	9.3	~0.2
~10	4.51	1.72	8.7	~0.2
6	3.98	1.67	5.7	2.1
1	5.12	2.21	9.4	~0.2
8	3.18	1.34	10.7	2.0
6	3.58	1.66	12.0	1.8
6	3.18	1.39	20	0.7
18	3.20	2.40	24.6	0.05
8	4.09	2.20	6.6	4.0
7	5.27	2.40	7.7	2.4
3	5.85	2.68	5.5	3.2
16	2.33	3.42	2.4	35
24	5.33	4.00	5.3	10
5	7.37	2.37	58	0.1

7. IR FILTERS [Ref.6]

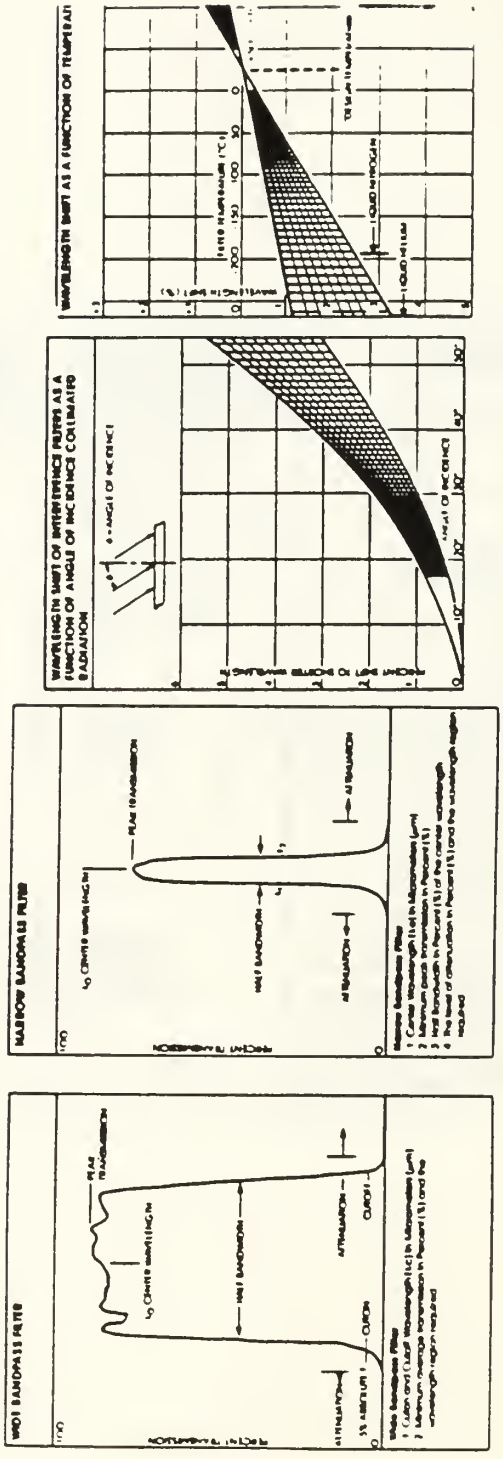

APPENDIX.C IR DETECTORS / COOLERS

1. THERMAL DETECTORS

THERMOCOUPLE	—	JUNCTION BETWEEN TWO METALS IN WHICH THE VOLTAGE OF THE THERMOELECTRIC JUNCTION IS MEASURED AS A FUNCTION OF TEMPERATURE
BOLOMETER	—	DETECTOR WHICH CHANGES ITS ELECTRICAL RESISTANCE WHEN HEATED. USUALLY CHARACTERIZED BY LONG TIME CONSTANTS
PYROELECTRIC FERROELECTRIC	—	AN UNCOOLED DETECTOR THAT RESPONDS TO THE TIME RATE OF CHANGE OF THE ABSORBED INFRARED RADIATION
PHOTOELECTRIC DETECTOR	—	INCIDENT PHOTON TRANSFERS ITS ENERGY TO AN ELECTRON IN THE DETECTOR MATERIAL. USUALLY THE MOST SENSITIVE, FASTEST RESPONSE AND TYPICALLY COOLED

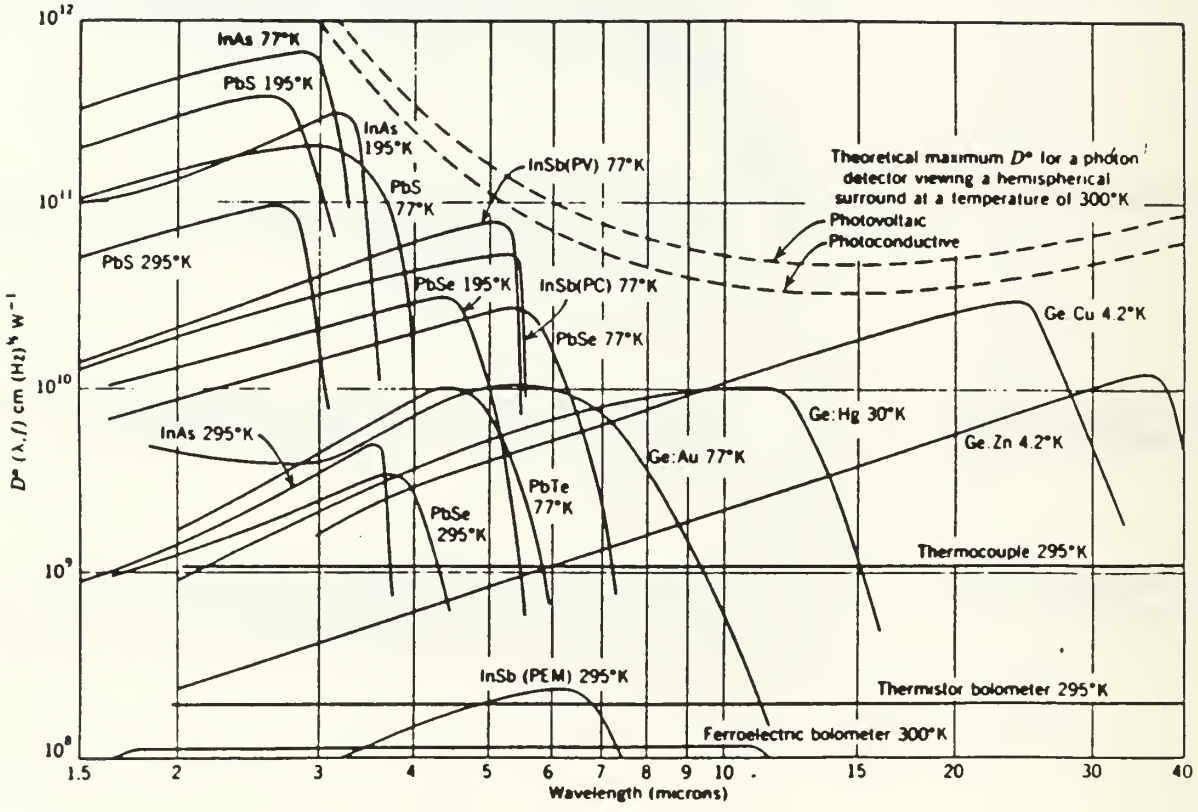
InAs 77°K
PbS 195°K
InAs 195°K
PbS 77°K
InSb(PV) 77°K
Theoretical maximum D* for a photon detector viewing a hemispherical surround at a temperature of 300°K
Photovoltaic
Photoconductive
PbS 295°K
PbSe 195°K
InSb(PC) 77°K
PbSe 77°K
Ge Cu 4.2°K
Ge:Hg 30°K
Ge Zn 4.2°K
InAs 295°K
Ge:Au 77°K
PbTe 77°K
PbSe 295°K
Thermocouple 295°K
InSb (PEM) 295°K
Thermistor bolometer 295°K
Ferroelectric bolometer 300°K
D* (λ,f) cm (Hz)^½ W^-1
Wavelength (microns)

AREA:	$A_d = XY\ (CM)^2$
RESISTANCE OF IMPEDANCE:	$Z\ (\Omega)$
RESPONSIVITY VS. WAVELENGTH:	$R\ (\lambda)\ (VW)^{-1}$
PEAK RESPONSE WAVELENGTH:	$\lambda_p (\mu m)$
CUTOFF WAVELENGTH:	$\lambda co (\mu M)$
NOISE EQUIVALENT POWER:	$P_n(\lambda)$ or NEP(W)
DETECTIVITY VS. WAVELENGTH:	$D^*\lambda\ (CM\text{-}Hz^{1/2}\text{-}W)$
TIME CONSTANT (RESPONSIVE TIME CONSTANT):	$\tau(\mu S$ or $S)$
BLIP DETECTIVITY:	$D^*\ \lambda BLIP\ (CM - Hz^{1/2}\text{-}W)$
D*f* PRODUCT:	f* = FREQUENCY WHERE D* FALLS TO 0.707 OF LOW FREQUENCY VALUE, ETC.

D STAR (D*)

$$D^* = \frac{(Ad\Delta f)^{1/2}}{NEP} \quad \text{UNITS CM(Hz)}^{1/2}\text{W}^{-1}$$

Δf IS THE ELECTRICAL BANDWIDTH MEASURED IN HERTZ

DETECTOR NOISE IN SOME DETECTORS (Si, Ge) IS PROPORTIONAL TO THE FLUCTUATIONS IN THE BACKGROUND PHOTONS. THESE DETECTORS ARE BACKGROUND LIMITED AND ARE REFERRED TO AS BLIP. BLIP STANDS FOR BACKGROUND LIMITED PHOTODETECTOR

$$\text{RESPONSIVITY (R)} = \frac{Vs}{HAd} \quad \text{UNITS} \quad \frac{\text{VOLTS}}{\text{WATT}}$$

H RMS VALUE OF THE IRRADIANCE ON THE DETECTOR
Ad SENSITIVE AREA OF THE DETECTOR
Vs RMS VALUE OF THE SIGNAL COMPONENT

NOISE EQUIVALENT POWER (NEP)
RADIANT FLUX NECESSARY TO GIVE AN OUTPUT SIGNAL EQUAL TO THE DETECTOR NOISE

$$\text{NEP} = \frac{HAdVn}{Vs} \text{ UNITS WATTS}$$

Vn IS RMS VALUE OF THE NOISE VOLTAGE

$$\text{NEP} = \frac{Vn}{R}$$

CAUTIONS

D* WAS INTENDED TO BE A FIGURE OF MERIT WHICH DEPENDED ONLY ON DETECTOR MATERIAL. NOT ALWAYS TRUE. DETECTOR PERFORMANCE ALSO VARIES WITH

- **CELL ASPECT RATIO** 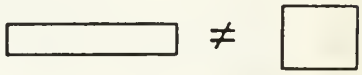
- **CELL THICKNESS**
- **CELL SIZE (AS IT INFLUENCES PROBABLITY OF GETTING DEFECTS)**
- **F/NO. OF INCIDENT RADIATION**
- **CELL TEMPERATURE**
- **QUALITY OF CONTACTS (OHMIC)**
- **SURFACE QUALITY (1/f NOISE)**
- **MICROPHONICS**

7. COMPARISON OF IR DETECTOR COOLERS [Ref.6]

THERMO ELECTRIC COOLERS

- WHEN CURRENT FLOWS IN A CIRCUIT CONSISTING OF TWO DISSIMILAR METALS, HEAT IS ABSORBED IN ONE AND RELEASED IN ANOTHER
- LOW VOLTAGE, HIGH CURRENT
- COOLDOWN TIME - SECONDS, SINGLE STAGE
- LOW TEMP (-120°C, 6 STAGE)

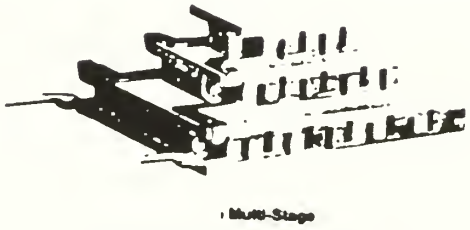

JOULE-THOMSON

- MINIATURE GAS LIQUEFIER THAT COOLS BY BLOWING EXPANDING GAS OVER A HEAT EXCHANGER
- CLOSED/OPEN CYCLE
- TEMPERATURE DEPENDS ON GAS (TYPICALLY 77° - 85° K)
- COOLDOWN, SECONDS TO MINUTES

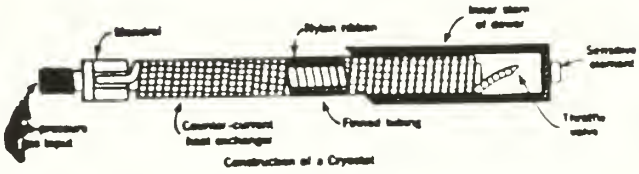

OTHERS

- CLAUDE, STIRLING

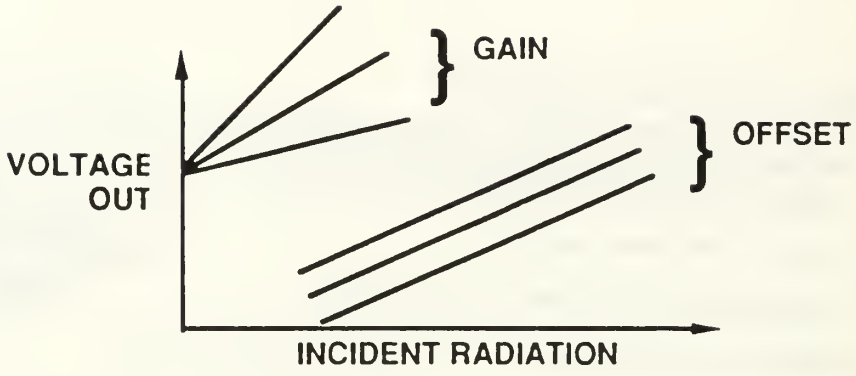

VOLTAGE OUTPUT = INCIDENT • RESPONSIVITY + OFFSET BIAS

$$= A \cdot X + B$$

GAIN ADJUSTMENT

OFFSET

SPECIAL NOTE: GAIN & OFFSET ARE NOT CONSTANT FROM DETECTOR TO DETECTOR

1. PREAMPS / POWER SUPPLIES

- **DYNAMIC RANGE OF INCIDENT RADIATION**

$$\text{DYNAMIC RANGE RADIATION} = \frac{\text{RADIANCE FOR MAXIMUM EXPECTED TEMP}}{\text{RADIANCE FOR MINIMUM EXPECTED TEMP}}$$

$$\text{DYNAMNIC RANGE PREAMP} = \frac{V_{MAX}}{V_{MIN}} = \frac{\text{R} \cdot \text{MAX RADIANCE ON DETECTOR}}{\text{R} \cdot \text{MINIMUM RADIANCE ON DETECTOR}}$$

V_{MAX} IS DETERMINED BY POWER SUPPLIES & PREAMP VOLTAGE SWING

V_{MIN} IS DETERMINED BY NOISE LEVEL OF SYSTEM

- **DETECTOR BIAS (VOLTAGES RANGE FROM 1V TO 250V)**

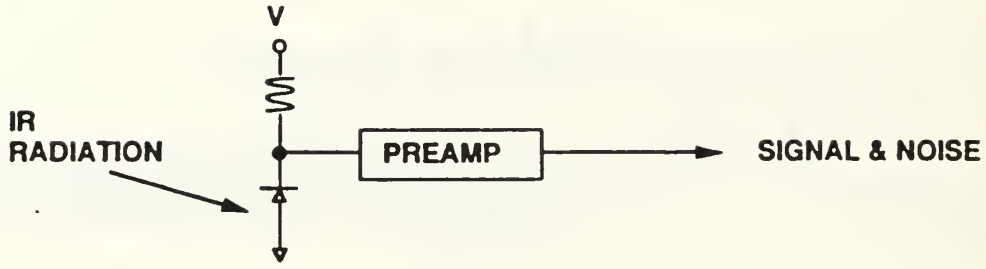

NOISE MAY BE DUE TO MANY DIFFERENT MECHANISMS:

1. THERMAL NOISE	$P = KT\Delta f$
2. SHOT NOISE	$(\overline{i^2})^{\frac{1}{2}} = (2IaC\Delta f)^{1/2}$
3. PHOTON NOISE	$\overline{\Delta n^2} = \bar{n}KT/(h\upsilon)$
4. GENERATION-RECOMBINATION NOISE	$\zeta = W_1^2/\mu V_D$
5. TEMPERATURE NOISE	$\overline{\Delta T^2} = KT^2/CH$
6. 1/f NOISE	$\overline{i^2} = KI^2/f^{\alpha}$
7. FLICKER NOISE	$= 1/f^{\alpha}$
8. PREAMPLIFIER NOISE	
9. QUANTIZATION OR PERIODIC NOISE	$(\overline{V_2})^{1/2} = d/2\sqrt{3}$

APPENDIX.E IR SENSORS AND PERFORMANCE

1. PASSIVE IR SENSOR [Ref.6]

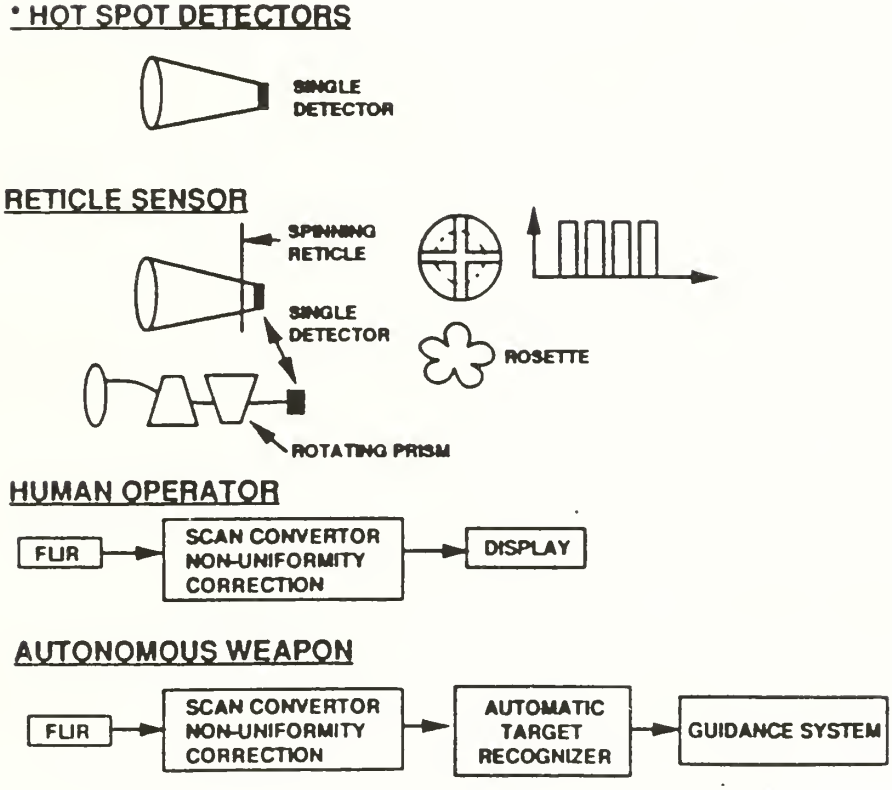

2. PASSIVE IMAGING IR SENSOR [Ref.6]

2-D SCANNING SYSTEM

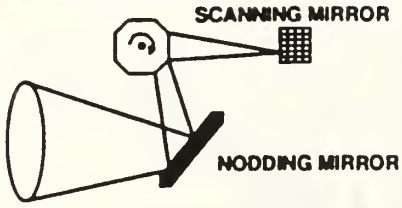

SCAN PATTERN

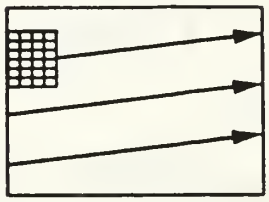

- SMALL NUMBER DETECTORS
- PERFORMANCE IMPROVED BY TDI
- VERY HIGH RPM OF SCANNING MIRROR

- COMPLICATED SCAN ELECTRONICS
- HIGH COST/HIGH PERFORMANCE
- VERY SMALL DWELL TIMES

1-D SCANNING SYSTEM

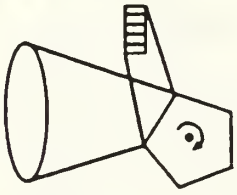

SCAN PATTERN

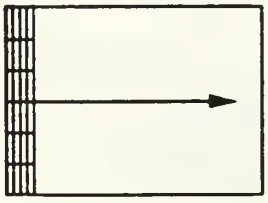

- LARGE LINEAR ARRAY (180 x 4)
- PERFORMANCE IMPROVED BY TDI
- MODERATE DWELL TIMES

STARING SYSTEM

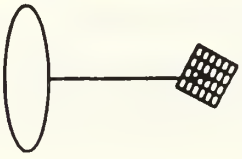

- LARGE ARRAY (512 x 256)
- PERFORMANCE IMPROVED BY LONG INTEGRATION TIME
- NO SCANNING

3. COMPARISON OF OTHER MEASURE FOR IR SYSTEM [Ref.6]

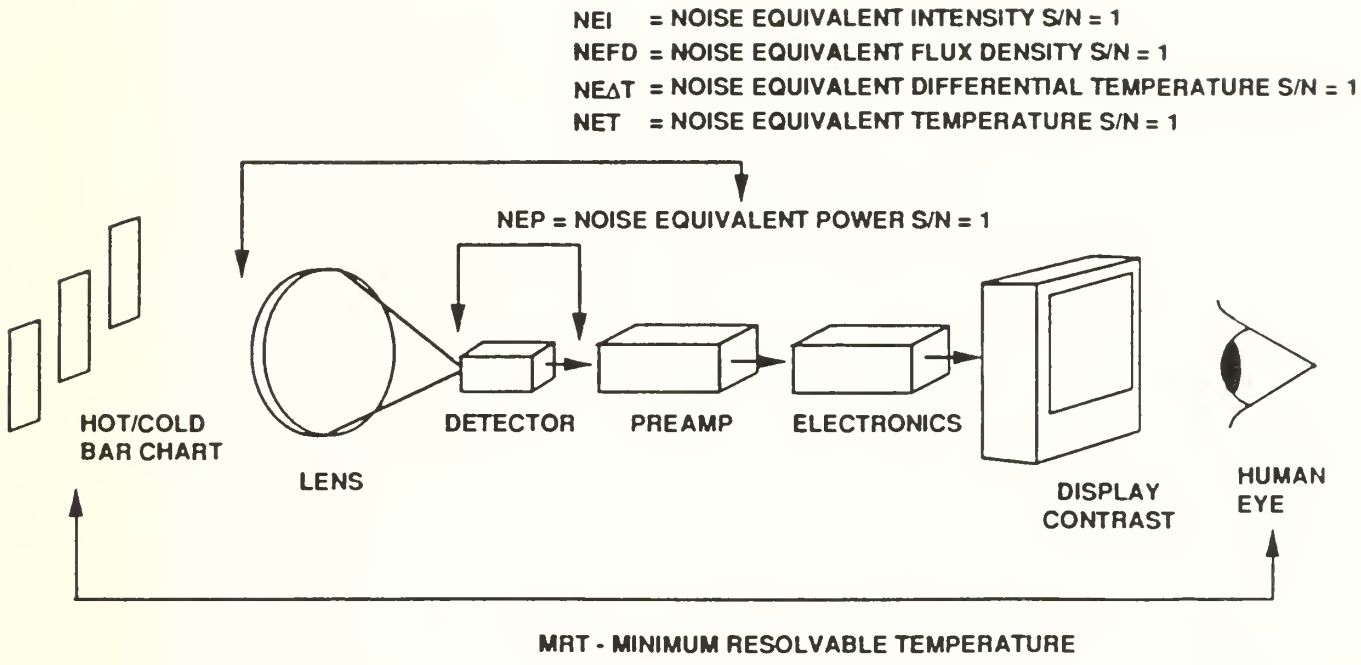

4. FUNDAMENTAL BLOCK DIAGRAM FOR A PASSIVE IR SENSOR [Ref.6]

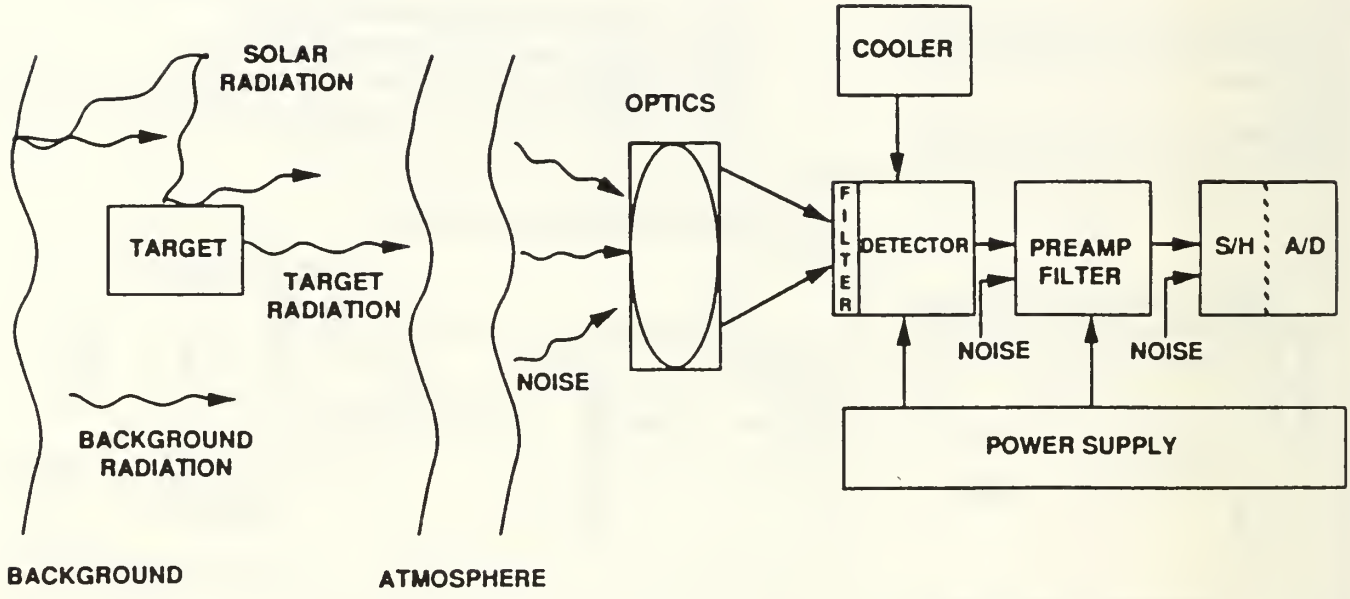

5. ANALYSIS OF IMAGING SYSTEM [Ref.6]

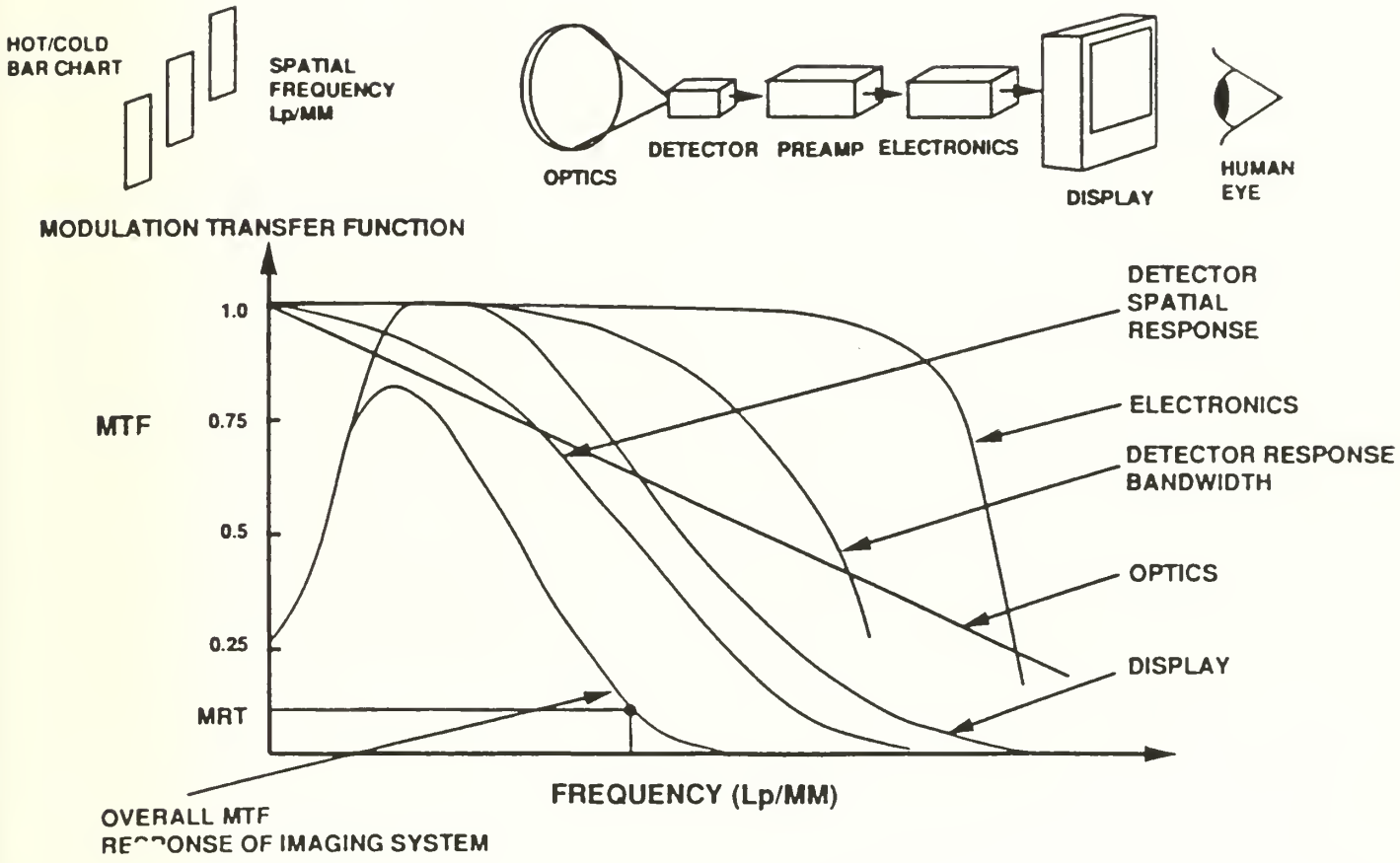

6. PROBABILITY OF DETECTION [Ref.6]

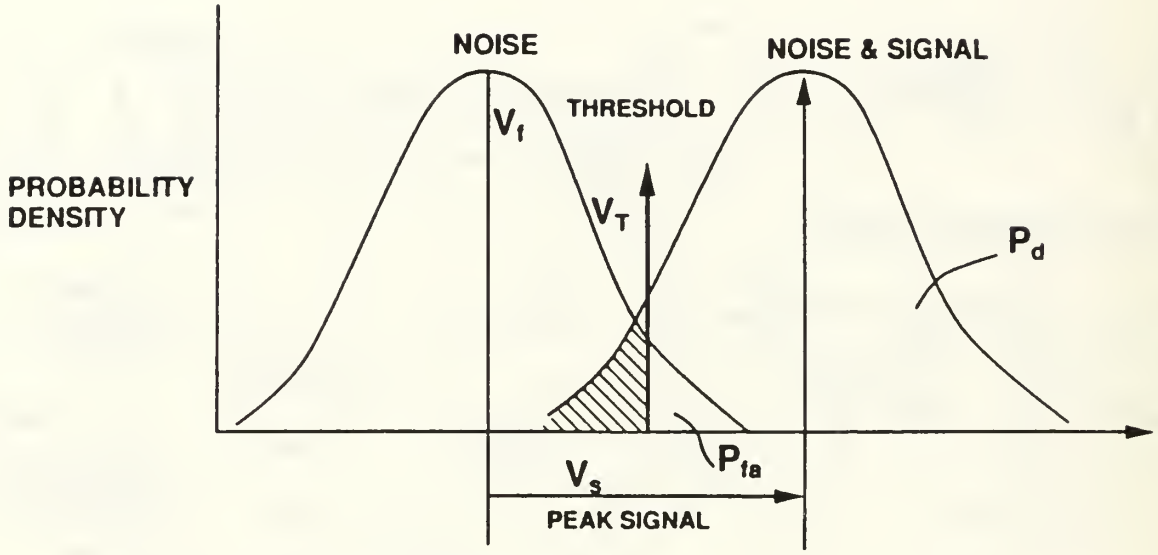

$$P_d = \frac{1}{\sqrt{2\pi}V_N}\int_{V_T}^{\infty} e^{-\frac{(V_1-V_s)^2}{2V_N^2}} dV \qquad V_N = \sigma$$

$$P_{fa} = \frac{1}{\sqrt{2\pi}V_N}\int_{V_T}^{\infty} e^{-\frac{V_1^2}{2V_N^2}} dV$$

7. PROBABILITY OF DETECTING A REAL TARGET [Ref.6]

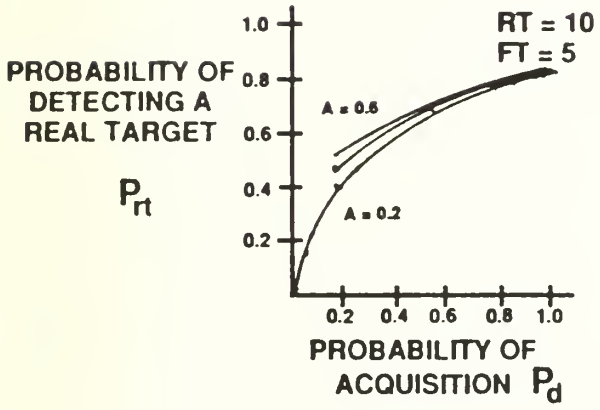

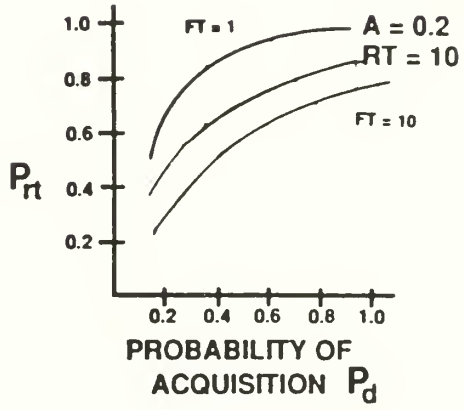

8. PROBABILITY VS. RANGE [Ref.6]

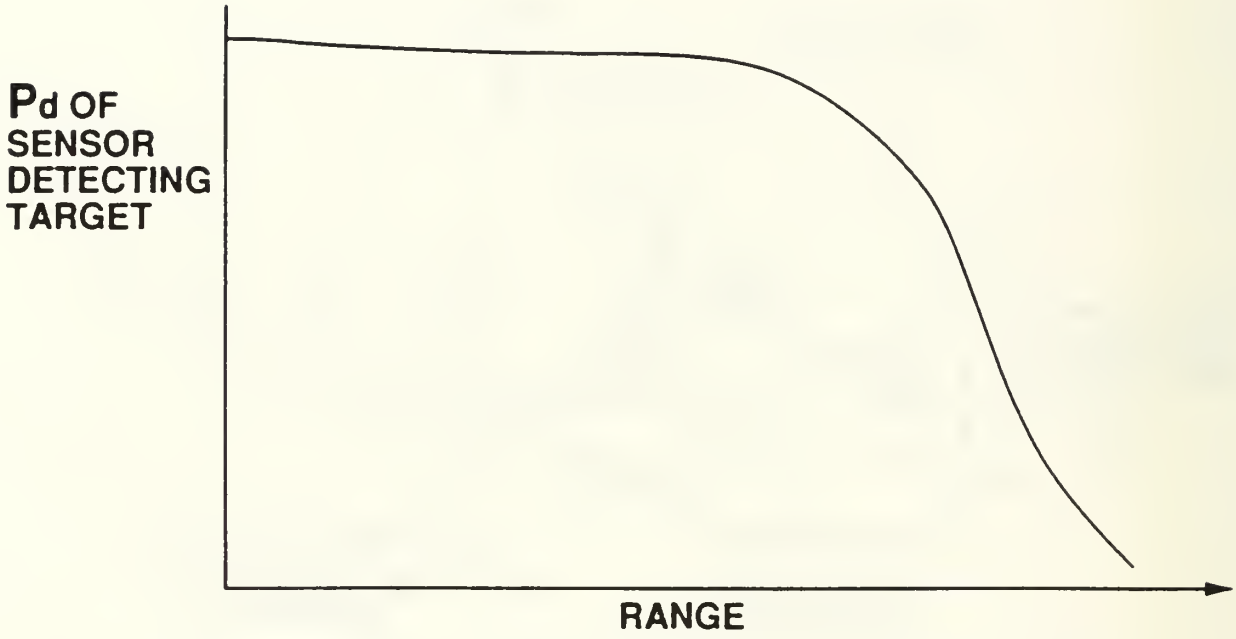

STEPS ① FROM SENSOR PARAMETERS CALCULATE SIGNAL/NOISE FOR RANGE

② CONVERT S/N RATIO TO Pd (RANGE)

9. IR DETECTION PERFORMANCE [Ref.6]

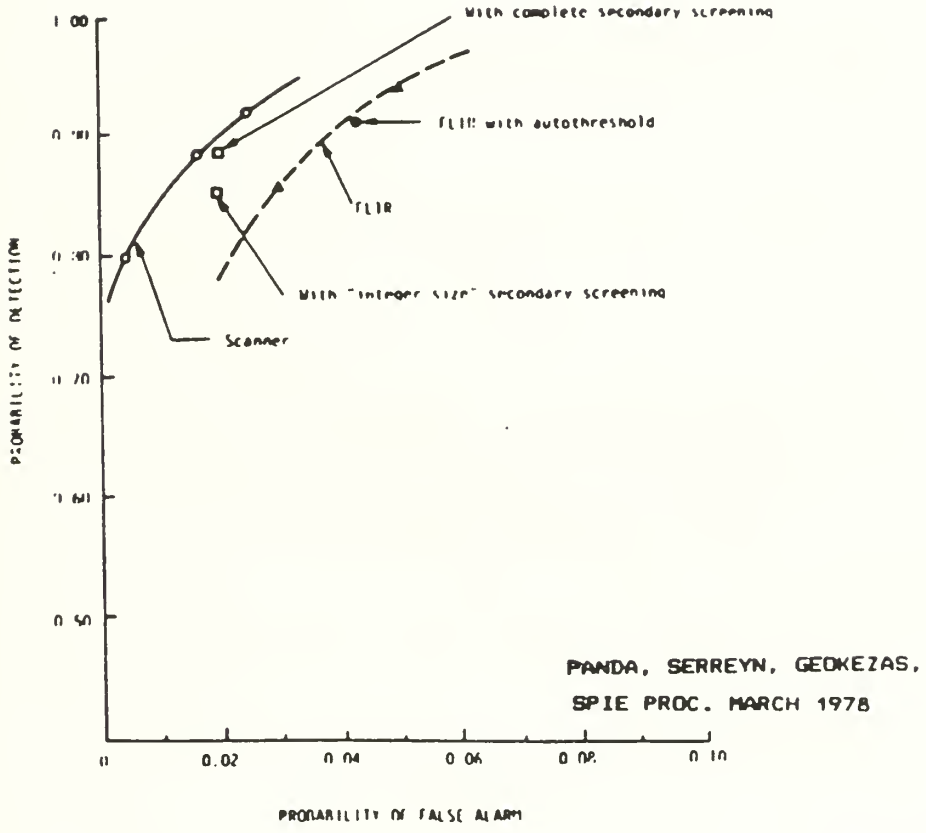

- FOR HOT SPOT DETECTION
  USE NOISE OR CLUTTER PROBABILITY DISTRIBUTION

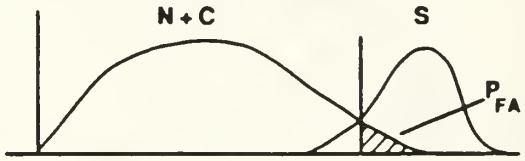

SABT40T

- FOR HIGH RESOLUTION IMAGE PROCESSING
  P_F = 0 FROM THERMAL SOURCES
  P_F = DISCRETE TARGET-LIKE PROBABILITY
  (ACTUAL OBJECTS USUALLY)
  (EMPIRICALLY ESTIMATED)

- IF 1KM^2 AREA IS SEARCHED; DESIRE RFTD < $\frac{1}{KM^2}$

- RFTD = RESIDUAL FALSE TARGET DENSITY

APPENDIX.F SENSOR GEOMETRY

1. DEFINITION OF TERMS

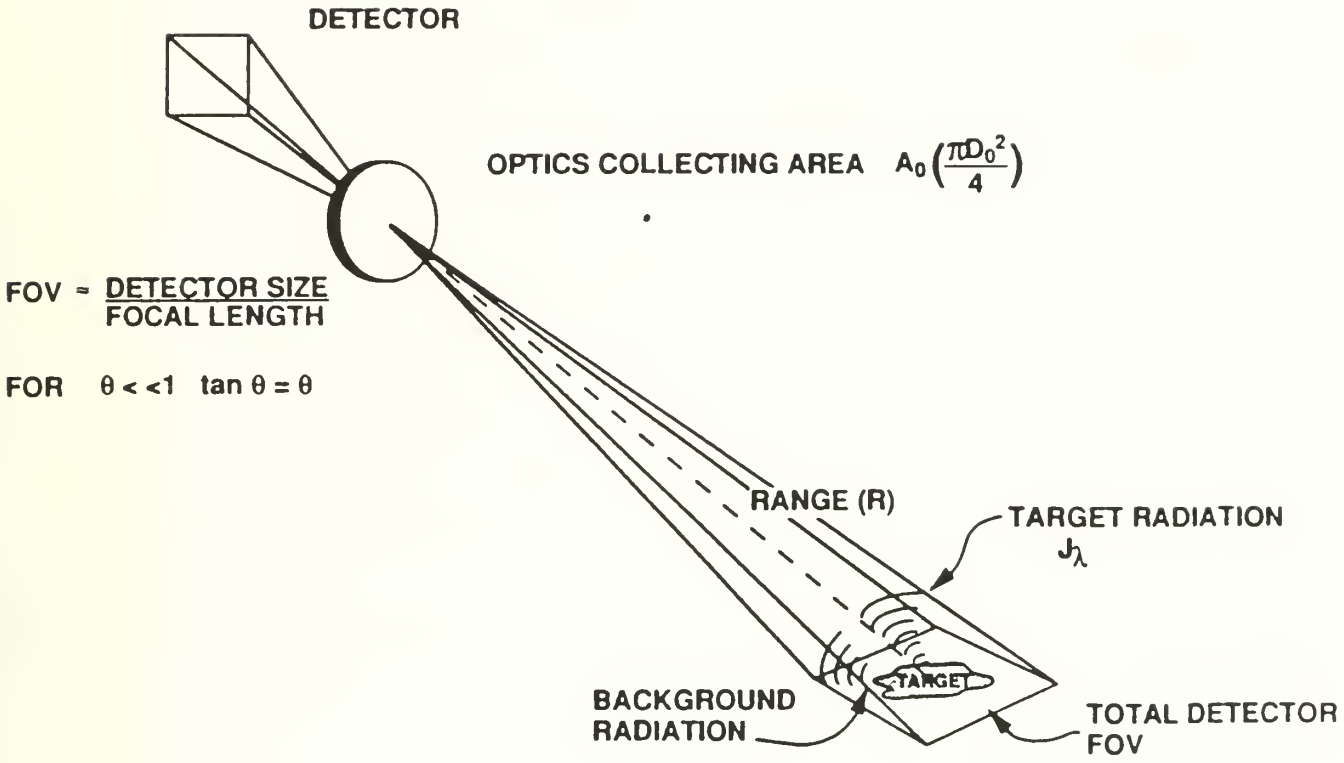

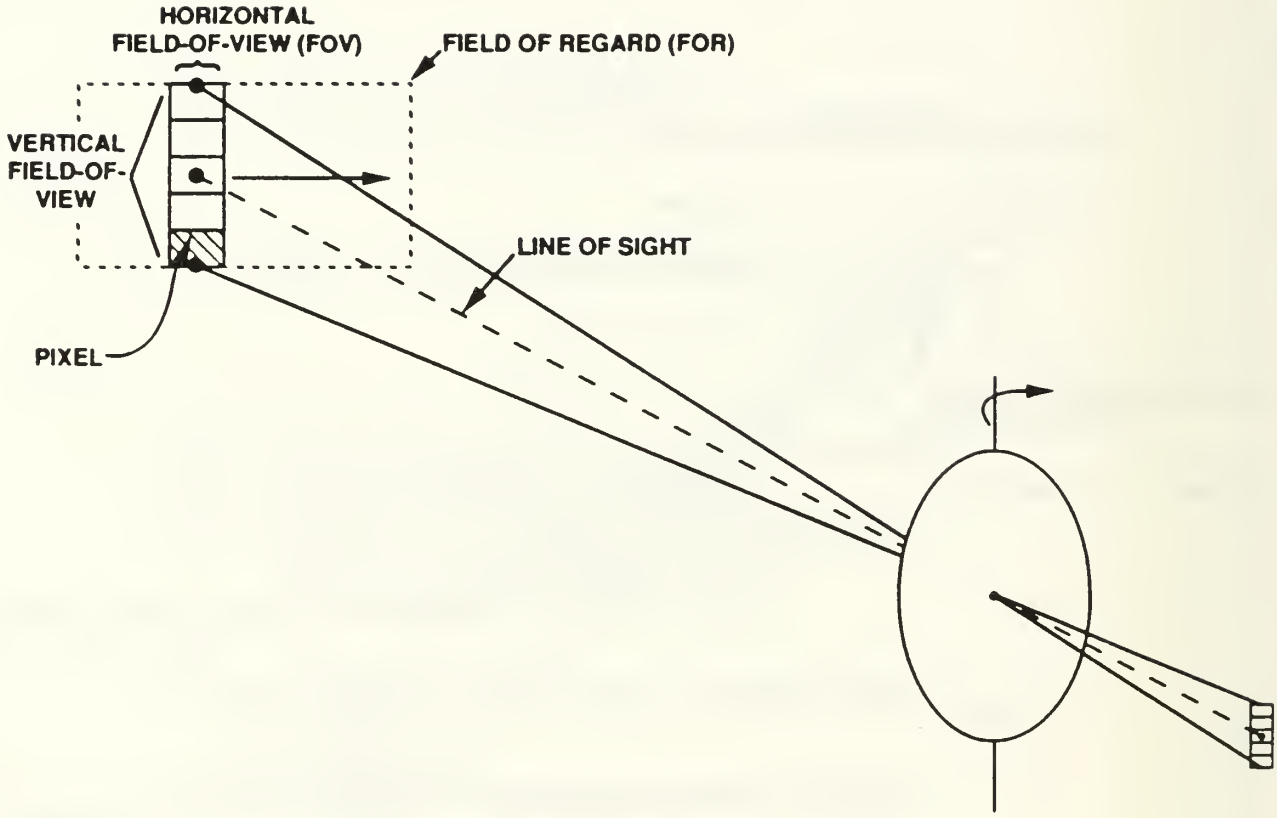
HORIZONTAL
FIELD-OF-VIEW (FOV)
FIELD OF REGARD (FOR)
VERTICAL
FIELD-OF-
VIEW
LINE OF SIGHT
PIXEL

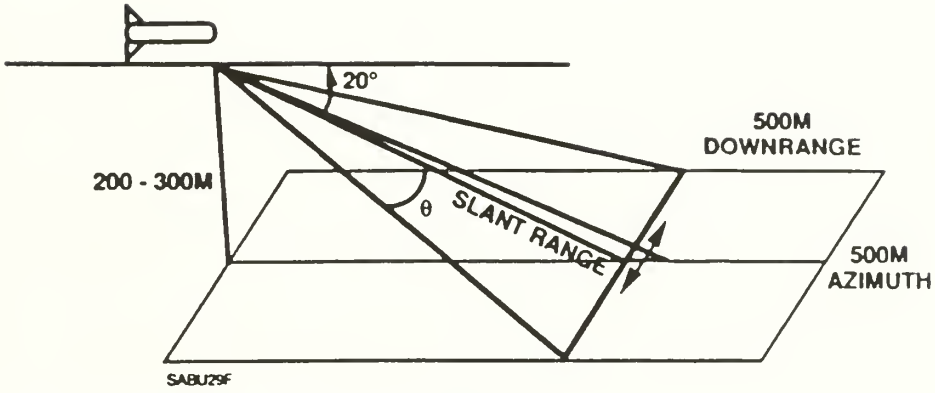

FOOTPRINT ~ 0.2 KM^2 ~ 500 M x 500 M

$$\text{SLANT RANGE} = \frac{\text{ALT}}{\cos^{-1}[70°]} \sim 500 - 800 \text{ m}$$

$$\text{SENSOR AZIMUTH (FOV)} \sim \tan^{-1}\left[\frac{500 \text{ M}}{\text{SL RGE}}\right] \sim 30° - 40°$$

$$\text{SENSOR DOWNRANGE (FOV)} \sim \tan^{-1}\left[\frac{\text{TARGET SIZE}}{\text{SL RGE}}\right] \sim 1°$$

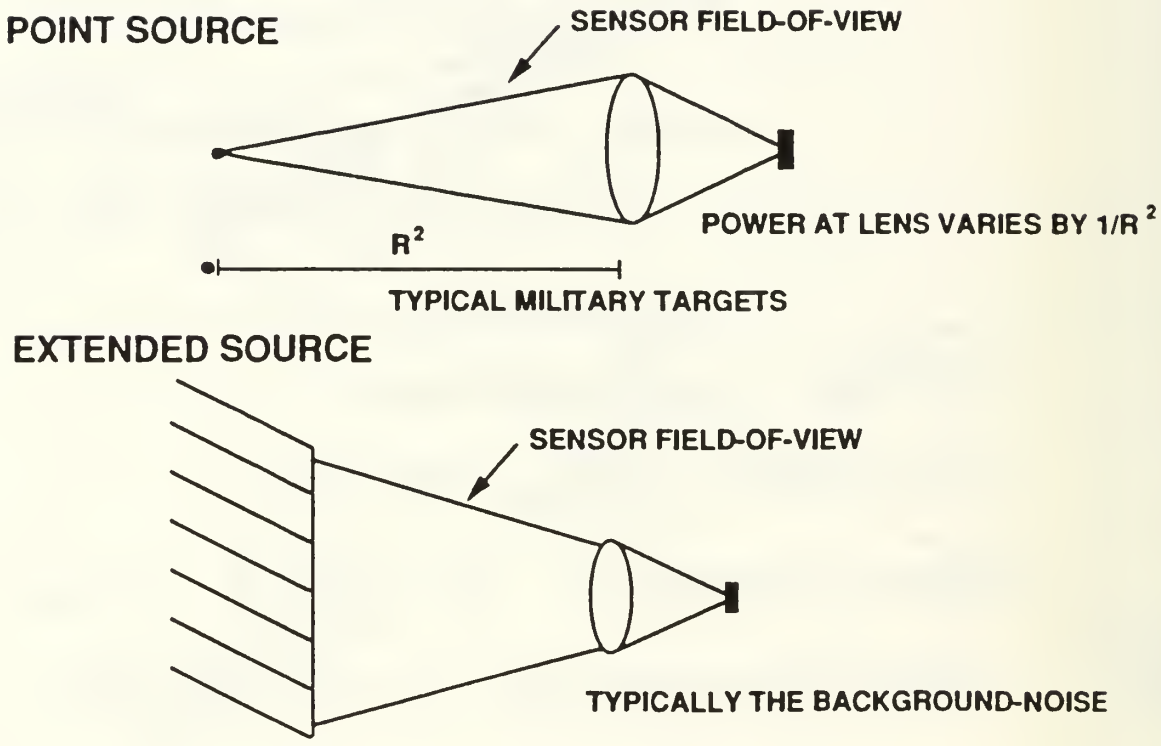
POINT SOURCE
SENSOR FIELD-OF-VIEW
POWER AT LENS VARIES BY 1/R 2
R2
TYPICAL MILITARY TARGETS
EXTENDED SOURCE
SENSOR FIELD-OF-VIEW
TYPICALLY THE BACKGROUND-NOISE

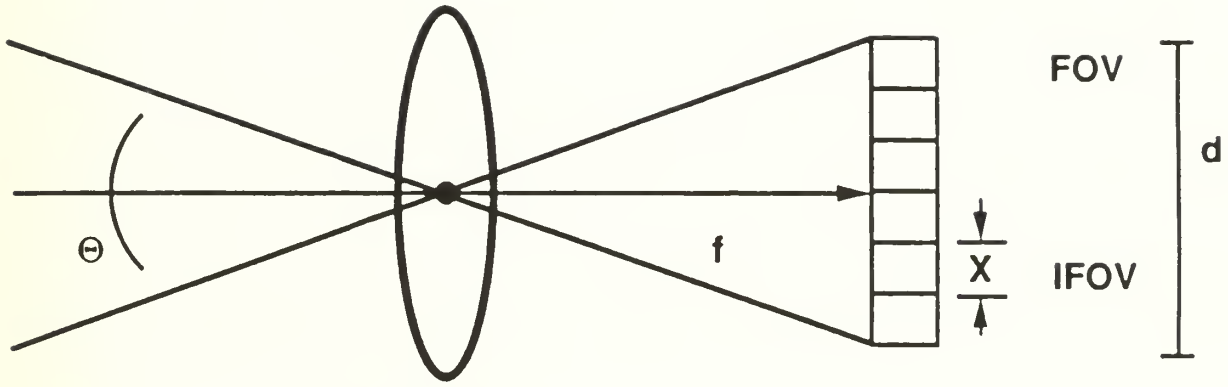

SENSOR FIELD OF VIEW (FOV)

$$\Theta = 2 \cdot \mathrm{TAN}^{-1} \left[\frac{d/2}{f} \right]$$

INSTANTANEOUS FIELD OF VIEW (IFOV)

$$\mathrm{TAN}\Theta \simeq \Theta = \frac{X}{f} \quad \text{PIXEL (IFOV)}$$

LIST OF REFERENCES

1. Robert J. Roy, *" Combat Operations Gardener Unmanned Aerial Support "*, Sinal Vol.45, April 1991.
2. H. Keith Parker, *" The Design and Initial Construction of a Composite RPV for Flight Research Applications "*, Naval Postgraduate School, Monterey, CA, Fall Quarter 1988.
3. US Marine Corps Development and Education Center, *" Remotely Piloted Vehicle Employment "*, Quantico, Virginia 22134-5001, April 1987.
4. M. R.Kruner, D. A. Scriber, and J. M. Killiany, *" IR Technology Development for Navy Applications "*, Optical Engineering Vol.26 NO.3, March 1987.
5. Richard D. Hudson, Jr, *" Infrared System Engineering "*, John Wiley & Sons, 1969.
6. John A. Hoschette and Edwin C. Thiede, *" IR/MMW Sensor Fusion "*, Technology Training Corp, Feb 1990.
7. J. D. E. Beynon and D. R. Lamb, *" Charge Coupled Devices and their Applications "*, Mc Graw-Hill Book Company (UK) Limited, 1980.
8. A. W. Cooper, *" Electro-Optic Principles and Devices "*, Department of Physics, NPS, 1980.
9. Richard D. Hudson, Jr, and Jacqueline W. Hudson, *" The Military Applications of Remote Sensing by Infrared "*, Proc. IEEE. Vol.36. No.1, 1975.
10. Donald J. Brock, *" Tactical Reconnaissance : Will It Survive Near-Real Time Reconnaissance "*, SPIE Vol. 496, 1975.

11. Willian T. Noel, " *Utilization of Imagery in Tactical Reconnaissance* ", SPIE Vol. 79, 1976.

12. William L. Wolfe, " *The Infrared Handbook* ", ERIM (3rd Ed.), 1989.

13. Richard A. Sturz, " *Payload Considerations for RPV/UAV Applications* ", SPIE Vol. 1156, 1989.

14. C. W. Ferguson and J. K. Taylor, " *FLIR System Today* ", SPIE Vol. 79, 1976.

15. Robert E. Fischer, " *Critical Issues in IR Imaging System* ", Photonics Spectra, July 1986.

16. R. Barry Johnson and William L. Wolfe, " *Infrared Design* ", SPIE Vol. 513 Part One, 1985.

17. K. J. Marsh and J. A. Savage, " *IR Optical Material for 8-13 μm Current Developments and Future Prospects* ", SPIE Vol. 513 Part One, 1985.

18. R. Barry Johnson, " *Relative Merits of the 3-5 μm and 8-12 μm Spectral Bands* ", SPIE Vol. 915, 1988.

19. James T. Woolaway, " *New Sensor Technology for the 3 - 5 μm Imaging Band* ", Photonics Spectra, Feb 1991.

20. John Heystead, " *Thermal Imaging Technology Has Versatile and Bright Future* ", Defense Electronics, Apr 1991.

21. M. Herzberger and C. D. Salzberg, " *Refractive Indices of IR Optical Materials and Color-correction of IR Lenses* ", J. Opt. Soc. Am., 53, 420, 1962.

22. Irving R. Abel, " *Radiometric Accuracy in a Forward Looking Infrared System* ", SPIE Vol. 513 part one, 1985.

23. Konrad J. Stahl, " *IR Detectors : State-of-the-art, Future Trends* ", Photonics Spectra, Sep 1989.

24. " *Infrared Detectors* ", Photonics Spectra, July 1985.

25. J. M. Lloyd, " *Thermal Imaging Systems* ", Plenum Publishing Corporation, 3rd Ed., Oct 1982.

26. L. Levi, Applied Optics, Wiley, 1968.

27. R. Barry Johnson and William L. Wolfe, " *Infrared Design* ", SPIE Vol. 513 Part Two, 1985.

28. Neil Sherman and Karl Stich, " *Imaging Sensor for RPVs* ", SPIE Vol.101, 1977.

INITIAL DISTRIBUTION LIST

	No. Copies
1. Defense Technical Information Center Cameron Station Alexandria, VA 22304-6145	2
2. Library, Code 052 Naval Postgraduate School Montery, CA, 93943-5002	2
3. Professor Donald D. Walters Department of Physics, Code PH/We Naval Postgraduate School Monterey, CA, 93943	2
4. Professor Ron J. Pieper Department of Electrical Engineering, Code EE/Pe Naval Postgraduate School Monterey, CA, 93943	1
5. Captain Kim Doo-Jong SMC 1587, NPS, Monterey, CA, 93943	1
6. Major Ji Yoon-Kyu SMC 1058, NPS, Monterey, CA, 93943	1

7. Library 1

Korea Military Academy, C.P.O. Box 77, Gong Neung-Dong,

Sung Book-gu, Seoul, Republic of Korea

8. Library 2

ROKA, Military Intelligence School

Changhowon-Eup P.O.BOX 88

Ichon-Gun, Kyunggi-Do

Seoul, Republic of Korea

9. Capt. Byung-Gook, Choi 3

ROKA, Military Intelligence School

Changhowon-Eup P.O.BOX 88

Ichon-Gun, Kyunggi-Do

Seoul, Republic of Korea

Thesis
C448842 Choi
c.1 The design of a FLIR sensor for the Korean Army RPV.